DELINEATION OF WATER TABLE USING THE GROUND PENETRATING RADAR

By

QUAYE, EVANS KANYI-KOI, Bsc. (Hons) Physics

A Thesis Submitted to the Department of Physics, Kwame Nkrumah University of Science and Technology in Partial Fulfilment of the Requirements of the Degree of

MASTER OF PHILOSOPHY (GEOPHYSICS)

College of Science

Supervisor: Dr. Kwasi Preko

April, 2015

DECLARATION

I hereby declare that this submission is my own work towards the M.Phil and that, to the best of my knowledge, it contains no material previously published by another person or material which has been accepted for the award of any degree of the university, except where due acknowledgement has been made in the text

Quaye Evans Kanyi-Koi	....	....
20290878	Signature	Date
(Student Name & ID)		

Certified by:

Dr. Kwasi Preko	....	....
Supervisor's Name	Signature	Date

Certified by:

Prof. S. K. Danuor	....	....
Head of Dept. Name	Signature	Date

ABSTRACT

This research work is aimed at investigating, determining and delineating the depth to water table and the water saturation level from the surface using the Ground Penetrating Radar (GPR) technique. The survey was conducted at the 55.5 hectare oil palm and citrus plantation portion of the Agriculture Research Station located in the town of Anwomaso which is under the Faculty of Agricultural Science – KNUST. The MALA GPR equipment with 25 MHz Rough Terrain Antenna (RTA) frequency was used for the data collection. GPR data were collected on thirty five profiles of different lengths (100-500 m) at 18 m inter profile spacing in the common offset mode. Results from the survey successfully revealed the average depth to the water table from the land surface to be 30.3 m. The implication of this is that boreholes must be sunk beyond this depth in the saturated zone in order to pump groundwater. It was further revealed that the water table in all cases traced the geometry or topography of the land at various elevations above mean sea level. Subsurface reflectors such as buried objects were also brought to fore. The water table data conform to hydro-geological data within the survey metropolis where most of the boreholes have an average depth of about 35 m.

ACKNOWLEDGEMENTS

Indeed I can do all things through Christ who strengthens me. First and foremost I would like to thank God for the wisdom and protection he bestowed on me during the entire duration of my postgraduate studies.

I also want to express my gratitude to my supervisor Dr. Kwasi Preko for his pain-staking effort in motivating and proof reading the draft work. Doc, when I was stranded on the project, you came to my rescue, this I truly appreciate.

I would also want to thank Prof. Sylvester Danuor, Dr. Akwasi Aning, Dr. Edem Donkor, Mr. Reginald Noye, Mr. Van-Dyke Asare, Mr. Samuel Arthur of ARS and all other lecturers who gave me direction at various stages of my postgraduate studies.

To the following friends: Mr. Obed Sedoawu, Mr. Emmanuel H. Tetteh, Mr George Hinson, Mr. Richard K. Akorlie, Mr. Jakalia I. Sontaa, Mr. Sackey Nathaniel, Mr. Desmond Appiah, Nana Kofi Appiah – Badu, Miss Bernice Danu, Adamu Iddrisu and other friends and course mates for their friendship.

Last but not least, I would like to thank my parents and siblings Rhoda Aryeley Quaye and Esther Naa Ayeley Commodore-Mensah for their unconditional support and to those who will prefer being anonymous.

TABLE OF CONTENTS

LIST OF TABLES

LIST OF FIGURES

LIST OF SYMBOLS AND ACRONYMS

a	Phase coefficient
α'	Attenuation constant
B	Magnetic flux density
b	Attenuation coefficient
c	Speed of light in Vacuum
D	Electric flux density
d	Distance
δ	Skin depth
E	Electric field strength of EM wave
ε	Absolute dielectric permittivity
ε^e	Complex effective permittivity
ε_0	Permittivity of free space
ε_r	Relative dielectric permittivity
f	Frequency
H	Magnetic field intensity
h	plank's constant
i	$\sqrt{-1}$
k	Wave number vector
σ	Conductivity
θ_v	Volumetric water content
ρ	Reflection coefficient
τ	Transmission coefficient
t	Time
T	Temperature
$tan(\delta)$	Loss tangent
μ_r	Relative magnetic permeability
μ_0	Permeability of free space
μ	Absolute magnetic permeability
v	Velocity
λ	Wavelength
ω	Angular frequency
π	Pie

Z

∇	Dirac delta function
Z	Impedance
AGC	Automatic Gain Control
ARS	Agriculture Research Station
EMR	Electromagnetic Radiation
LED	Light Emitting Diode
GIS	Geographic Information System
GPS	Global Position System
GPR	Ground Penetrating Radar
NW	North West
RTA	Rough Terrain Antenna
SW	South-West
SMP	Symmetric Multiprocessing
RADAR	Radio Detection and Ranging
ZOP	Zero-offset Profiling

CHAPTER 1

INTRODUCTION AND LITERATURE REVIEW

1.1 General Introduction

The definition of geophysics is done in several ways. In the broadest sense, it can be defined as the application of physical principles to study the earth (Sheriff, 2002). This general definition encompasses a wide range of disciplines such as hydrogeology, meteorology, physical oceanography, seismology, techno-physics and so on. Specifically, geophysics is the application of physical quantity measurement techniques to provide information on conditions or features beneath the earth's surface.

Ground-penetration radar (GPR) is a geophysical technique employed to obtain subsurface information from surface-based measurements. The GPR equipment operates by transmitting and receiving polarised pulses of electromagnetic wave from the ground to the surface (Reynolds, 2011). This technique responds to variations in the electrical properties of subsurface materials such as dielectric constant and conductivity. The responses are also functions of material type, moisture content and pore-fluid type. When there is a contrast in the dielectric properties between adjacent materials, a portion of the electromagnetic pulse will be reflected. Subsurface structures and conditions such as water table can be mapped by measuring the amplitude and travel time of the reflected energy (Reynolds, 2011).

Water table at a particular place beneath the earth surface affects soils and its agricultural use. High water table has the potential to restrict rooting of plants and also retard warming of soil (Hughes et al., 1993).

In understanding the formation of groundwater, it is important to understand the water saturation profile in the subsurface. The portion of the profile between the ground surface and the ground water table is called the vadose zone. This zone can be divided into a number of regions (Ziaqiang et al., 2009). Water is held at a minimum in the upper part of the vadose zone where there is the residual saturation. In the lower part of the vadose zone also known as the transition (funicular) zone, the water saturation rises above residual levels which increases with depth to the point where the ground water surface is reached. The capillary fringe is located below the funicular zone where saturation approaches 100 % as in figure1.1 (Garambois et al., 2002). The common boundary between the saturated and unsaturated zones is described as the water table. It can also be described as the depth where the pore water pressure is equal to the atmospheric pressure (Ziaqiang et al., 2009). The thickness of the capillary fringe and transition zone depends largely on the grain size distribution. The distinguishable electromagnetic wave reflections of main concern occur at the top of the water saturated zone which is located at the top of the capillary fringe above the water table (Ziaqiang et al., 2009). The GPR response from the top of the capillary fringe is assumed to be the location of the water table (Al Hagrey and Mauller, 2000). Annan (2005) showed that radar reflections from the water saturated zone become more dispersed as the thickness of the transition zone above the capillary fringe increases.

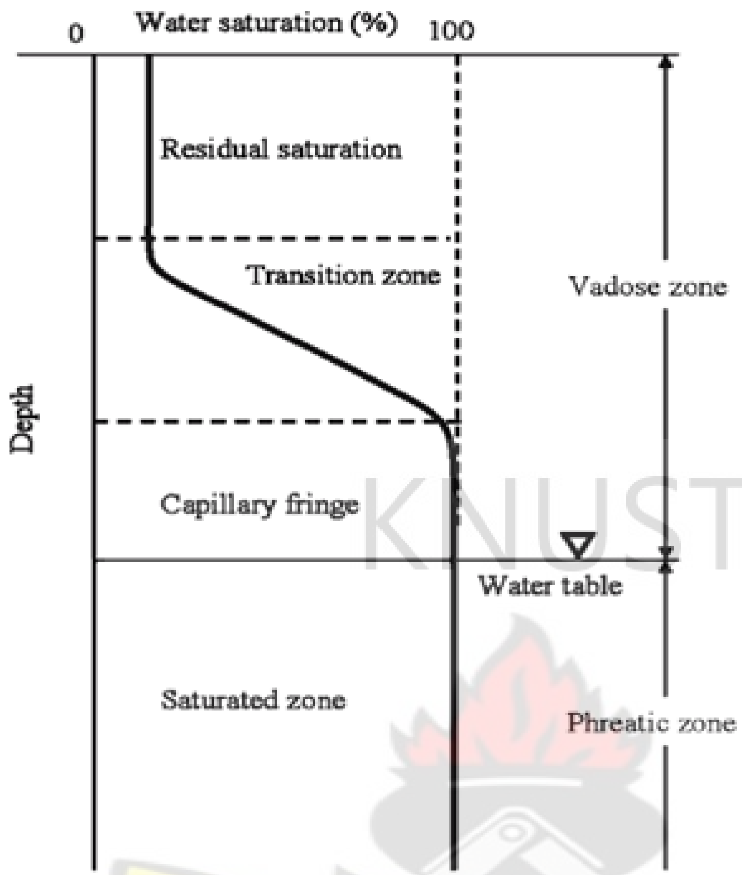

Figure 1.1: A conceptual model of the water saturation profile in the subsurface (Ziaquiang et al., 2009)

Water table behaviour can be influenced by certain variables. These include topography, soil characteristics and rainfall intensity (Dunne and Black, 1970, Cheng et al., 1975). These variables are capable of acting individually or together in causing water table to rise at a specific point.

Dunne and Black (1970) and Anderson and Burt (1978) investigated the role topography plays in influencing soil moisture level. They both showed that in hollow regions (surface concavities), the levels of the water table were generally higher than in spurs (surface concavities). Although the effect of topography on water table levels was observed, no attempt was made to correlate water table levels with topographic variables.

This was first attempted by Sinai et al., (1981), who found a strong correlation between soil moisture content at a depth of 40 cm and soil surface curvature.

The occurrence of higher moisture levels in concave areas was also noted by Beven (1979), Huff et al., (1982), and Petch (1988). Anderson and Burt (1978) also noticed the generation of saturated zones away from topographic hollows at their pasture site. They concluded that topographic variables should only be used in steep topographies. Their findings were however contradicted by Petch (1988), who found that the highest probability of saturation existed in areas of strong topographic convergence regardless of slope angle, as well as in areas of low slope close to stream channels.

Soil characteristics and surface topography are closely linked. This has led to the development of the catena theory (Thompson, 1991). This theory states that soils derived from the same parent material and of the same age may have varying characteristics due to difference in topographic relief and drainage. The theory is based on the fact that lateral movement of soil water in a down slope direction will carry soil solutes and suspensions with it, thereby affecting down slope soil development (McCaig, 1984).

Highly variable water tables and the existence of long-term soil saturation have also been linked to the colour of the soil as well as the presence of mottles and gleying. These soil characteristics are used by soil scientists to determine soil drainage class and to evaluate the duration of high water tables. Even though it is used widely, some researchers have discovered the inaccuracy of these indicators to describe saturated conditions depending on factors such as the season in which saturation occurs (Cogger et al., 1992).

Moreover, it is also not easy to evaluate water table depths by use of redoximorphic features as depth increases. According to Moore et al., (1990), soil parameters influencing water table behaviour include saturated hydraulic conductivity, organic content and moisture release.

The influence of rainfall intensity and volume on water table response has been found in a number of studies. Factors that can influence water level include amount and volume of precipitation. These may cause water level to rise as well as increasing the likelihood of saturation (Thompson, 1991).

Manu (2013) conducted a survey over the Subenso-north gold deposit to delineate the possible fracture zones of mineralization using GPR. Among his results the author found out that different radar responses were obtained from the saprolites and the inferred structural patterns established were interpreted as zones of possible gold mineralization.

Preko (2007) also used the guided wave sounding method, an invasive application of GPR to determine volumetric soil water content and proved to be successful. In his abstract statement, the author concluded that GPR has further advantage over discrete point data acquisition geophysical techniques.

Snow covered crevasse in alpine areas were also discovered using GPR. After the usual processing steps to synchronize and enhance the reflected signals, the anomalies occurring in any crevasse could be seen clearly since the reflection horizon from the snow/ice boundary is non-continuous and the diffraction from the walls of the crevasse show curvatures towards the crevasse.

Ground penetrating radar exploration for ground water and contamination was conducted by Ziaqiang et al., (2009). He highlighted the effect of a capillary fringe over water table with groundwater survey and hydraulic properties estimation. They found out that water contents vary from severally in the capillary fringe in the Changsha province of China.

GPR also plays a very important role for stratigraphy recognition. Azwin et al., (2012) used three-dimensional GPR to study water table and the subsurface in Seri Iskandar, Tronoh and Perak in Malaysia. They concluded that layer of reclaimed sand were detected at depth less than 3 m with non-uniform sand sedimentation and dipping layers were detected at depth less than 10 m.

Liang (1990) noted that due to the difference between dielectric constants of water and soil, a reflection wave would be generated GPR comes into contact with an underground water surface. Hence, GPR could be used to test underground water level. Beres and Haeni (1991) mentioned that the underground water surface could be detected more easily in sandy soil layer than in clay layer.

A run-through of the results obtained by Lee (1996) brought to the fore, the likelihood of using GPR to detect ground water level as well as its content and mud rock. Daniels (1994), Dominic (1995) and Benson (1993) concluded that the stratum of underground water level is formed by coarse materials.

These attest to the significant information obtained regarding the application and use of GPR. Reflections are visible and distinct at boundaries with different dielectric properties. Reflections from fluid surfaces are also visible and the energy reflected at this interface is significant and can be coupled with the geology and other hydro-geological information to map the water table in the Agriculture Research Station (ARS) at Anwomaso.

1.2 Research Problem Definition

Over the years, the Agriculture research Station located at Anwomaso in the Kumasi Metropolis of Ghana with an arable land size of about 554.5 hectares has played a leading role in providing food stuff to the KNUST community and beyond. However, the station continues to operate without basic amenities such as potable water, for domestic usage and farm management. The situation is even dire since the only hand dug well continues to remain dry. This problem has made it imperative to employ a geo-scientific approach to determine the water table in the subsurface; hence, the choice of the GPR. Also, Ground penetrating radar is increasingly becoming successful in ground water geophysics and other disciplines in engineering and the earth sciences. From many researchers and literature reviewed especially in Ghana, groundwater detection as well as water table detection has become common with the use of other prospecting methods such as electrical resistivity and electromagnetic methods but that of the GPR technique has received low attention and application for this purpose. The strong relationship between the physical properties of geologic materials including water and their electromagnetic properties enables the identification of physical structures in the subsurface (Davis and Annan, 1989; Dallimore and Davis, 1987; Delany and Arcone, 1982; Scott et al., 1978).

The ability to achieve this can go a long way to ameliorate the challenge of lack of basic amenities like water at the ARS which has bedevilled the farm over the past years both for research purposes and farm management. It is envisaged that borehole construction in the near future will see a facelift with this project since the farm lacks groundwater table map or data which has resulted in the inability to detect groundwater after boreholes have been dug. Lack of proper and thorough geophysical and hydro-geological work may have accounted for this or simply put the depths at which these boreholes were dug were inaccurate and shallow per the information obtained from workers and managers of the farm.

1.3 Research Purpose and Objectives

The main objective of this research work is to map the water table of the subsurface at the Agricultural Research Station at Anwomaso using the Ground Penetration Radar technique.

There are other objectives which will help to achieve the overall aim, these include:

- Estimating the depth of the water table
- Evaluating the hydro-geological composition of the vadose zone
- Locating aquifer depth
- Determining the average propagation velocity of radar signal through subsurface materials
- Establishing the influence of topography on groundwater table behaviour

These objectives can be accomplished through the interpretation of information derived from the radar pulses and in conjunction with geophysical and hydro-geological data.

1.4 Justification of the Research

Water is an indispensable natural resource for life sustenance and its availability is always and almost at a threat by many factors including climate change. Climate change for instance is interrelated with agriculture, both of which take place on a global scale.

Research station like the ARS depends solely on rain for farm management. However, erratic rainfall which is characterised by unpredictable patterns of rainfall, poor rainfall both in volumes and distribution and increase incidence of pests and diseases result in low crop yields and possible extinction of some species of plants. To buttress this point, the 20th October 2011 edition of the Ghanaian Chronicle newspaper reported that, according to researchers, production of cassava for instance is expected to reduce by up to 53% by 2080, and cocoyam by 68%. According to the report Ghana is vulnerable due to its high level of dependence on agriculture with its attendant adverse climate conditions.

The ARS is no exception to this, a well-defined map detailing the water table depths and water distribution of the farm is important in making projections and decision making in the construction of mechanised wells for farm management.

1.5 Structure of thesis

This thesis comprises six main chapters.

Chapter 1 gives an overview of the research. This includes a discussion of the ground water saturation profile. The variables that also influence water table depths such as topography, soil and precipitation were also discussed. This is followed by the literature review of the research topic and overview of related research works.

Chapter 2 provides a background of groundwater concept and the physiography of the project site. Climate, vegetation and soil, location and hydrogeology of the research site are major subtopics explained here.

Chapter 3 outlines the theory and physics of GPR; including a discussion of the various GPR survey techniques and the significance of some physical properties such as dielectric, electrical conductivity and magnetic permeability of materials.

Chapter 4 provides an overview of the research methodology and GPR equipment adopted to address the objectives. It also explains the measurement procedure. Data processing at various stages to obtain sharp radar records are also described in this chapter.

Chapter 5 deals with the display and interpretation of the radar records for some profiles. The subsurface water saturation profile including the depth of water table is also discussed in this chapter. Subsurface reflectors that were revealed were identified and radar velocities through them were estimated on the radar records to determine whether they have any geologic significance or otherwise.

Chapter 6 draws possible conclusion from the research work based on information derived from the method, equipment and processing of data. This is done with the help of hydro-geological data available and other materials associated in achieving the objectives of this research work.

CHAPTR 2

PHYSIOGRAPHY AND GEOLOGICAL SETTINGS

2.1 Concept of Groundwater and Water-table

Some water can be found beneath the earth's surface almost everywhere, plains, mountains and even deserts. This water may occur close to the land surface, as in a marsh, or it may lie many hundreds of feet below the surface, as in some arid zones or hot climatic regions (Philip et al., 2003)

Water found at shallow depths might be just a few hours or days old; and can even be 100 years old or more. When the depth is greater and after flowing over long distances, water may be several thousands of years old. Ground water is stored in permeable rocks called aquifer after slowly moving into it. Aquifer is derived from two Latin words, aqua which means water, and ferre which means to bear or carry. Aquifers literally carry water underground. An aquifer may have sizeable openings and may compose of sand or gravel layer, cavernous limestone or sandstone. It may also be composed of a rubble top or base of lava flows, or even a large body of massive rock, such as fractured granite, that has sizable openings. In terms of storage at any one instant in time, ground water is the largest single supply of fresh water available for use by humans (Philip et al., 2003)

Ground water has been known to humans for thousands of years. The biblical flood as captured in the Scripture in Genesis 7:11 "the fountains of the great deep (were) broken up," and Exodus 20:4 "water under the Earth" are part of many references to ground water.

Ground water simply means subsurface water that saturates pores or cracks in rocks below the ground surface (Harter, 2003). Ground water is recharged by rainfall, melted snow and so on. When it rains or snow melts, some infiltrates into the pores of cracks and rocks while some are collected in streams and on land (Fig 2.1). Water that enters the soil first of all replaces the water that has evaporated or used by plants during a preceding dry period (Philip et al., 2003). The distance between the land surface and the water bearing rock is a zone referred by hydrologists as the unsaturated zone. The water content in this unsaturated zone is usually little, mostly in smaller openings of the soil and rock. The larger openings usually contain air instead of water. After a heavy rainfall, the unsaturated zone may be almost saturated; after a long dry period, it may be almost dry. Water is held in the unsaturated zone by molecular force of attraction and this prevents water from entering or flowing towards a well. After plants have satisfied their requirements, excess water will infiltrate to the water table. Below the water table, all the openings in the rocks are full of water. Water then moves through the aquifer to streams, springs, or wells from which water is being withdrawn. Natural refilling of aquifers in the subsurface is a slow process since ground water moves slowly through the unsaturated zone and the aquifer (Philip et al., 2003).

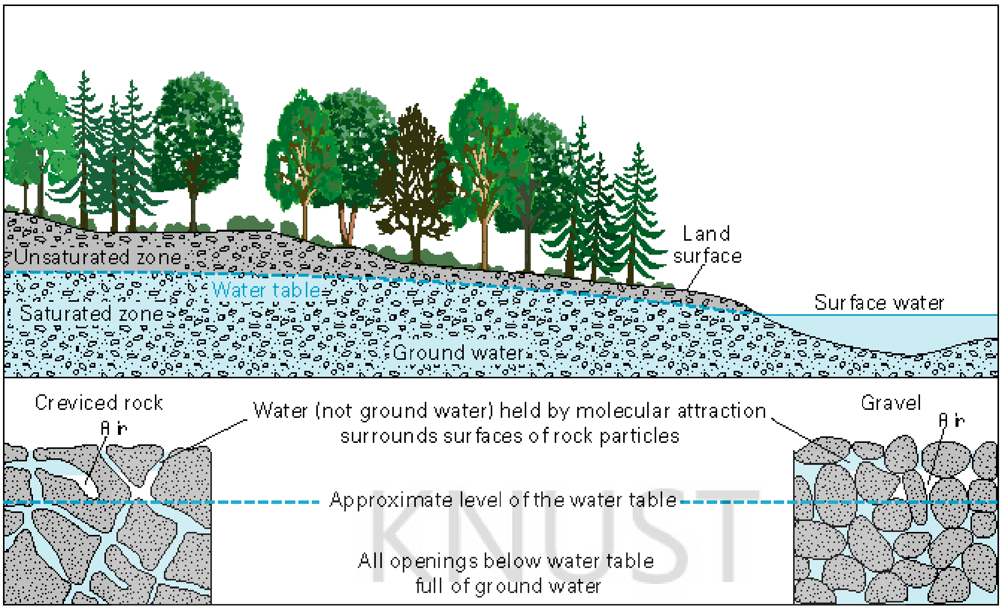

Figure 2.1: Occurrence of ground water in rocks

The wide range applications of subsurface radar can involve distances of many hundreds of meters. In general, the frequencies involved have been between 10 MHz to 1 GHz for different resolutions of subsurface materials. Much of the long-range radar probing work has been carried out by academic establishments and research organizations.

Water table depth can vary from a meter depth or less when it is found on the land surface or near permanent water bodies such as streams, lakes and wetlands, to several meters on certain landscapes. One significant characteristic of the water table is that its depth varies seasonally and from year to year because of groundwater recharge. The accumulation of water to the upper surface of the saturated zone is related to the wide variation in the quantity, distribution, and timing of precipitation (Winter, 1999).

2.2 Climate and Vegetation

The project site falls within the wet semi-equatorial climatic region of Ghana (Benneh and Dickson, 1977). It has two rainfall maxima (214.3 mm in June and 165.2 mm in September). The first rainy season lasts from May to June, and the second one from September to October. The average humidity is about 84.16 % at 0900 GMT and 60 per cent at 1500 GMT. The mean minimum and maximum temperatures are 21.5℃ and 30.7℃ respectively while the average annual temperature is about 24℃

With respect to vegetation, the area falls within the moist semi-deciduous South-East Ecological Zone. Predominant species of trees found are Ceiba, Triplochlon, Celtis with exotic species. The rich soil is coarse in texture and has promoted agriculture in the periphery. Infrastructural facilities such as hospitals, schools, police station and telecommunications are available. Electricity is supplied from the national grid. Some notable towns around the project site are Boadi, Fomesu and Oduom.

2.3 Location and Accessibility

The project was undertaken at the KNUST Agriculture Research Station at Anwomaso in the Kumasi Metropolis in the Ashanti Region of Ghana. It is located on latitude 6^{o} 41' 838" N and longitude 1^{o}31'533" W. The town is bordered on the north by Fomesua, to the east by the KNUST campus, to the West by Oduom and to the south by Boadi. Anwomaso is about 15 kilometres from the centre of Kumasi- the capital city of the Ashanti Region of Ghana (Fig 2.2).

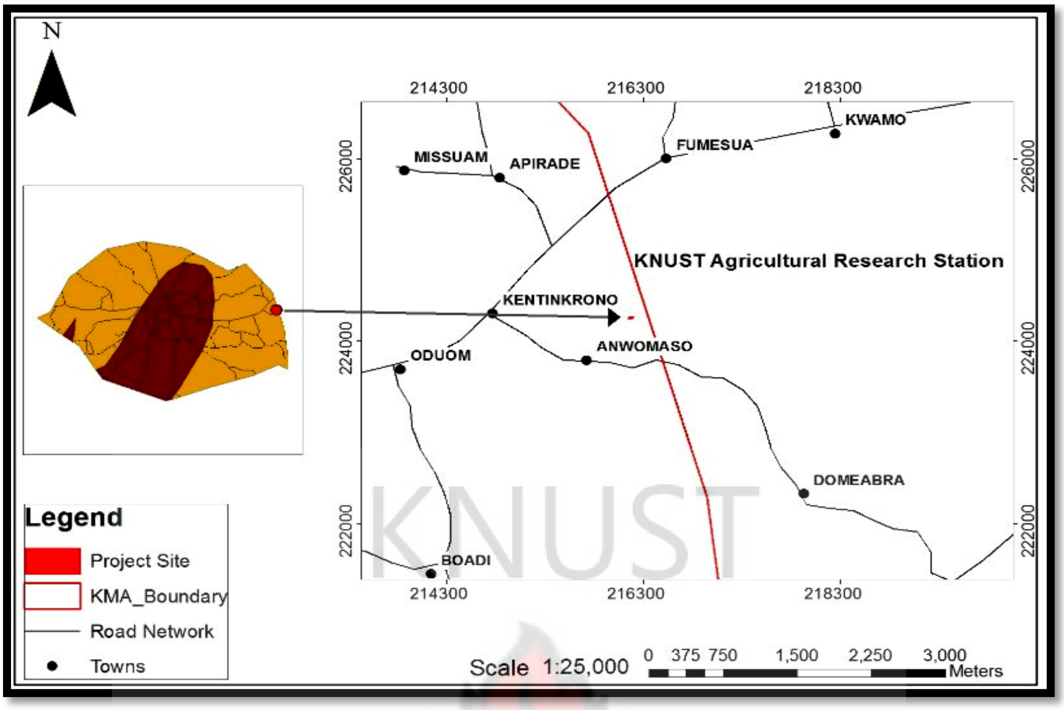

Figure 2.2 Geological map of the Kumasi metropolis showing location and accessibility to study area (Geological Survey Department, Ghana, 2009)

2.7 Local Geology and Hydrogeology

The Anwomaso is dominated by the middle Precambrian Rock. The Birimian phyllite, schist, slate, greywacke, tuff, and lava are generally strongly foliated and fractured. Where they crop out or are near the surface, considerable water may percolate through them Fig 2.3.

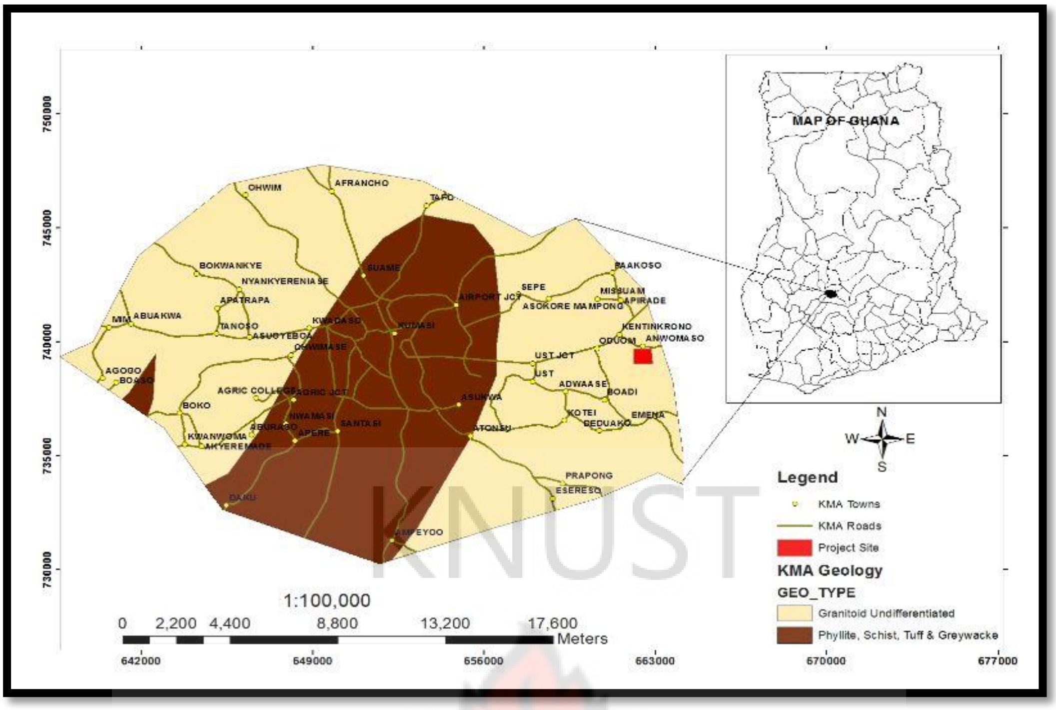

Figure 2.3: Geology map of Kumasi Metropolis showing the study area
(Geological Survey Department, Ghana, 2009)

Boreholes in the Upper and Lower Birimian rocks have average yield of about $12.7 m^3/h$. Kumasi and its surrounding areas have higher borehole yields. Most of the boreholes in the Birimian System are fitted with hand pumps and have an average depth of about 35 m compared to the granite, where it is more difficult to construct successful wells. Boreholes in this zone are drilled to an average depth of 60 m (Dapaah-Siakwa and Gyau-Boakye, 2000)

The major hydrogeological province of the metropolis is the Basement Complex and the sub-province is the Birimian system.

CHAPTER 3

THEORY OF THE GROUND PENETRATING RADAR

3.1 Basic Radar Theory

GPR uses high-frequency polarized radio waves typically in the 1 to 5000 MHz frequency range and transmits into the ground. When the waves hit a buried object or a boundary with different dielectric constant, the receiving antenna records the variations in the reflected signal. The principle also involves the scattering of electromagnetic energy in the form of an electromagnetic wave to locate buried objects. One basic principle of interpreting GPR is to understand electromagnetic (EM) theory and have an empirical understanding of how electromagnetic energy travels or propagates in the subsurface (Allred et al., 2008).

A propagating wave is described by a frequency, a velocity and a wavelength. Adding two waves together must be informed by the phase or time offset of the waves. Also from basic physics, to form any wave shape, the waves should have different frequencies and different phases. A wave composed of multiple frequencies with resulting finite time duration such as a pulse of electromagnetic energy is called a time-domain wave. The most fundamental underpinning principle of GPR according to Allred et al., (2008) is as follows:

a. A pulse of time-domain electromagnetic energy is generated by a transmitting antenna which propagates into the earth with a particular velocity and amplitude, and recorded by a receiving antenna, and
b. The energy of the pulse recorded over time provides a time-history of the pulse travelling through the subsurface.

Electromagnetic waves travel at a specific velocity which is determined by the permittivity of the material.

Also, investigating the subsurface by GPR is based primarily on the relationship between the velocity of the wave and material properties. This therefore explains that the velocity is different between materials with different electrical properties, and a signal passing through two materials with different electrical properties over the same distance will arrive at different times (Daniels, 2000). The time interval for the wave to travel from the transmitter to the receiver is called the ‘travel time’. The basic unit of EM wave travel time is the nanosecond (ns), where 1 ns = 10^{-9} s. The velocity of an electromagnetic wave in air is approximately 0.33 m/ns. The velocity is directly related to the inverse square root of the permittivity of the material, and since the permittivity of earth material is greater than the permittivity of the air, the velocity of a wave in a material other than air is always greater than 0.33 m/ns (Daniels, 2000).

3.2 Electromagnetic Radiation

A better understanding of radar remote sensing can be achieved when the nature of electromagnetic radiation (EMR) is explained. Kip (1969) and Drury (1993) explained this in a simple way. EMR is made up of quanta of energy which are the smallest defined units of energy. They can also be described as particles (photons) or as waves of oscillating magnetic and electric fields.

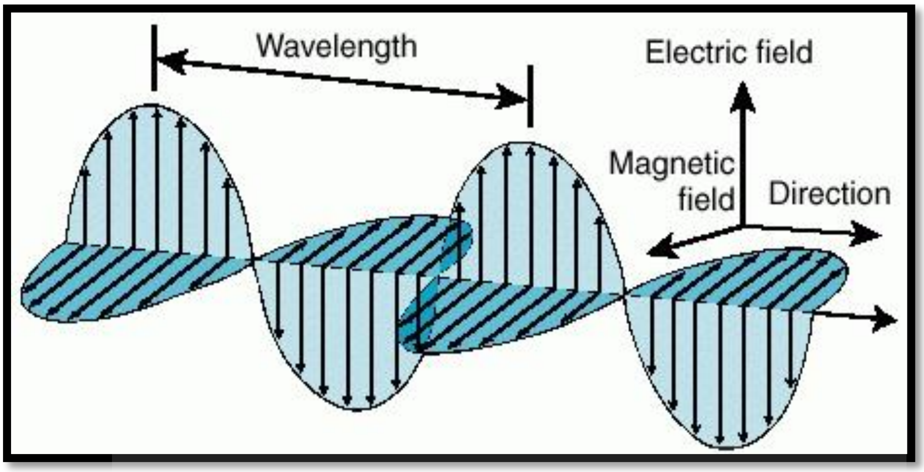

Figure 3.1 EM wave propagation (Drury 1993)

These oscillating fields which are described as sine wave stand in right angles to each other and to the direction of propagation (Fig 3.1). Radiations are called polarised if the electric fields of all quanta are lined in one direction. The velocity of propagation for EMR in a vacuum is given as c = 3.0 × 10^8 ms^{-1}. In matter this velocity changes. The EMR velocity (c) can also be written as:

$$c = \frac{1}{\sqrt{\varepsilon_0 \mu_0}} \tag{3.1}$$

where ε_0 and μ_0 are the free space constants for permittivity and permeability respectively. Permittivity is the property of a dielectric substance that determines the degree to which it modifies an electric field. Permeability describes the property of a substance that can be magnetised and also determines the degree to which it modifies the magnetic flux in the region occupied by it in a magnetic field.

The frequency of the wave oscillation f and the wave length λ are inversely proportional and it is given by the equation (Conyers and Goodman, 1997):

$$c = \lambda f \tag{3.2}$$

Frequency and wavelength vary as a function of the energy of the quanta according to Planck's law:

$$E = hf \tag{3.3}$$

where Planck's constant $h = 6.62 \times 10^{-34}$ Js

EMR of different wavelengths and different frequencies and are emitted from different sources and through different processes as shown in fig 3.2. Also, the behaviour of EMR changes with its wavelength.

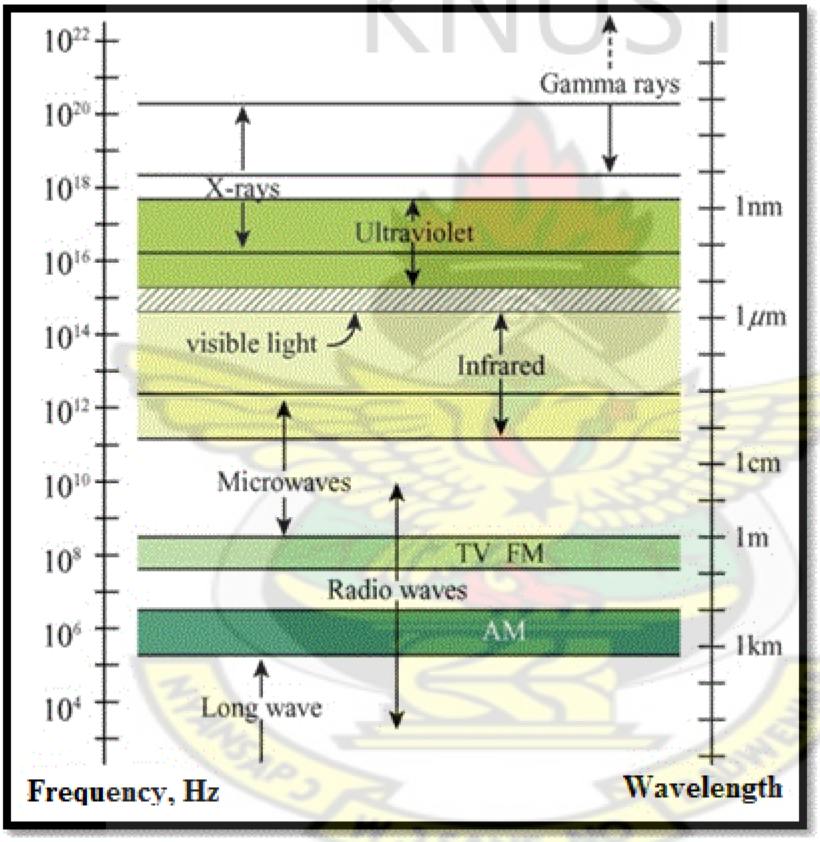

Figure 3.2: Electromagnetic wave spectrum

3.2.1 Maxwell's Equations

Maxwell's equations represent one of the most concise ways in stating the basics of electricity and magnetism. From these equations one can build most of the working relationships in the field. Because of their concise statement, they represent a high level of mathematical sophistication and are therefore not generally introduced in an introductory treatment of the subject, except perhaps as summary relationships.

In regions of space where there are no charges or currents Maxwell's equations are as follows:

$$\nabla \cdot E = 0 \tag{3.4}$$

$$\nabla \cdot B = 0 \tag{3.5}$$

$$\nabla \times E = -\frac{\partial B}{\partial t} \tag{3.6}$$

$$\nabla \times H = \mu_0 \varepsilon_0 \frac{\partial E}{\partial t} \tag{3.7}$$

Where $\boldsymbol{E}$ is the electric field strength vector (Vm^{-1}), $\boldsymbol{H}$ is the magnetic field intensity vector (Am^{-1}), $\boldsymbol{B}$is the magnetic flux density vector (Tm^{-2}).

Maxwell's equations are a set of coupled, first order, partial differential equations for **E** and **B**. They can be decoupled by applying curl to equations 3.6 and 3.7.

$$\nabla \times (\nabla \times E) = \nabla(\nabla \cdot E) - \nabla^2 E = -\nabla \times \frac{\partial B}{\partial t} = -\frac{\partial}{\partial t}(\nabla \times B) = -\mu_0 \varepsilon_0 \frac{\partial^2 E}{\partial t^2} \tag{3.8}$$

$$\nabla \times (\nabla \times B) = \nabla(\nabla \cdot B) - \nabla^2 B = \nabla \times \left(\mu_0 \varepsilon_0 \frac{\partial E}{\partial t} \right) = \mu_0 \varepsilon_0 \frac{\partial}{\partial t}(\nabla \times E) = -\mu_0 \varepsilon_0 \frac{\partial^2 B}{\partial t^2} \tag{3.9}$$

Since $\nabla.\boldsymbol{E} = 0$ and $\nabla.\boldsymbol{B} = 0$ we have

$$\nabla^2 E = \mu_0 \varepsilon_O \frac{\partial^2 E}{\partial t^2} \tag{3.10}$$

$$\nabla^2 B = -\mu_0 \varepsilon_O \frac{\partial^2 B}{\partial t^2} \tag{3.11}$$

The equations for **E** and **B** are of second order as a result of decoupling them. In vacuum, each Cartesian component of **E** and **B** satisfies the three-dimensional wave equation,

$$\nabla^2 f = \mu_0 \varepsilon_O \frac{\partial^2 f}{\partial t^2} \tag{3.12}$$

The solution of this equation is a wave. So Maxwell's equations suggest that empty space supports the transmission of EM waves traveling at a speed which happens to be precisely the velocity of light, c. This implies that light is an electromagnetic wave.

$$c = \frac{1}{\sqrt{\mu_0 \varepsilon_0}} = 3.00 \times 10^8 \text{ m/s} \tag{3.13}$$

3.2.2 Electromagnetic Wave in Non-conducting Medium

One of the most important consequences of the Maxwell's equation is the equations for electromagnetic wave propagation in a non-conducting medium. In the absence of free charges and current densities, Maxwell's equations are given by equations 3.4 to 3.7 and the wave equations for **E** and **B** are derived by taking the curl of $\nabla \times \boldsymbol{H}$ and $\nabla \times \mathbf{E}$,

$$\nabla \times \nabla \times E = -\nabla \times \frac{\partial B}{\partial t} \tag{3.14}$$

$$\nabla \times \nabla \times H = \nabla \times \frac{\partial D}{\partial t} \tag{3.15}$$

For uniform isotropic and linear medium we have $\mathbf{D} = \varepsilon \boldsymbol{E}$ and $\mathbf{B} = \mu \boldsymbol{H}$ where ε and μ are in general complex functions of frequency ω.

Then we obtain

$$\nabla \times \nabla \times E = -\varepsilon\mu \frac{\partial^2 E}{\partial t^2} \tag{3.16}$$

$$\nabla \times \nabla \times B = -\varepsilon\mu \frac{\partial^2 B}{\partial t^2} \tag{3.17}$$

Since $\nabla \times \nabla \times \mathbf{E} = \nabla(\nabla.\boldsymbol{E}) - \nabla^2\boldsymbol{E} = -\nabla^2\mathbf{E}$ and, similarly, $\nabla \times \nabla \times \mathbf{B} = -\nabla^2\boldsymbol{B}$

$$\nabla^2 E = \varepsilon\mu \frac{\partial^2 E}{\partial t^2} \tag{3.18}$$

$$\nabla^2 B = \varepsilon\mu \frac{\partial^2 B}{\partial t^2} \tag{3.19}$$

Monochromatic waves may be described as waves that are characterized by a single frequency. Assuming the fields with harmonic time dependence $e^{-i\omega t}$, so that

$\boldsymbol{E}(x,t) = \boldsymbol{E}(x)e^{-i\omega t}$ and $\boldsymbol{B}(x,t) = \boldsymbol{B}(x)e^{-i\omega t}$ we get the Helmholtz wave equations.

$$\nabla^2 E + \varepsilon\mu\omega^2 E = 0 \tag{3.20}$$

$$\nabla^2 B + \varepsilon\mu\omega^2 B = 0 \tag{3.21}$$

3.2.3 Electromagnetic Wave Propagation through Vacuum

Suppose that the medium is a vacuum, so that $\varepsilon = \varepsilon_0$ and $\mu = \mu_0$, and suppose $\boldsymbol{E}(x)$ varies in only one dimension, say the z- direction then equations 3.20 becomes

$$\frac{d^2 E(Z)}{dz^2} + k^2 E(z) = 0 \tag{3.22}$$

where $k = {}^{\omega}/_{c}$. This equation is mathematically the same as the harmonic oscillator equation and has solutions

$$E_k(z) = E_0 e^{\pm ikz} \tag{3.23}$$

where ε is a constant vector. Therefore, the full solution is

$$E_k(z,t) = E_0 e^{\pm ikz - i\omega t} = E_0 e^{-i\omega\left(t + \frac{-z}{c}\right)} \tag{3.24}$$

This represents a sinusoidal wave travelling to the right or left in the z-direction with the speed of light c. Using the Fourier superposition theorem, we can construct a general solution of the form

$$\boldsymbol{E}_k(z,t) = \boldsymbol{F}(z - ct) + \boldsymbol{G}(z + ct) \tag{3.25}$$

3.2.4 Electromagnetic Wave Propagation through Soil

The propagation velocity v of the electromagnetic wave in soil is characterised by the dielectric permittivity ε and magnetic permeability μ of the medium:

$$v = \frac{1}{\sqrt{\varepsilon\mu}} = \frac{1}{\sqrt{\varepsilon_0 \varepsilon_r \mu_0 \mu_r}} \tag{3.26}$$

where $\varepsilon_0 = 8.854 \times 10^{-12}\mathrm{F/m}$ is the permittivity of free space, $\varepsilon_r = {}^{\varepsilon}/_{\varepsilon_0}$ is the relative permittivity (dielectric constant) of the medium, $\mu_0 = 4\pi \times 10^{-7}\mathrm{H/m}$ is the free space magnetic permeability, and $\mu_r = {}^{\mu}/_{\mu_0}$ is the relative magnetic permeability. In most soils, magnetic properties are negligible, yielding $\mu = \mu_0$, equation 3.26 becomes

$$v = \frac{c}{\sqrt{\varepsilon_r}} \tag{3.27}$$

where $c = 3 \times 10^8 \mathrm{m/s}$ is the speed of light. The EM wave propagation in one period of oscillation is known as the wavelength λ and is obtained by (Takahashi et al., 2012)

$$\lambda = \frac{v}{f} = \frac{2\pi}{\omega\sqrt{\varepsilon\mu}} \tag{3.28}$$

where f is the frequency and $\omega = 2\pi f$ is the angular frequency.

In general, dielectric permittivity ε and electric conductivity σ are complex and can be expressed as

$$\varepsilon = \varepsilon' - i\varepsilon'' \tag{3.29}$$

$$\sigma = \sigma - i\sigma'' \tag{3.30}$$

where ε' represents the dielectric polarisation term, ε'' depicts the energy loss due to the polarisation lag, σ' depicts the ohmic conduction, and σ'' is stands for the faradaic diffusion (Knight and Endres, 2005). A complex effective permittivity expresses the overall loss and storage effects of the material as a whole (Cassidy, 2009):

$$\varepsilon^e = \left(\varepsilon' + \frac{\sigma''}{\omega}\right) - i\left(\varepsilon'' + \frac{\sigma'}{\omega}\right) \tag{3.31}$$

The ratio of the imaginary and real parts of the complex permittivity is defined as $\tan\delta$ (loss tangent):

$$\tan\delta = \frac{\varepsilon''}{\varepsilon'} \cong \frac{\sigma'}{\omega\varepsilon'} \tag{3.32}$$

where ε'' and σ'' are small, it is approximated as the correct expression. In Maxwell's equations plane wave solution, the electric field $\boldsymbol{E}$ of an EM wave that is travelling in z - direction is expressed as

$$E(z,t) = E_0 e^{i(\omega t - kz)} \tag{3.33}$$

where E_0 is the peak signal amplitude and $k = \omega\sqrt{\varepsilon\mu}$ is the wave number, which is complex if the medium is conductive, and it can be separated into real and imaginary parts:

$$k = \alpha + i\beta \tag{3.34}$$

The real α and imaginary β parts are respectively called the attenuation constant (Np/m) and phase constant (rad / m) and are given as:

$$\alpha = \omega\left[\frac{\varepsilon'\mu}{2}\left(\sqrt{1+\tan^2\delta}-1\right)\right]^{1/2} \tag{3.35}$$

$$\beta = \omega\left[\frac{\varepsilon'\mu}{2}\left(\sqrt{1+\tan^2\delta}+1\right)\right]^{1/2} \tag{3.36}$$

The attenuation constant is also expressed in dB/m by $\alpha' = 8.686\alpha$. The inverse of the attenuation constant is known as the skin depth:

$$\delta = \frac{1}{\alpha} \tag{3.37}$$

It is also a useful parameter to describe how lossy the medium is and also how EM wave decays inside a material. Table 3.1 provides the typical range of permittivity, conductivity and attenuation of various materials.

Table 3.1. Dielectric characteristic ranges of various materials measured at 100 MHz (Daniels,2004; Cassidy, 2009)

Material	Relative Permittivity	Conductivity S/m	Attenuation constant dB/m
Air	**1**	0	0
Fresh water	81	10^{-6}-10^{-2}	0.01
Clay, dry	2-6	10^{-3}-10^{-1}	10-50
Clay, wet	5-40	10^{-1}-10^{-0}	20-100
Sand, dry	2-6	10^{-7}-10^{-3}	0.01-1
Sand, wet	10-30	10^{-3}-10^{-2}	0.5-5

3.3 Reflection and Transmission of GPR Waves

GPR normally measures signals of reflected or scattered EM waves from the difference in the electric properties of geologic structures (Takahashi et al., 2012.).

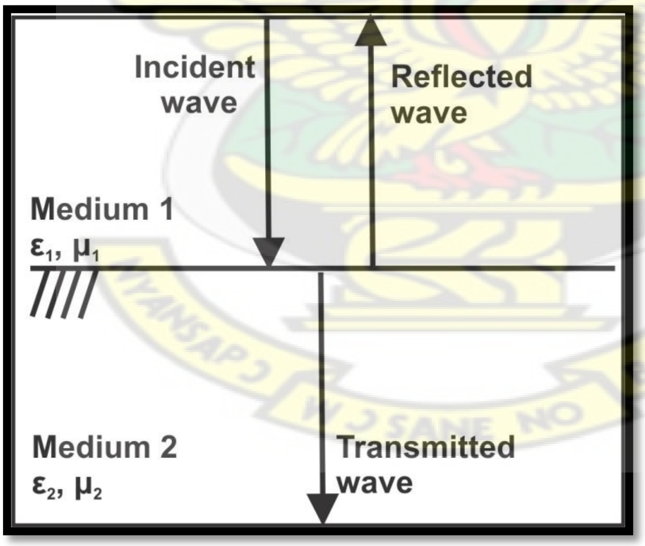

Figure 3.3: Reflection and transmission of an incident EM wave normal to a planar interface between two media

When EM waves strike a planar interface, part of the energy is reflected at the interface and the rest is transmitted into the second medium (Fig 3.3). The transmitted, incident and reflected energies are related as follow:

$$E^i = E^r + E^t \tag{3.38}$$

$$E^r = \rho \cdot E^i \tag{3.39}$$

$$E^t = \tau \cdot E^i \tag{3.40}$$

where ρ and τ are reflection and transmission coefficients respectively.

$$\rho = \frac{\eta_2 - \eta_1}{\eta_1 + \eta_2} \tag{3.41}$$

$$\tau = 1 - R = \frac{2\eta_2}{\eta_1 + \eta_2} \tag{3.42}$$

Where η_1 and η_2 are the intrinsic impedances of medium 1 and medium 2 respectively (Daniels, 2004)

$$\tau \cong \frac{\sqrt{\varepsilon_{r1}} - \sqrt{\varepsilon_{r2}}}{\sqrt{\varepsilon_{r1}} + \sqrt{\varepsilon_{r2}}} \tag{3.43}$$

3.4 GPR Signal Velocity and Depth Determination

The ability of GPR to image below the surface depends on three main factors (Moorman, 2001)

a. the number of interfaces that generate reflections and the dielectric contrast at each interface: When a GPR signal arrives at a particular interface, a portion of the signal is reflected to the surface while the rest continues through the interfaces. When this happens, the proportion of energy that propagates to these interfaces at their various depths reduces as the interfaces increase. Moreover, at each interface, a greater proportion of energy is reflected back to the surface leaving just a small proportion of the energy to propagate deeper into the ground. In sediment, localized dielectric contrasts can create chaotic reflections. This limits the depth of investigation because the reflections of interest get masked by the clutter of the chaotic returns.

b. the rate at which the signal is attenuated as it travels through the subsurface: Conductivity of the area where the GPR signal propagates has a major influence on the depth to which the signal will propagate. As the conductivity increases, the medium of propagation acts more like a conductor which generates conductive current in the medium. These conductive currents are an energy dissipating mechanism for an EM field. This extracts energy from the EM field and it is transferred to the medium it propagates. Figure 3.4 illustrates the impact conductivity has on the potential depth of penetration

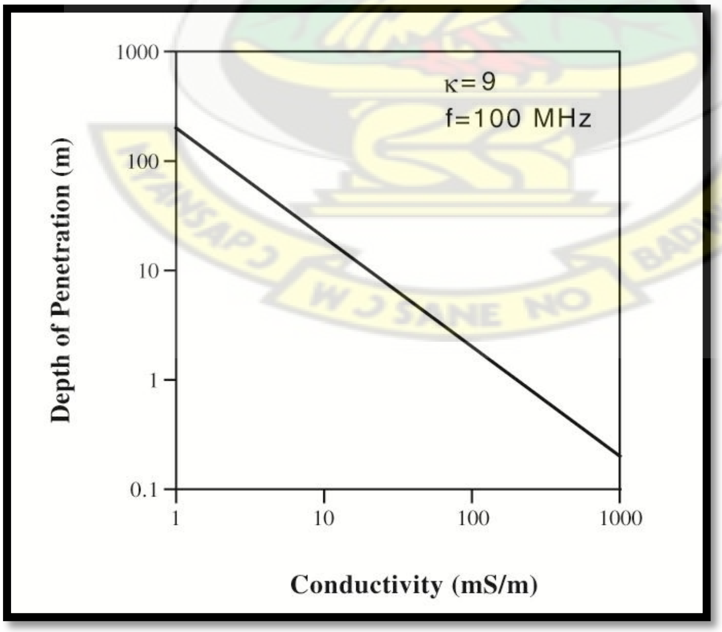

Figure 3.4: Impact of conductivity on depth of penetration (Moorman 2001)

c. the center frequency of the antennas: The frequency used is very important since the rate of signal attenuation and the resolution of the system is proportional to the frequency of the GPR system (Fig. 3.5). A lower frequency antenna produces a longer wavelength and as a result attenuation is less due to conductive losses and less scattering from the chaotic reflections. However using very low frequencies decrease resolution such that the thickness of small layers may not be measured and small objects are not detected. Practically, as the frequency decreases, the antenna lengths increase in size and become more difficult to work with

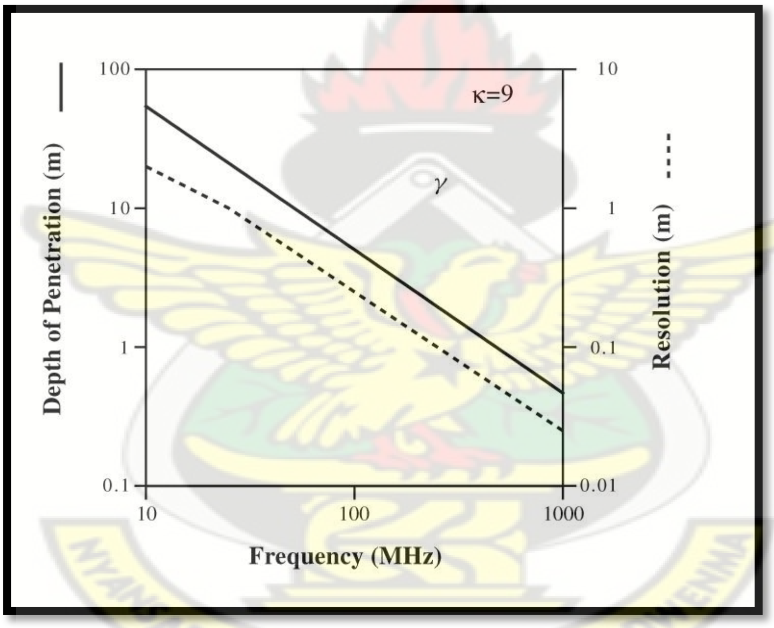

Figure 3.5: depth of penetration and resolution of frequency selection for a survey (Moorman 2001)

3.5 Feature Detection and Resolution

According to Moorman J. (2001), the three major factors that determine where an object or a thin layer of material is detectable are the object size or layer thickness, the frequency of the GPR system, and the velocity of propagation in the medium. Higher frequency antennas generate shorter waves and thus have finer resolution and can detect smaller objects. The velocity of propagation in the medium is critical in the sense that the size of the wavelet in the subsurface is not only influenced by the frequency of the antenna that created it, but also the velocity at which it propagates through the subsurface.

The vertical resolution achievable by the GPR is greatly determined by the signal wavelength which in turn is affected by the materials dielectric properties, with higher frequency signals having better resolution. The vertical resolution achievable by GPR is generally taken to be between one-half $\left(\frac{\lambda}{2}\right)$ to one quarter $\left(\frac{\lambda}{4}\right)$ of the signal wavelength (Martinez and Byrnes, 2001, Sheriff and Geldart, 1982).

The minimum distance that GPR can identify between two features at the same depth separated horizontally is known as the horizontal resolution of the GPR. When two features are spaced closer than the horizontal resolution, they appear on GPR data as one single feature. GPR horizontal resolution is influenced by factors such as the number of traces (and number of scans) per meter and the geometry of the EM radiation pattern which results in the size of the 'Fresnel zone' or antenna 'footprint' at a given depth (Daniels, 2004).

The size of the wavelets which are recorded on a GPR profile is a function of the pulse width of the original transmitted pulse. The pulse width which is produced by the 50 MHz and 100 MHz antennae and the resultant maximum theoretical resolution in various geologic materials is presented in Table 3.2.

Table 3.2: Pulse width and theoretical resolution of 50 MHz and 100 MHz GPR antennas with a bandwidth to frequency ratio of 1. (Annan, 1992; Davis & Annan, 1989; Ulriksen, 1982)

Material	50 MHz		100 MHz	
	Pulse width (m)	Theoretical Resolution (m)	Pulse width (m)	Theoretical Resolution (m)
water	0.66	0.16	0.33	0.08
Ice	3.2	0.8	1.6	0.4
Saturated sand	1.2	0.3	0.6	0.15
Saturated clay	2.0	0.5	1.0	0.25
Limestone	2.4	0.6	1.2	0.3
Shale	2.0	0.5	1.0	0.25
Granite	2.6	0.66	1.3	0.33

The horizontal resolution is related to the spacing between traces and the footprint of the radar pulse. In a lake survey, for example, the footprint represents the area over which the pulse of the GPR is reflected from the bottom of the lake. The size of the footprint is determined by the wavelength, radiation pattern and water depth. For common dipole antennas, Annan (1992) provides a way to estimate the footprint using:

$$A = \frac{\lambda}{2} + \frac{d}{\sqrt{k-1}} \qquad (3.44)$$

where A represents the long axis diameter of the oval footprint, d represents the distance (or depth), and k in this instance represents the dielectric constant of the medium (80 for water). The short axis of the oval foot print is roughly half the length of the long axis. For example, at 20 m depth, in water, the effective footprint of a 50 MHz pulse has a mean diameter of approximately 10 m. This is quite smaller than the footprint of an acoustic sub bottom profiler (Sellmann et al., 1992).

3.6 GPR Surveys

According to Annan (2009), GPR surveys are categorized into reflection and transillumination measurements. Measurement of reflections normally uses configurations known as the common offset and common midpoint. Antennas placed on the ground have propagation paths both in and above the ground, as shown in Fig. 3.6. Transillumination measurements are often carried out using antennas installed into drilled wells or trenches.

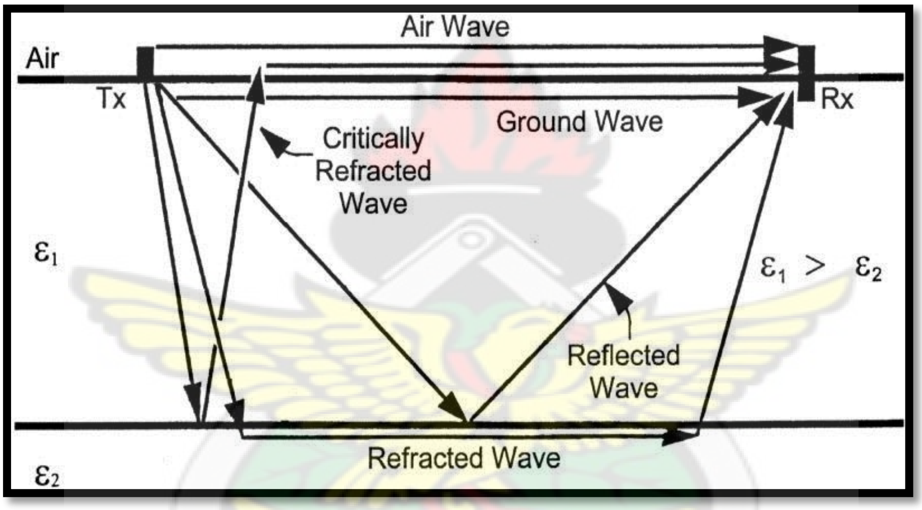

Figure 3.6: Travel paths of EM waves for a surface GPR survey.

3.6.1 Common Offset Survey

Common-offset surveys normally have both the transmitting antenna and receiving antenna placed at a fixed spacing. The transmitting and receiving antennas scan the survey area while keeping a constant space and acquiring the data at each measurement location, as shown in Fig. 3.7. For a single survey line, the acquired GPR data corresponds to a 2D reflectivity map of the subsurface below the scanning line called a radar record or radargram. By setting multiple parallel lines, 3D data can be obtained and horizontal slices and 3D maps can be constructed.

The parameters defining a common-offset survey are GPR center frequency, the recording time window, the time sampling interval, the station spacing, the antenna spacing, the line separation spacing, and the antenna orientation (Harry, 2009).

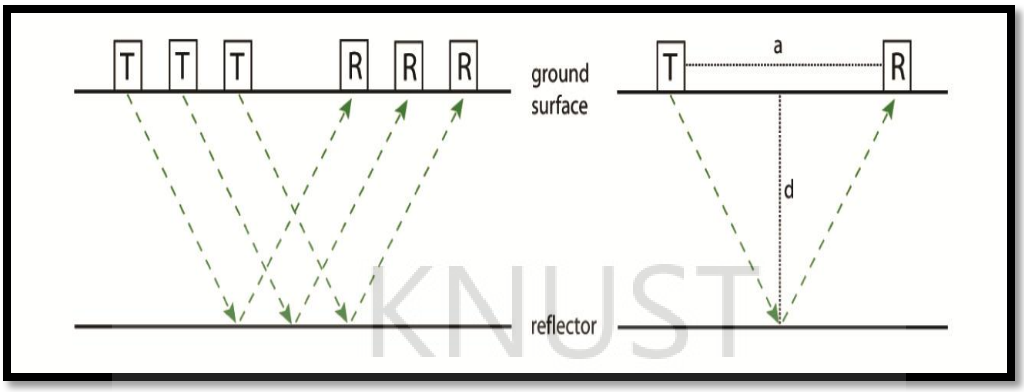

Figure 3.7: Common Offset Survey

From the measured travel time t of the reflected electromagnetic signal, the depth d of a reflector can be determined (Fig 3.7) from,

$$s = 2\left(\sqrt{d^2 + \left(\frac{a}{2}\right)^2}\right) = \sqrt{4d^2 + a^2} \qquad (3.45)$$

where a is the distance between transmitting and receiving antennas and s is the distance from the transmitting antenna to the reflector and to the receiving antenna

3.6.2 Common Midpoint Survey

Common midpoint survey CMP normally employs a separate transmitting and receiving antennas which are placed on the ground. In the CMP survey, the center position of the antennas remains constant while the separation between the antennas is varied. For a layered subsurface structure with varying separation, various signal paths with the same point of reflections can be obtained and the data can be used to determine the velocity distribution versus subsurface depth of the radar signal (Annan, 2005; Annan, 2009). A Schematic CMP survey configuration is illustrated in Fig. 3.8. With the transmitting antenna fixed instead of being moved from the midpoint together with the receiving antenna, and if only the receiving antenna is moved away from the transmitting antenna, the setup is known as a wide-angle reflection and refraction (WARR) gather.

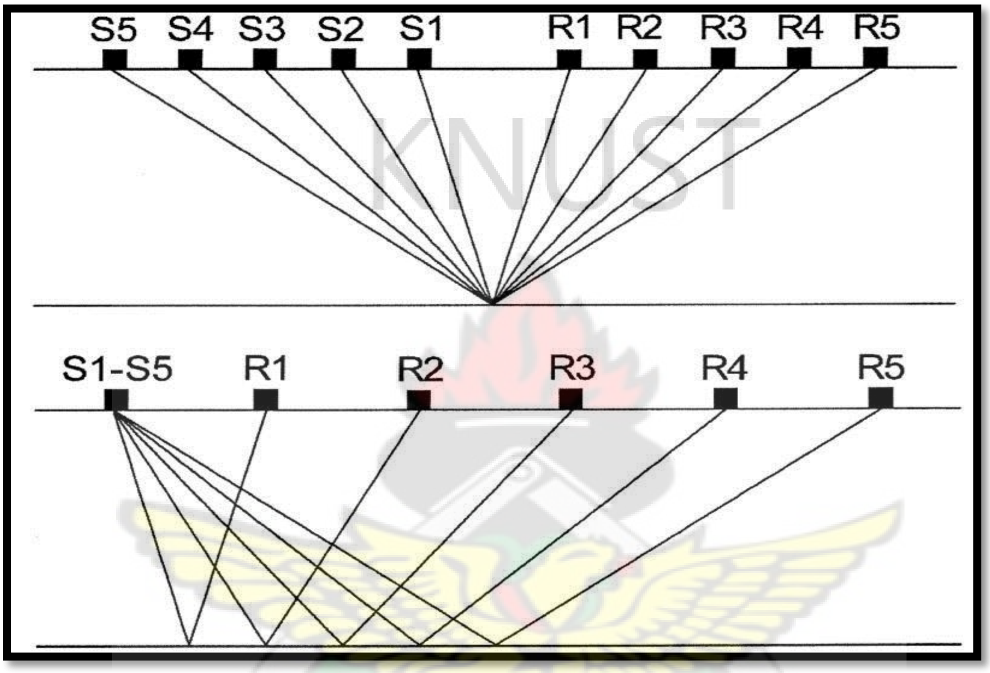

Figure 3.8: Schematic illustration of common-midpoint (top) and wide angle reflection and refraction (down) surveys. S and R indicate transmitter and receiver antennas respectively

3.6.3 Transillumination Measurements

Zero-offset profiling (ZOP) employs a configuration whereby the transmitting and receiving antennas are moved in two parallel boreholes at a constant distance. (Fig.3.9, left), resulting in parallel ray paths especially when the subsurface medium is homogenous. This configuration is a simple and quick way in locating anomalies.

Transillumination multi-offset gather surveys are the basis of tomographic imaging. The survey measures transmission signals through the volume between boreholes with varying angles (Fig.3.9, right). Tomographic image derived from the survey data is capable of providing the distribution of dielectric distribution of dielectric properties of measured volume.

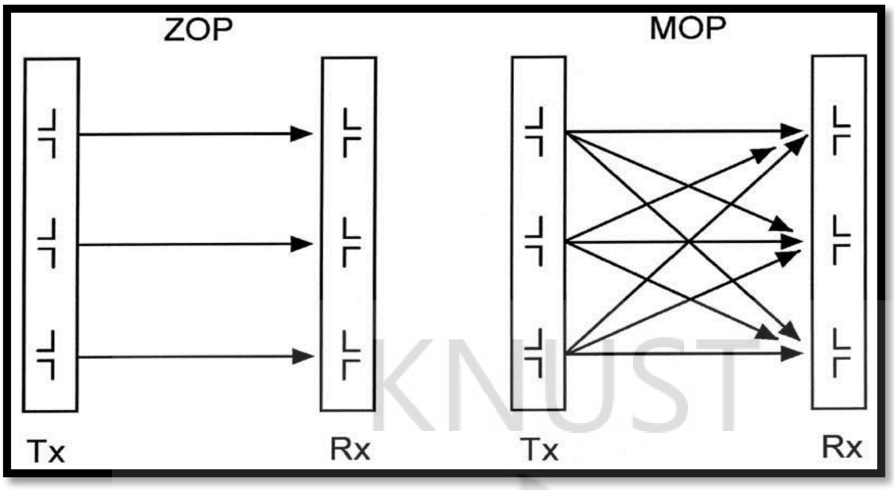

Figure 3.9: Schematic illustration of transillumination zero-offset profiling (left) and transillumination multi-offset gather (right) configurations

3.7 Dielectric Permittivity

According to Takahashi et al., (2012), material's ability to store and discharge electric charge describes the permittivity of the material. This is classically related to the storage ability of capacitors (Cassidy, 2009). Intrinsic impedance, reflectivity and velocity of an EM wave are greatly influenced by Permittivity. Dielectric permittivity in natural soils has a larger influence than magnetic permeability and electric conductivity (Lampe & Holliger, 2003; Takahashi et al., 2012).

Soil may be seen as a three-phase composite where the soil matrix and the pore spaces are filled with water and air. The water in the pore of soil is divided into free and bound water where the mobility is restricted by absorption to the soil matrix surface. The relative permittivity of air is 1 and that of common minerals in soils and rocks is between 1 and 2.7 (Ulaby et al., 1986). That of water is 80 and this value depends on the temperature. Thus, the permittivity of water-bearing soil is largely affected by its water content (Robinson et al., 2003). Hence, by analyzing the dielectric permittivity of soil that is measured and monitored with GPR, it is possible to determinate the water content of the soil.

Water plays a vital role in the determination of the dielectric characteristic of soils. The frequency-dependent dielectric permittivity of water influences the permittivity of soil. GPR frequency range dependence is caused by polarization of the dipole water molecule, which leads to relaxation. A straight forward model that describes the relaxation time τ is related to the relaxation frequency $f_{relax} = {}^{1}/_{(2\pi\tau)}$. From this model, the real component of permittivity ε' and imaginary component ε'' are given by

$$\varepsilon'(\omega) = \varepsilon_\infty + \frac{\varepsilon_s - \varepsilon_\infty}{1+\omega^2\tau^2} \tag{3.46}$$

$$\varepsilon''(\omega) = \omega\tau\left(\frac{\varepsilon_s - \varepsilon_\infty}{1+\omega^2\tau^2}\right) \tag{3.47}$$

Where ε_s is the static (DC) value of the permittivity and ε_∞ is the optical or very-high frequency value of the permittivity. Pure free water at room temperature (at 25℃) has a relaxation time $\tau = 8.27$ ps (Kaatze, 1989), which corresponds to a relaxation frequency of approximately 19 GHz. In view of this, free water losses will only begin to have a significant effect with high-frequency surveys (i.e. above 500 MHz; Cassidy, 2009). Various mixing models provide the dielectric permittivity of soil. One of the most popular models is an empirical model called Topp's equation (Topp et al., 1980), which describes the relationship between relative permittivity ε_r and volumetric water content θ_v of soil:

$$\varepsilon_r = 3.03 + 9.3\theta_v + 146\theta_v^2 - 76.6\theta_v^3 \tag{3.48}$$

$$\theta_v = -5.3 \times 10^{-2} + 2.92 \times 10^{-2}\varepsilon_r - 5.5 \times 10^{-4}\varepsilon_r^2 + 4.3 \times 10^{-6}\varepsilon_r^3 \quad (3.49)$$

The model is often seen as inappropriate for organic soils and clays, but it agrees generally well for sandy and loamy soils over a wide range of water contents (5-50%) in the GPR frequency range between10 MHz and1 GHz. The model does not account for the imaginary component of permittivity (Takahashi et al., 2012).

3.7.1 The Relative Dielectric Permittivity of Soil

According to Ludwig et al., (2011), soil can be considered as a three phase medium consisting of the soil matrix, air and water. Therefore knowledge of the permittivity of each constituent and then the mixture is paramount. Since the permittivity is determined by measuring the wave propagation velocity, equation 3.28 is considered. Because the relative permittivity of air ($\varepsilon_{air} \approx 1$) and the soil matrix ($\varepsilon_{matrix} \approx 4 - 5$), Ludwig et al., (2011), can be considered as constant values and more emphasis will be put on the relative permittivity of water and that of the mixture.

3.7.2 The Relative Permittivity of Water

Each molecule of water can be considered as polar which can be oriented according to an incoming electromagnetic field. This orientation of the molecules depends on the frequency of the incoming field. Hence three cases have to be distinguished (Ludwig et al., 2011)

i. For a very high frequency, the molecules cannot store electromagnetic energy since they cannot flow. This results in a smaller value of the relative permittivity of water.

ii. For a very slow frequency relative to the time of orientation of each molecule, the polarization of the water can reach its maximum, which results in the highest number of the relative permittivity value.

iii. For the frequency between the above limits, the molecules can follow partially the alternating electromagnetic fields. Therefore, electromagnetic energy is needed to orientate the molecules. This energy is either re-emitted or transformed into thermal energy.

This phenomenon is called relaxation process, because the reemission is not instantaneous. Furthermore, it is coupled with absorption of the EM waves. The frequency at which the energy is absorbed is called relaxation frequency.

The ability of water molecules to be polarized as well as the relaxation process and the absorption of electromagnetic energy is a function of temperature. For frequencies below 1 GHz, the dielectric permittivity of water may be assumed to be frequency independent and the imaginary part can be neglected, Gerhards (2008). Including temperature, the dielectric permittivity ε, can be described as a function of temperature according to Kaatze (1989) as

$$\log_{10} \varepsilon_{water} = 1.94404 - 1.991 \times 10^{-3} K^{-1} (T - 273.15K) \quad (3.50)$$

where T is temperature in Kelvin

3.8 Electrical Conductivity

The electrical conductivity(σ) of a material describes the flow of electrical charges during the passage of an EM wave, and can greatly affect the energy loss or attenuation of the EM signal. Conductivity, as well as signal frequency, is one of the main influences on signal attenuation, which in turn governs signal penetration depth. A high conductivity will generally attenuate GPR signals rapidly. Factors that increase conductivity include a high amount of salts present in water in the material, and the presence of clay minerals because of the molecular ionic structure particular to clays that have high levels of exchangeable cations.

Hence, the presence of water and clay minerals can reduce the effective penetration depth of a GPR survey (Evans, 2009).

3.9 Magnetic Permeability

Where EM sources are used, the voltage induced into a buried conductor varies with the rate of change of magnetic field and also with the magnetic permeability of the conductor. From Maxwell's equation $\nabla \times E = -\mu \frac{\partial H}{\partial t}$, currents induced in the ground are enhanced by the factor μ. Practically, however, the permeability rarely is appreciably greater than unity, except for a few magnetic minerals; consequently it is of no particular significance in electrical work, except when Fe_2O_3 is present in large concentration (Telford et al., 1976).

CHAPTER 4

MATERIALS AND METHODS

4.1 Site Description

The site for the project is the Agriculture Research Station (ARS) which is located at Anwomaso, a suburb of Kumasi in the Ashanti region of Ghana. It is under the faculty of Agricultural Science in the College of Agriculture and Natural Resources of the Kwame Nkrumah University of Science and Technology (KNUST).The ARS is located on latitude 6^{o} 41' 838" N and longitude 1^{o}31'533" W (Fig 2.2). The activities of the station include research, plant development and arable crop production, extension and community services, forage and weed museum establishment and so on. It is about 10 km from the KNUST campus and includes approximately 554.492 hectares of extensive arable land suitable for livestock and crop production. Less than 10% of the total land area is developed into the station's oil palm plantations where the data for the project was taken. The area is generally topographically flat.

The oil palm trees are arranged in rows with a tree to tree spacing of 9 m. As a result of the already established tree arrangement, the space between three successive trees was used as the profile line during data collection. Based on this, the inter-profile spacing was 18 m. The density of the oil palm plantation is 50 trees per hectare.

4.2 Field Reconnaissance

Field reconnaissance survey was carried out on 15^{th} January 2014 to gather initial information regarding the manner to acquire the data for the research work. It was discovered that the RTA snake like antenna was the preferred choice because of the bushy and dense vegetation cover at the site. This would have made it difficult to for measurement to have been taken. Accessibility played a major role in the field work for which the profile length and number of profiles were determined during the period of the reconnaissance survey.

One significant discovery was the fact that a borehole that was drilled some years back did not contain water as at the time of the reconnaissance survey. According to workers, the well got dried some few months after completion. This revelation was very paramount in determining some of the objectives of this project.

4.3 Description of the GPR equipment

The RAMAC GPR system made by the MALA Company Sweden of was employed in this research work. The system comprises the MALA ProEx control unit, the XV monitor and the antenna unit. The XV monitor is powered by a 12 V standard Li-Ion rechargeable batteries which operates for six hours when used continuously. Operating temperature for the equipment is between $-20°C$ to$+50°C$. Specifically for this research work, the MALA Rough Terrain 25 MHz frequency Antenna (RTA) was used (Fig 4.1). The RTA contains the transmitter and receiver electronics as well as their antennas which are 6.2 m apart, within a rugged yet flexible tube. The advantages of dragging the flexible MALA RTA along a survey line allows for perfect ground coupling, as well as the ability to access nearly any environment or terrain and achieve finer spacing between radar readings at much higher speeds than conventional systems. The system allows the entire GPR system to be towed by a single survey.

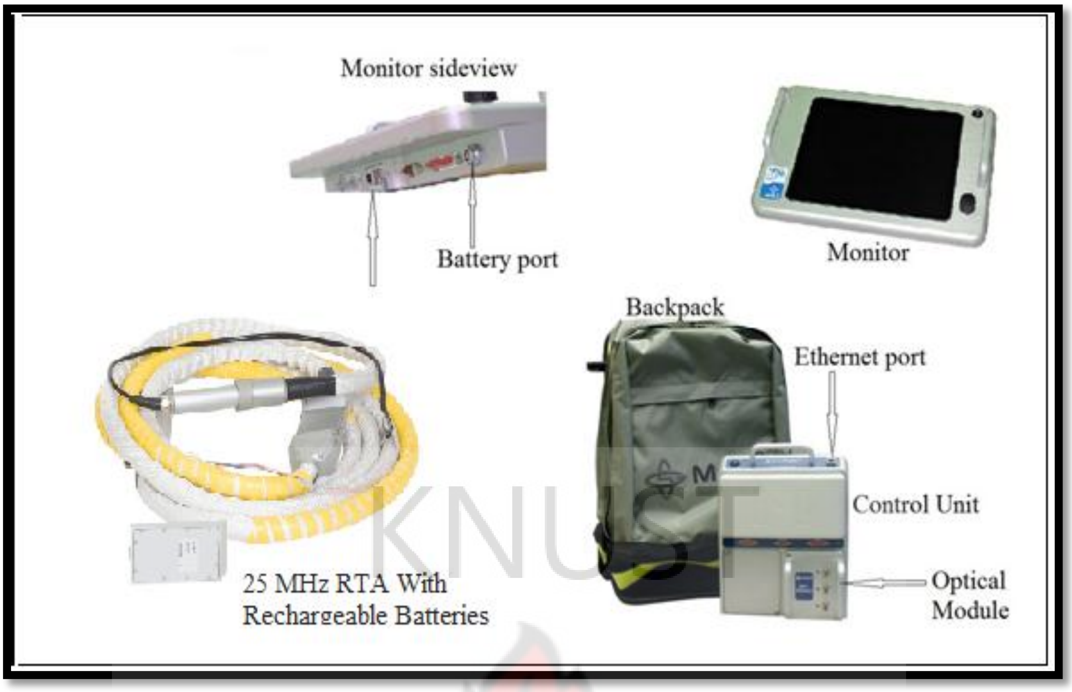

Figure 4.1: MALA GPR equipment

4.4 Operation of the GPR equipment

As shown in figure 4.1, the MALA GPR equipment comprises basically three main components which are the control unit, antennas, and monitor or display module.

Parameters for the survey are received from the interface which then generates timing signal for the transmitting and receiving antennas. This is done by the control unit. The control unit receives the data from the receiving antenna which quickly initiates processing before transmitting the data for storage. For other systems, the control and display units as well as the storage medium and interface are merged in one system. However, the control unit may be separated in other systems and a palmtop or laptop computer may be employed to enter the survey parameters, store the data and display the data.

When a command is issued on the control unit, the transmitting antenna generates the EM pulse which is emitted through an antenna connected to it. The transmitting antenna pair is able to determine the bandwidth and center frequency and of the signal that is sent into the ground. An antenna identical to that attached to the transmitter is attached to the receiver. This receiving antenna receives reflected energy which is then transmitted to the receiving antenna where amplification and digitization take place and sent to the control unit. The captured wave is recorded on a digital storage device for later interpretation. The time against received energy graph is known as a trace. Data are collected frequently at intervals along a profile, so that the traces can be plotted side by side which creates a pseudo-section through the ground (Leucci, 2012)

4.4.1 Data Acquisition

Data for the project was collected in January 2014. In all, thirty five profiles with different profile lengths were traversed. The difference in profile length was primarily as a result of accessibility. The smallest and longest profile lengths were 130 m and 500 m respectively with the average being 348 m and inter-profile spacing of 18 m. Fig. 4.2 is a schematic layout of the profiles.

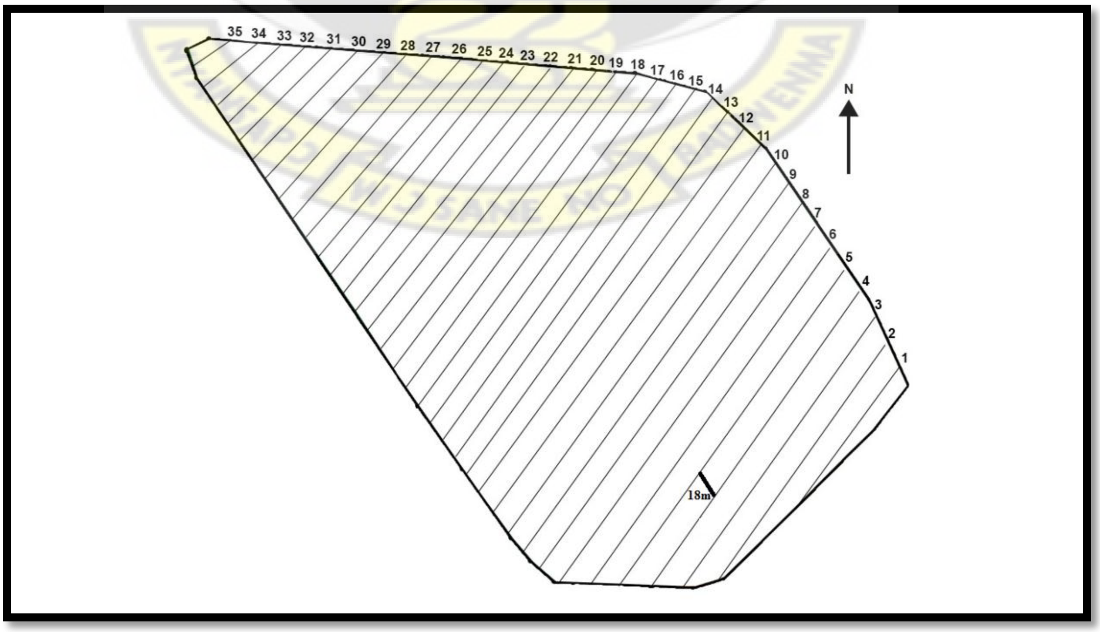

Figure 4.2: Profile lines and profile numbers at project site

Data were acquired using the Mala ProEx GPR recording unit which is owned by the Department of Physics, KNUST with 25 MHz RTA using common offset technique. For full operation of the components of the equipment, a 12 V battery was used to power the monitor which was then connected to the control unit through fibre optic cables. The 25 MHz RTA was also powered with in-line rechargeable batteries contained in battery housing protectors and a removable skid to solidly protect the cables in the RTA. The RTA was then connected to the control unit by wired cables.

On pressing the power button, a beep is heard and the light emitting diodes (LED's) on the control unit began to blink indicating a well-established connection between the various components of the equipment.

The survey parameters for this project were carefully selected to obtain optimum results. The time window which defines the total trace lengths of the electromagnetic wave transmitting time was chosen as 1016.0 ns (53.81 m, 560 smp). The velocity was set at 100 m/μs and this parameter determined the speed of propagation of the measured EM wave in the ground. A 1.0 s sampling interval time with a sampling frequency of 521.64 MHz was used.

The acquisition mode which determines how the measurements were to be gathered was set at the time triggering mode. Stacking was set at the 'auto stack' mode and the maximum time window medium was selected. The control unit was then held in position in a pack bag which was worn at the back (Fig 4.2B) with the monitor fixed in front for easy viewing (Fig 4.2A). The RTA was towed continuously over the ground during measurement (Fig 4.2C and D). This moving mode arrangement kept the transmitter and receiver antennas at a fixed distance with the antenna pair moved along the surface by pulling them by hand (Allred et al., 2008.)

Figure 4.2:A and B Showing GPR monitor and control unit in use, C and D showing complete set-up of equipment for data collection

The flexible “snake” like design in the form of a long tube allowed the antenna to be manoeuvred easily and efficiently through the dense vegetation of the project site without affecting ground contact. The most important benefit was that it was not necessary to clear the profile route prior to the survey (Daniels 2004; Mala 2010).

Figure 4.3: Data collection in the field

4.5 GPR Data processing and Presentation

Processing and display are an integral part of being able to effectively interpret GPR data. GPR data can rarely be interpreted thoroughly without some form of processing. This is done to improve the resolution of coherent signals that represent the targets, and a display that enables the interpreter to easily identify the anomalies that identify the time–space location of the targets. Processing and display can be conducted in the field, but in many cases, it is more convenient to process and display data at a later time in the office or laboratory (Allred et al., 2008.)

GPR data are recorded digitally and need extensive processing. Most GPR data analysis requires some conditioning of the raw recorded pulses before construction of images from closely spaced profiles is implemented. The use of specialized filters to enhance and adjust digitized data as well as noises in the raw data is achieved by

Radargram Signal Processing (RSP). What signal processes are needed will depend on a variety of factors observed in the raw data. There are a variety of RSP that are essential and some are only used if certain noises are found to exist in the data.

The REFLEXW software, which is a program package for the processing of reflection and transmission data, was used for the RSP.

The basic processing steps used before the GPR data became ready for interpretation were as follows:

1. In the first step the data was edited in order to correct mistakes in the fields. The end direction of every profile was selected as the start of a new profile during measurement and as a result; profile direction was maintained during processing.
2. Background removal filter (subtract average trace to remove banding) was the next processing step. Background noise is a signal that repeats itself and it is created by slight ringing in the antennae, which produces a coherent banding effect, parallel to the surface wave, across the section (Conyers and Goodman, 1997). The filter involved a simple arithmetic process that summed all the amplitudes of reflections that were recorded at the same time along a profile. The time window where the filter operated was specified so that the filter was not applied until after the surface wave.
3. The next processing step was the filtering out wow noises or the elimination of the possible low frequency part. This is called dewowing (subtract mean).The filter acted on each trace independently. With this option activated, a running mean value was calculated for each value of each trace. This running mean was subtracted from the central point.

4. Zero-time adjustment (static shift) was performed after the data was ‘dewowed’. During GPR surveys, the first waveform to arrive at the receiver is the air wave. Time of arrival of the first break of the air wave on the radar section arrives late due to the length of the cable connecting the antennae and the control unit. Therefore the zero-time was associated to the zero-depth so that time offset due to instrument recording was removed. After activating the option ‘static correction’ on the REFLEXW processing software, a table with the parameters distance and time appeared which made it possible for interactive input of the static correction values.
5. Topographic correction was finally done to determine how the land’s topography behaves with respect of the surface geometry.

It is worth mentioning that other processing parameters, though not applied here, can be used depending on the objective behind a particular project as well as the target of interest such as migration and deconvolution.

Migration is a processing technique which attempts to correct for the fact that energy in the GPR profile image is not necessarily correctly associated with depths below the 2-D survey line (Leucci, 2012). According to Goodman and Piro (2013), most GPR antennas transmit a broad beam of microwave energy into the ground. The net effect of having a broad beam in the ground is to cause hyperbolic reflections being recorded from round objects in the ground. Objects that are not directly beneath the antenna get recorded as microwaves and are sent over a broad range of angles. The travel times however from objects that are recorded off to the side of an antenna take progressively longer travel times the further they are from being directly beneath the antenna.

Deconvolution which is a signal processing method can be applied to help reduce multiple reflections and echoes recorded on radargrams as well as to minimize the effects of the transmitted pulse. The pulses that are transmitted by GPR antenna have a defined impulse response function. One kind of deconvolution filter is designed to remove the transmitted impulse response function from the recorded radargram.

The water table depth map was constructed using the Pitney Bowes Geographic Information System (GIS) software called MapInfo Professional; version 11.5. Various points were located on every profile using a Global Position System (GPS) which were then fed into the aforementioned software for geo-referencing. The geo-referenced points were later fed into another processing software called ArGIS and the maps in this project were generated (Fig 5.11 and Appendix B).

CHAPTER 5

RESULTS AND DISCUSSIONS

5.1 Introduction

This chapter displays the radar records for some selected profiles in the survey area and it is intended to give a visual display of water table depths for every location at the project site. The rest of the radar records are displayed in Appendix A. Other noticeable dipping and hyperbolic reflections revealed on the radar records were also identified and interpreted based on their estimated velocities.

5.2 Estimated Water Table Depths

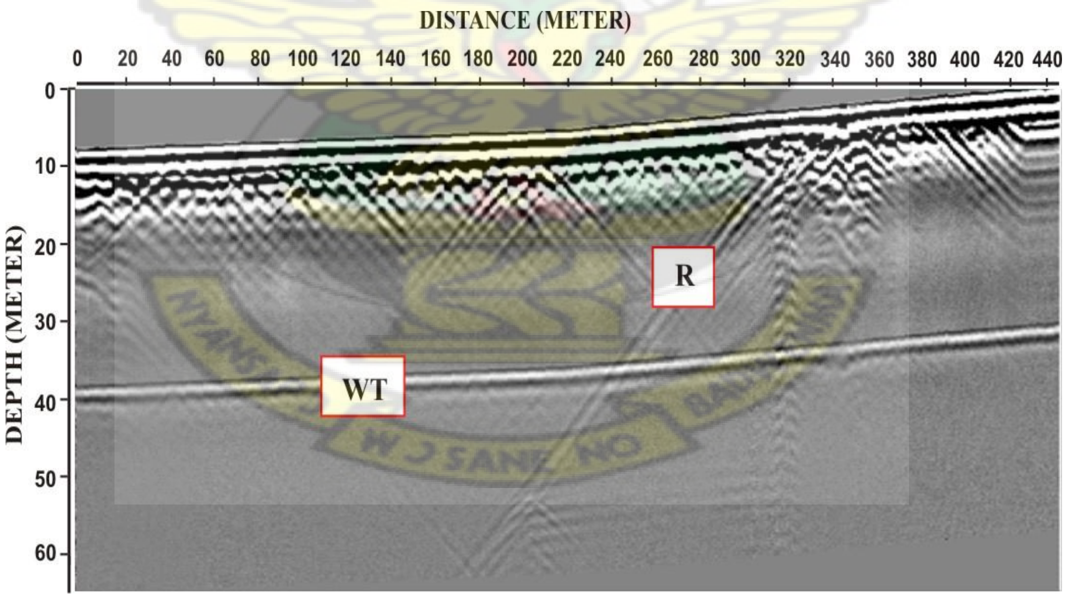

Figure 5.1 Radar record for profile 1

Figure 5.1 displays the radar record for profile 1. The length of the profile is 440 m. The unique continuous reflection signature shown on the radar record was interpreted to be the water table (WT). This is because water table provides continuous and high amplitude reflections across radar records and appears as series of uninterrupted bands making it distinct from other reflections.

As revealed, the depth of the water table ranges between 39.2 m from the beginning and decreases to about 31.1 m at the end as revealed on the radar records. This was because topographic correction was factored into the processing of the data. Topographic correction was applied to better explain the behaviour and nature of the water table. The average depth to the water table from the land surface was assumed to be equal to the vertical thickness of the unsaturated zone or the vadose zone which was estimated to be 30.9 m. This thickness was interpreted to be the average depth of the water table from the land surface for this profile. As depicted on the radar record, the water table follows a similar pattern as the geometry or topography of the land. Water bearing indicator rock at this depth is assumed to be permeable, hence ground water is able to move through and form zones of saturation. Also revealed on the radar record is a dipping reflector marked R. A velocity check of the radar signal of this reflector suggested that the reflection was from outside environment rather than the subsurface; hence has no geological significance.

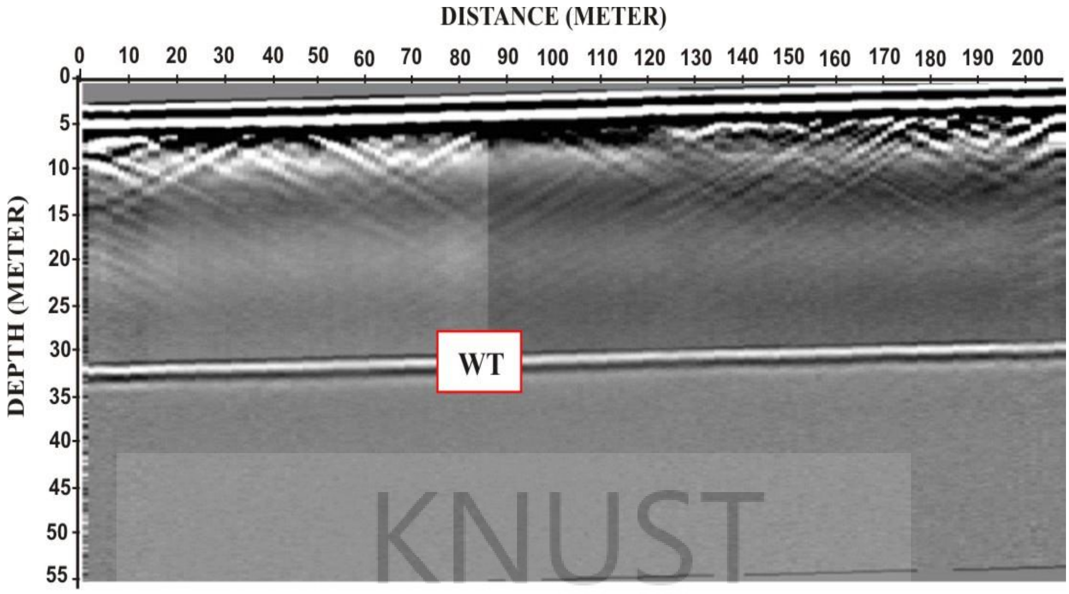

Figure 5.2: Radar record for profile 2

Figure 5.2 is a radar record of the profile 2 and has a profile length of 218 m. The continuous reflections marked WT represents the water table. As a result of the topography of the land, the water table was revealed at depth from 38.1 m from the beginning and decreases steadily to 32.5 m at the end as revealed in figure 5.2. Top soil reflections also began to appear at depth between 4.5 m from the beginning and 1.6 m at the end as a result of the slopping nature of the land. The reflections from the top soil become evidence after zero-time adjustment is applied during the processing of the data. Air waves are first to be recorded by the receiving antenna during measurement and this may be misconstrued as coming from the top soil. Therefore the estimated depth of the water table from the land surface for this profile was 30.2 m. The saturated zone is located beneath this depth and a possible location of the aquifer. A strong relation exists between the topography of the area and the water table.

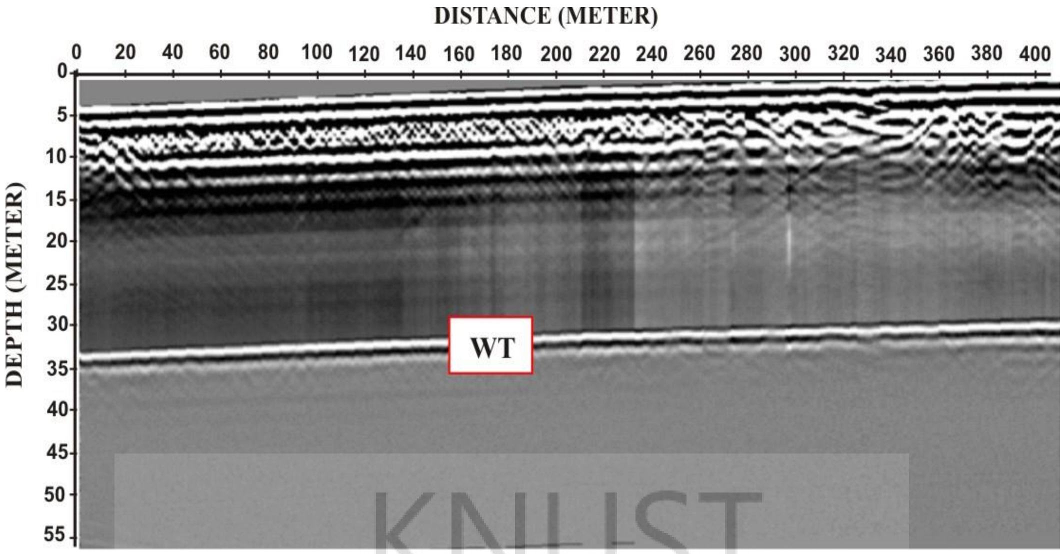

Figure 5.3: Radar record for profile 3

Figure 5.3 is the radar record of profile 3 with a length of 407 m. The continuous reflections marked WT across the radar record was interpreted to be the water table. Reflections from the top soil from the beginning of the profile were revealed on the radar record at depth of 5.0 m. That of the water table reflections was also between 35.3 m and 30.4 m respectively. The estimated average vertical thickness was 30.3 m for all points between these two reflections. This therefore suggests that the water table depth from the land surface was 30.3. The subsurface was also assumed to be uniform and fine textured as a result of the smooth and regular reflections.

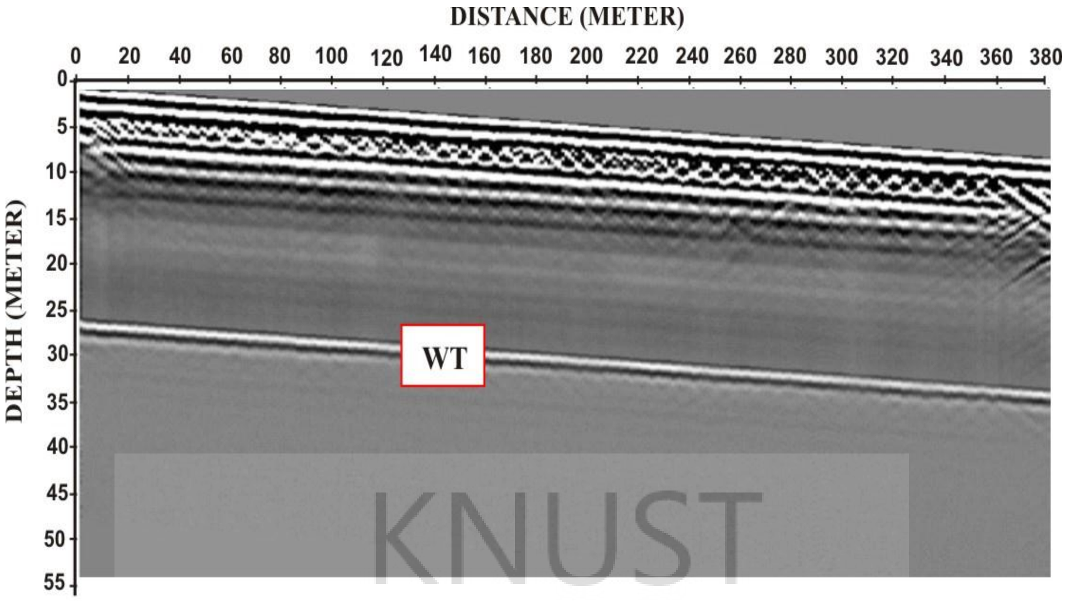

Figure 5.4: Radar record for profile 7

Figure 5.4 shows a radar record representing the result obtained for profile 7 and has a profile length of 381 m. The water table (WT) also reveals a smooth and continuous pattern at a depth of 30.3 m from the land surface and it is clearly revealed on the radar record. Reflections from the land surface or top soil appeared just at the start of the profile. At a depth of about 15 m from the land surface, the reflections were pronounced; this zone was interpreted to be the area of residual saturation where groundwater is held at a minimum quantity. Beneath this depth, these reflection events evanesce as the water table interface is reached; this was interpreted to be the transition capillary fringe. Attenuation of radar signals is higher as water content increases. The capillary fringe in the vadose zone contains much water compared to the zone of residual saturation. These subsurface characteristics were also evident for other profile as shown in appendix A.

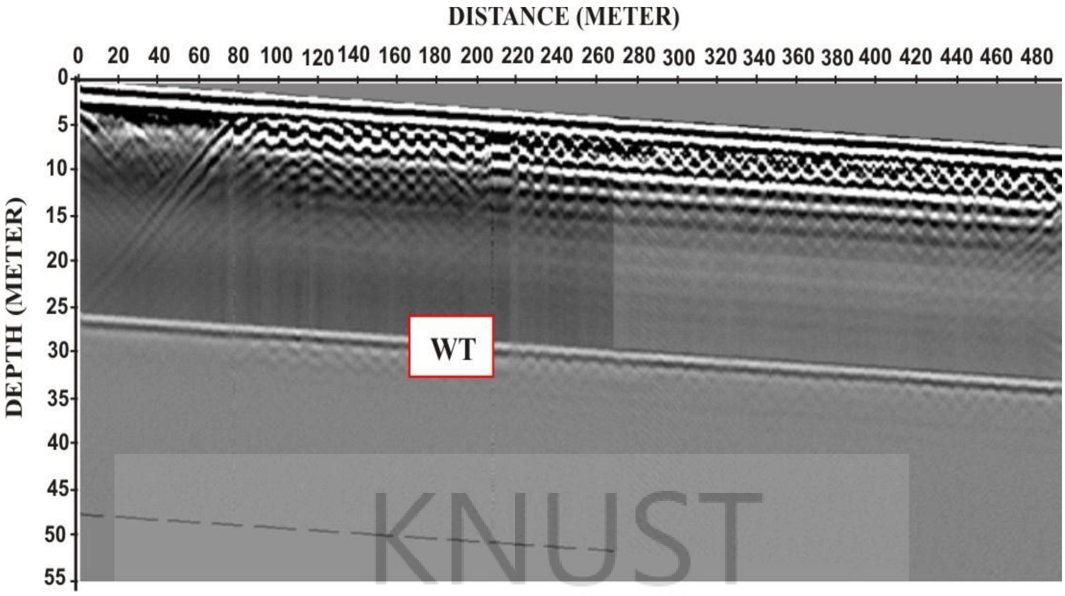

Figure 5.5: Radar record for profile 13

Figure 5.5 is a radar record of profile 13, which has a profile length of 494 m. As shown, smooth continuous reflections labelled as WT was inferred to be the water table reflections. The average depth from the land surface was estimated to be 30.1 m which also represented the depth of the vadose zone. Similar to other radar records; the water table takes the form or geometry of the land surface. From the beginning to about 80 m along the profile, reflections were irregular to depth of 20 m. This could be the fact that the subsurface at this location was unconsolidated and the soil was coarse textured as against the smooth reflections from 80 m to the end of the profile.

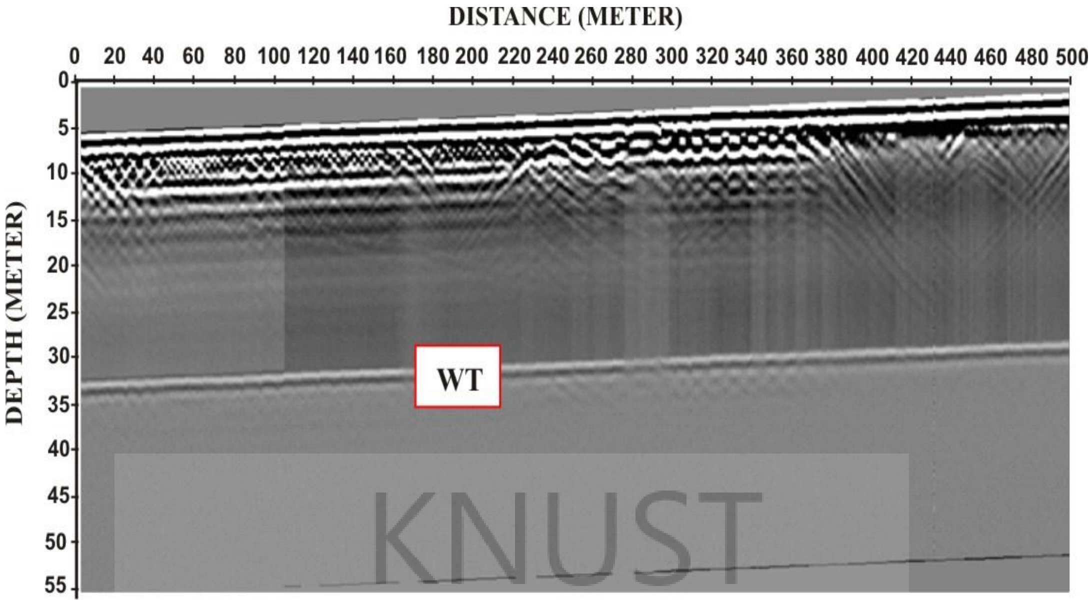

Figure 5.6: Radar record for profile 16

Figure 5.6 is the result for profile 16. It was the longest profile traversed and had a profile length of 500 m. The inferred water table (WT) as shown appears smooth and continuous and it is estimated to have an average depth from the land to be 28.1 m. Top soil or surface reflections began to appear at a depth of 5.1 m and 1.0 m from the beginning and end of the radar record respectively. Water table reflections were also recorded at depth between 33.5 m and 30.1 m at the beginning and end respectively. Reflections on this profile were irregular at distance between 360 m and 500 m at depth 5-15 m. This suggests a loose unconsolidated medium in this area.

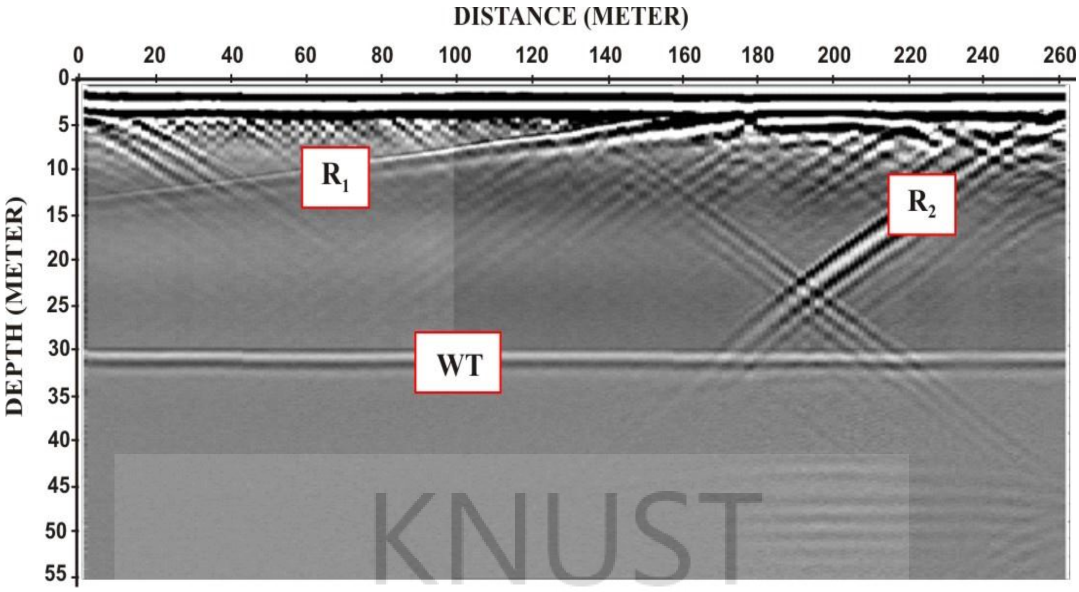

Figure 5.7: Radar record for profile 19

Fig 5.7 is the radar record for profile 19 which has a profile length of 265 m. The estimated water table (WT) is revealed at an average depth of 30 m from the land surface. The water table appears smooth, continuous and horizontal. This emphasizes a strong correlation between the behaviour and nature of the land surface and that of the water table. Noticeable dipping reflections marked R_1 and R_2were revealed on this radar record. These reflections were from outside environment such as high tension electrical cables rather than the subsurface and therefore have no geologic significance. This was also revealed on other radar records in appendix A.

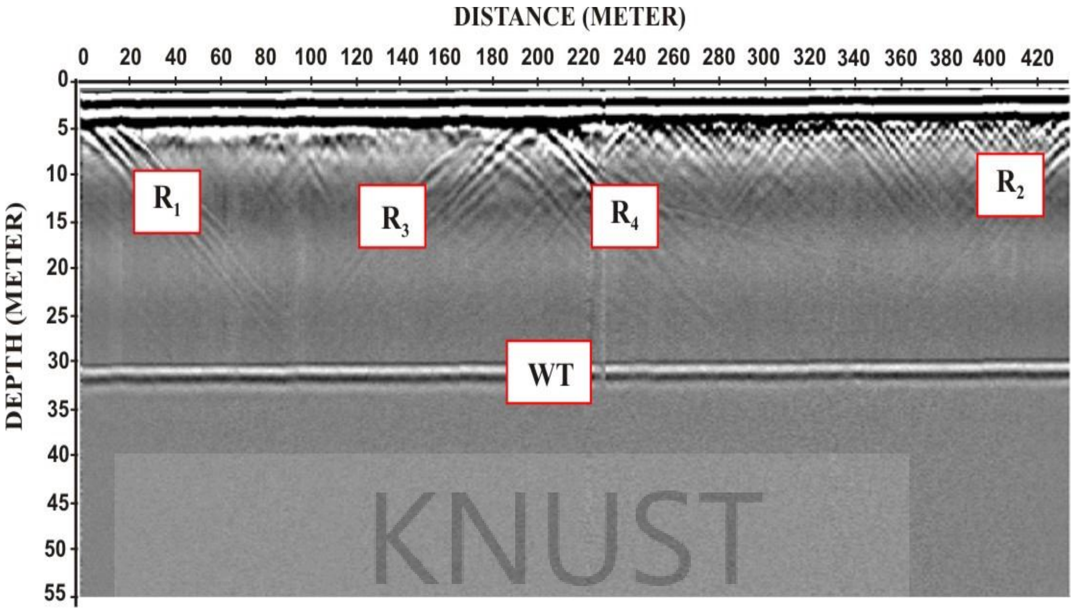

Figure 5.8: Radar record for profile 22

Fig 5.8 represents the result for profile 22. It has a profile length of 435 m. The estimated water table is revealed at a depth of 30.1 m. The area of residual saturation is revealed to have thickness of about 7 m which is revealed at depths between 5 m and 12 m along the profile. Below this depth to the top of the inferred water table is the transition zone where the radar velocity continuously decreases with depth. Other subsurface reflections marked R_1 as well as hyperbolic reflections marked R_2 and R_3 were also recorded. These reflectors may have come from subsurface reflectors since radar velocity check for these reflections have an average value of 0.18 m/ns which is less than 0.33 m/ns which represents radar velocity in air.

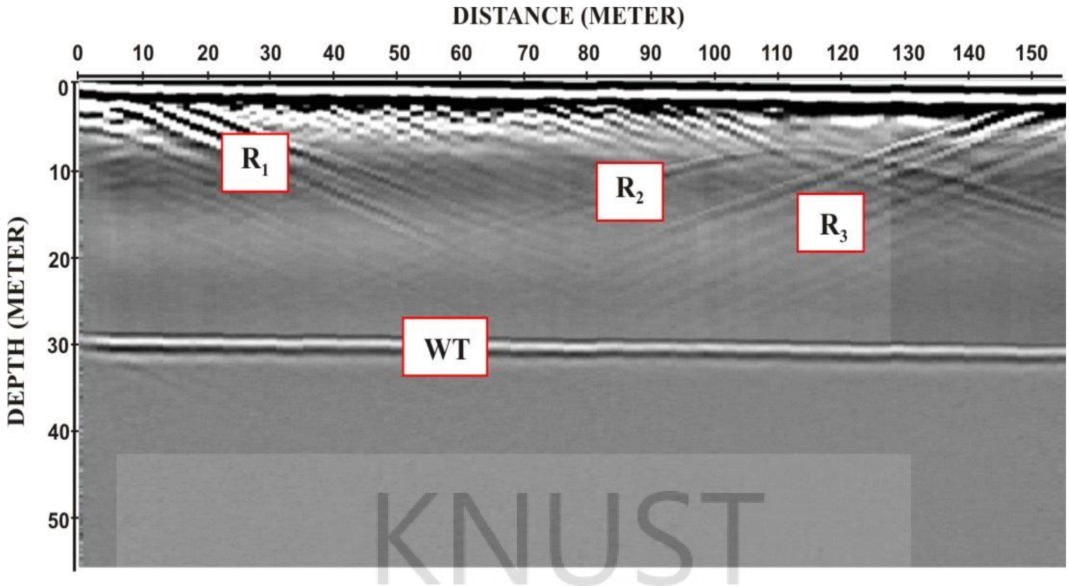

Figure 5.9: Radar record for profile 33

Figure 5.9 represents the result of profile 33 which has a profile length of 155 m. The radar record of this profile reveals the inferred water table (WT) at an average depth of 28.8 m. Top soil reflections were recorded between 0.1 and 3.5 m at the ends of the profile as against 29.9 m and 32.2 m for the water table reflections. This gave rise to the aforementioned water table depth from the land surface which is assumed to be the vertical thickness of the vadose zone. Other subsurface reflections were recorded on the radar records which are marked R_1, R_2 and R_3. Their velocities suggest that they are geologic features which may be significant upon determination. An average radar velocity of these reflectors was estimated to be 0.16 m/ns which suggest that they are from buried objects.

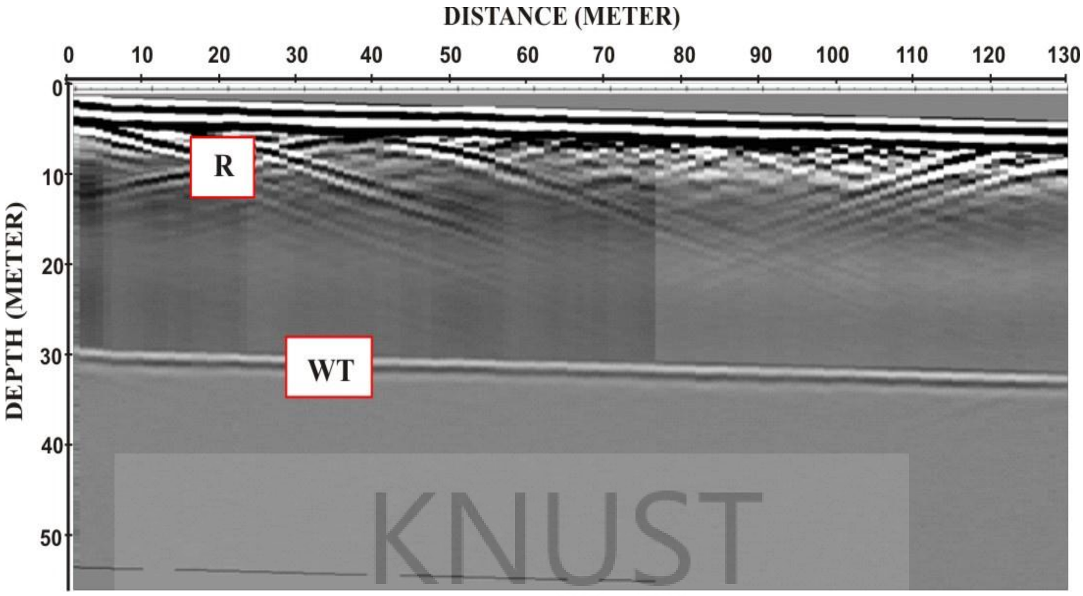

Figure 5.10: Radar record for profile 34

Figure 5.10 is a radar record of profile 34 with a profile length of 130 m. The revealed water table (WT) was estimated to have a vertical thickness of 30.3 m from the land surface. The irregular or chaotic nature of the reflections in the vadose zone suggests that the subsurface was unconsolidated at a vertical thickness of 10 m just beneath the topsoil reflection. Noticeable reflections marked R were also revealed on the radar record. The average velocities of the radar signal through these reflectors were estimated to be 0.22 m/ns. These were interpreted to be buried objects such as bottles and pipes since the area is close to an abandoned dump site.

5.3 Interpretation of Results

The water table provides a continuous and high amplitude reflection that is conspicuous across radar records. As a result of oscillations in the reflected radar signals, the water table interface appeared on the radar records as a series of three bands.

This distinguishable reflection as shown on the radar records was as a result of the sharp and abrupt contrast in the dielectric property between the saturated and unsaturated zone. This phenomenon normally happens in coarse textured soils (Smith et al., 1992; Bentley and Trenholm, 2002). As a result of this, water content increases with increasing depth from the unsaturated to the saturated zone where the capillary fringe is located. The consequence of this is that the GPR could not measure the water table depth directly but rather responded to saturated conditions within or near the top of the capillary fringe and this was inferred to be the water table.

The use of the 25 MHz non-shielded antennas made it possible to also emit electromagnetic waves into the air. Reflection events from objects originating from the air due to contrast in the electrical properties in air caused obscure reflections from the subsurface. Reflections indicated on the radar records depending on their velocities were interpreted to be from objects in the subsurface or above the earth surface. The reason being that electromagnetic wave propagates in air with the speed of light which is 0.3 m/ns. This speed is proportional to the inverse square root of the permittivity of the earth material and since the permittivity of earth material is always greater than the permittivity of air, the speed of a wave in a material other than air is always greater than 0.3 m/ns.

There exists an inverse relation between EM wave velocity and the permittivity; in view of this; higher velocities due the low-loss character of electromagnetic propagation in air are assumed to come from above the land surface. The converse of this that lower velocities than 0.3 m/ns could originate from the subsurface.

5.4 Water Table Map

The water table contour map in figure 5.11 is the map representing the water table depths of the project site and it is intended to show the general pattern of the water table depth from the surface with respect to the geometry or elevation at locations of the project site. It is important to state that the water table map is a representative of a specific time and season; which is the time of data acquisition (January 2014). This time forms part of the dry season of Ghana where the land is most often dry. The depth may change when rain sets in as a result of hydraulic conductivity. As shown on the map, the site were the apparent dry borehole is located on the farm has a water table depth of about 30.2 m which is far deeper than the 15 m depth of the borehole. The dryness of this borehole amongst others could be as a result of the fact that it was dug in the dry season where water table depth is relatively low.

The contour map is spaced at 1 m interval and the datum is the land surface. The depth ranges between 29.5 m and 32.7 m on the entire map. About 70 % of the project site has water table depth range between 30.2-30.5 m which is evenly distributed over the entire oil palm and citrus plantation. Water table beyond 31 m is hardly found in this area.

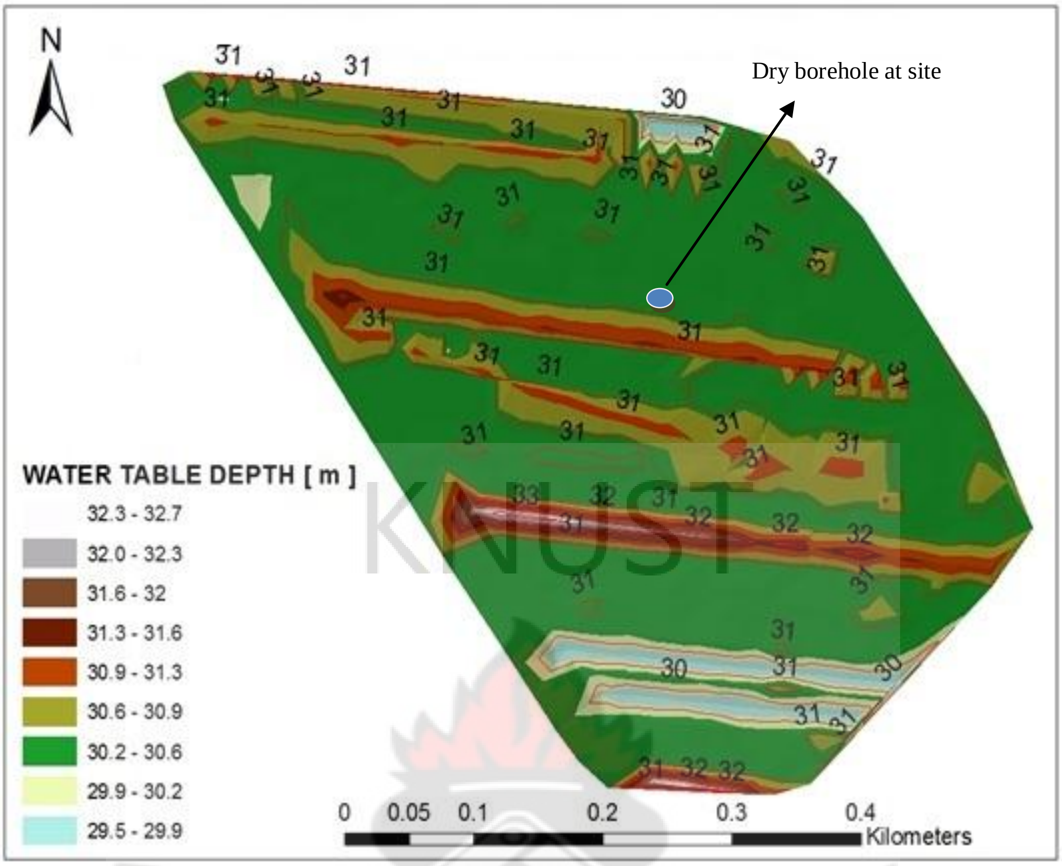

Figure 5.11: Water table depth map of the project site

CHAPTER 6

CONCLUSIONS AND RECOMMENDATIONS

6.1 Conclusions

The study appraised the effectiveness of GPR a tool for determining depth to the water table at the Agriculture Research Station-Anwomaso. It therefore confirms the efficiency and effectiveness of the use of GPR as a geophysical technique.

The result and analysis of this research work revealed the average water table depth to be 30.3 m from the surface of the land to the top of the capillary fringe which marks to interface between the saturated and unsaturated zone. This implies that water is saturated at this depth below the surface where groundwater can be pumped.

The underground water saturation divisions of the vadose zone were revealed at various depths. The vadose zone was estimated to have the same vertical thickness as the depth of the water table from the land surface (30.3 m). The upper part of the vadose zone where water is held at a minimum was estimated to have an average depth of 9 m. Below this depth to the top of the water table is the capillary fringe which is estimated to be 21 m.

The aquifer in the survey area could be located at a depth of about 30 m. This conclusion was arrived at because by definition, the saturated zone beneath the water table is the impermeable rock that stores the groundwater. Therefore wells must be sunk below this point in the region to pump water from the ground.

Noticeable dipping and hyperbolic reflections in the surface were recorded at various locations at the borders of the project site which were revealed at the extreme ends of some of the radar records. The average propagation velocity of the radar signal through these earth materials was estimated to be 0.18 m/ns. Theses reflectors could be buried objects since that area of the project site serves as a dumping site for refuse by residents who leave near the Agriculture Research Station.

The topography of the land directly influences the water table. From the radar records, the land pattern or the geometry of the land surface was similar to that of the water table; in that a slopping land surface gave rise to relatively deeper water table.

6.2 Recommendation

1. Farm practices such as wetland creation and shallow water development and management should be carried out during the rainy season when high water table depth is expected. This would ease the shortage of water during the dry season when groundwater decreases in the existing borehole.
2. Further research should be conducted on subsurface topography in the form of depth to bedrock, to ascertain the influence of subsurface topography on water table behaviour.
3. Other geophysical technique such as Electrical Resistivity should be used as a confirmatory tool to further validate this research work.

REFERENCES

1. Al Hagrey, S. A. and C. Mauller, GPR study of pore water content and salinity in sand,"Geophysical Prospecting, Vol. 48, 63{85, 2000}.
2. Allred, B.J; Daniels, J.J; and Ehsani, M.R. (2008). Handbook of Agricultural Geophysics. CRC Press, first edition.
3. Anderson, M. G., and T. P. Burt. "The role of topography in controlling throughflow generation." Earth Surface Processes 3, no. 4 (1978): 331-344.
4. Annan, A. P., 1992. Ground Penetrating Radar Workshop Notes. Sensors and Software Inc., Mississauga, Ontario, 56 pp.
5. Annan, A.P. (2005). Ground penetrating radar in near-surface geophysics, In: Near-Surface Geophysics, Investigations in Geophysics, No. 13, Society of Exploration Geophysics, Butler, D.K., pp.357-438, ISBN 1-56080-130-1, Tulsa, OK.
6. Annan, A.P. (2009). Electromagnetic principles of ground penetrating radar, In: Ground,Penetrating Radar: Theory and Applications, Jol, H.M., pp. 3-40, Elsevier, ISBN 978- 0-444-53348-7, Amsterdam, The Netherlands.
7. Azwin, I. N., Rosli, S., Nordiana, M. M., & Saufia, A. T. (2012). A Study of Water Table and Subsurface Using 3-Dimensional Ground Penetrating Radar. International Journal of Environmental Science and Development.
8. Benneh, G. and Dickson K. (1977). A new Geography of Ghana. Longman.
9. Benson, A. K., 1993. Case studies using ground penetrating radar to help assess groundwater contamination, shallow faulting, faults, and cavities, Proceeding of the 29th Symposium on Engineering Geology and Geotechnical Engineering.

10. Bentley, L.R., Trenholm, N.M., 2002. The accuracy of water table elevation estimates determined from ground penetrating radar data. Journal of Engineering and Environmental Geophysics 7, 37– 53.

11. Beres, M. J. and Haeni, E. P., 1991. Application of ground-penetrating –radar methods in hydrogeologic studies, Ground Water, 29, 3: 375-386.

12. Beven, K.J. 1979. Experiments with a finite element model of hillslope hydrology. The effect of topography. In: H.J Morel-Seytoux (Editor), Surface and Subsurface Hydrology: Proceedings of the Fort Collins Third International Hydrology Symposium, Water Resourses Publication: 37-51.

13. Brabham, G., 1998. The regional geological setting and nature of the Damang stockwork gold deposit – a new type of gold deposit in Ghana. MSc Thesis, Dept. of Geology and Geophysics, Univ. of Western Australia, 101pp.

14. Cassidy, N.J. (2009). Electrical and magnetic properties of rocks, soils, and fluids, In: Ground Penetrating Radar: Theory and Applications, Jol, H.M., pp. 41-72, Elsevier, ISBN 978-0-444-53348-7, Amsterdam, The Netherlands.

15. Cheng, JD., Black, T.A., and Willington, R.P. 1975. The generation of storm flow from small forested watersheds in the Coast Mountains of south western British Columbia. In: Proceedings, Canadian Hydrology Symposium 1975, National Research Council of Canada: 542-55.

16. Cogger, C. G., P. E. Kennedy, and D. Carlson. "Seasonally saturated soils in the Puget Lowland II. Measuring and interpreting redox potentials." Soil Science 154, no. 1 (1992): 50-58.

17. Conyers L. B. and Goodman D., (1997). Ground-penetrating radar – An introduction for archaeologists, Altamira Press, A Division of Sage Publications, Inc.

18. Dabowski, C. N., 1972. The geology of 1/4° field sheet no. 81 Wiawso SW and 122 Kukuom SW; Ghana Geological. Survey. [unpubl rept.].

19. Dallimore, S. R. & J. L. Davis, 1987. Ground probing radar investigations of massive ground ice and near surface geology in continuous permafrost. GSC Paper 87–1A. Current Research Part A: 913–918.

20. Daniels, D.J. (Ed.). (2004). Ground Penetrating Radar (2nd Edition), IEE, ISBN 0-86341-360-9, London.

21. Daniels, J.J. (2000). Ground Penetrating Radar Fundamentals. Appendix to a report to the U.S.EPA, Region V.

22. Daniels, J. J., 1994. "Ground penetrating radar for geo-technical applications, Geophysical Characterization of Sites", Volume Prepared by ISSMFE, TC # 10:1-13.

23. Dapaah-Siakwan, S., & Gyau-Boakye, P. (2000). Hydrogeologic framework and borehole yields in Ghana. Hydrogeology Journal, 8(4), 405-416.

24. Davis, J. L. & A. P. Annan, 1989. Ground-penetrating radar for high-resolution mapping of soil and rock stratigraphy. Geophysical Prospecting 37: 531–551.

25. Delaney, A. J. & S. A. Arcone, 1982. Laboratory Measurements of Soil Electric Properties between 0.1 and 5 GHz. U.S. Army Cold Regions Research and Engineering Laboratories, Hanover, New Hampshire, 7 pp

26. Dominic, D. F., 1995. Delineation of shallow stratigraphy using ground-penetrating radar, Journal of Applied Geophysics, 33, 1-3: 167-176.

27. Drury, S.A. 1993. Image interpretation in geology. pp. 1-4, 41-47, 175-203. Chapman & Hall, London, 1993.

28. Dunne, T ., and Black, R.D. 1970. An experimental investigation of runoff production in permeable soils. Water Resources Research, 6: 478-490.

29. Dunne, Thomas, ToR Moore, and C. H. Taylor. "Recognition and prediction of runoff-producing zones in humid regions." Hydrol. Sci. Bull 20, no. 3 (1975): 305-327.

30. Eisenlohr, B. N. and Hirdes, W. (1992). The structural development of early Proterozoic Birimian and Tarkwaian rocks in southwest Ghana,West Africa. Journal of African Earth Science, 14(3):313–325.

31. Evans, R.D. (2009). Optimising Ground Penetrating Radar (GPR) to Assess Pavements. PhD thesis, Loughborough University.

32. Garambois, S., P. Senechal, and H. Perroud, On the use of combined geophysical methods to assess water content and water conductivity of near-surface formations," Journal of Hydrology, Vol. 259, 32{48, 2002}.

33. Geological Survey Department (2009).l Geological, Geophysical and Geochemical Investigations in the Bui Belt Area in Ghana. Geol. Jb. Reihe B, 88, 269p.

34. Gerhards, H. 2008. Ground Penetrating Radar as a Quantitative Tool with Applications in Soil Hydrology, PhD thesis, Heidelberg University.

35.Goodman, D., & Piro, S. (2013). GPR Remote Sensing in Archaeology (Vol.9). New York: Springer.Griffis, R. J., Barning, K., Agezo, F. L., and Akosah, F. K. (2002). Gold deposits of Ghana.

36. Harter, T. (2003). Basic concepts of groundwater hydrology.

37. Harry, M. J. (2009). Ground Penetrating Radar Theory and Application. Elsevier Science, first edition.

38. Hirdes, W., & Davis, D. W. (2002). U–Pb geochronology of paleoproterozoic rocks in the southern part of the Kedougou-Kenieba Inlier, Senegal, West Africa: evidence for diachronous accretionary development of the Eburnean province. Precambrian Research, 118(1), 83-99.

39. Hirdes, W. and Nunoo, B. (1994). The Proterozoic paleoplacers at the Tarkwa gold mine, SW - Ghana -sedimentology, mineralogy, and precise age dating of the main reef and west reef, and bearing of the investigations on source area aspects. In Oberthür, T. (ed.), Metallogenesis of Selected Gold Deposits in Africa, pages 247–298. Geologische Jahrbuch, Reihe D, Heft 100, Hannover.

40. Huff, D. D., R. V. O'Neill, W. R. Emanuel, J. W. Elwood, and J. D. Newbold. "Flow variability and hillslope hydrology." Earth Surface Processes and Landforms 7, no. 1 (1982): 91-94.

41. Hughes, Paul A., Krysztof A. Lesniewicz, and Robert V. Rouke. "Water tables, soil temperatures, and morphological characteristics in selected Maine soils." (1993).

42. Junner, N. R. (1940). Geology of the Gold Coast and Western Togoland. Geological Survey Bulletin No.1.

43. Kaatze, U. (1989). Complex permittivity of water as a function of frequency and temperature. Journal of Chemical and Engineering Data, Vol. 34, pp. 371-374.

44. Kesse, G. (1985). The Mineral and Rock Resources of Ghana.

45. Kiessling, R., 1997. Sedimentation and Structure in the Tarkwaian Group of the Bui Basin in West-Ghana; in A. Zitzmann (ed.),

46. Kip, A.F., 1969. Fundamentals of Electricity and Magnetism. International student edition. McGraw-Hill Kogakusha Ltd, Tokyo.

47. Knight, R.J. & Endres, A.L. (2005). An introduction to rock physics principles for nearsurface geophysics, In: Near-Surface Geophysics, Investigations in Geophysics, No. 13, Society of Exploration Geophysics, Butler, D.K., pp.357-438, ISBN 1-56080-130-1, Tulsa, OK.

48. Lampe, B. & Holliger, K. (2003). Effects of fractal fluctuations in topographic relief, permittivity and conductivity on ground-penetrating radar antenna radiation. Geophysics, Vol. 68, pp. 1934-1944.

49. Ledru, P., Milesi, J. P., Vinchon, G., Ankrah, P. J., Johan, V., and E. Marcoux, 1991. The Geology of the Lower Proterozoic Succession of Ghana; in Kesse G.O (ed.)., Proc. Of the Int. Conf. On the Geology of Ghana. Geol. Soc. Ghana, v. 3, pp. M1 to M33, Accra.

50. Lee, K. T., 1996. “Initial study of GPR applications on civil engineering”, Master thesis for Institute of Civil Engineering, National Cheng Kung University.

51. Leube, A., and W. Hirdes, 1986. The Birimian Supergroup of Ghana – depositional environment, structural development and conceptual model of an Early Proterozoic suite. Rept No 99529, Arch. BGR: 260 p, Hannover (unpubl.).

52. Leube, A., Hirdes, W., and Kesse, G. (1990). The early proterozoic birimian supergroup ofghana some aspects of its associated gold mineralization. pages 139–165.

53. Leucci, G. (2012). Ground Penetrating Radar: A Useful Tool for Shallow Subsurface Stratigraphy Characterization. Stratigraphic Analysis of Layered Deposits, 978-953.

54. Liang, S. 1990. Principles of GPR echo wave and application on testing underground water level, Journal of Agriculture and Forestry, 39, 2 : 201-219 .

55. Liegeois, J. P., Classens, W., Camara, D., and J. Klerkx, 1991. Short-lived Eburnian Orogeny in southern Mali: Geology, tectonics, U-Pb and Rb-Sr geochronology. Prec. Res., v.50, pp. 111-136.

56. Ludwig, R., Gerhards H., Wollschlager., Buchner, 2011. Electromagnetic Methods in Applied Geophysics. Institute of Environmental Physics, Heidelberg University.

57. Mala (2011). Mala geoscience, "RAMAC/GPR" software manual. pages 7–18.

58. Manu, E. (2013). Application of Ground Penetrating Radar in delineating zones of Gold Mineralization at the Subenso-North Concession of Newmont Ghana Gold Limited. International Journal of Scientific and Research Publications.

59. Martinez, A. & Byrnes, A. P. 2001. Modeling Dielectric-constant values of Geologic Materials: An Aid to Ground-Penetrating Radar Data Collection and Interpretation. Current Research in Earth Sciences, Bulletin 247, part 1, Kansas Geological Survey, Lawrence, KS, USA. 2001.

60. McCaig, M. 1984. Soil properties and subsurface hydrology. In: K.S. Richards, A.R. Arnett, and S. Ellis (Editors), Geomorphology and Soils. London: Geotge Allen and Unwin.

61. Milési, J. P., Ledru, P., Ankrah, P., Johan, V., Marcoux, E., & Vinchon, C. (1991). The metallogenic relationship between Birimian and Tarkwaian gold deposits in Ghana. Mineralium Deposita, 26(3), 228-238.

62. Moore, I. D., George. Foster, M. G. Anderson, and T. P. Burt. "Hydraulics and overland flow." Process studies in hillslope hydrology. (1990): 215-254.

63. Moorman, B.J. (2001). Ground-Penetrating Radar Applications in Paleolimnology. Earth Science Program, University of Calgary, Alberta, Canada.

64. Petch, R. A. "Soil saturation patterns in steep, convergent hill-slopes under forest and pasture vegetation." Hydrological Processes 2, no. 1 (1988): 93-103.

65. Petters, SW., 1991. Regional Geology of Africa. Springer-Verlag (Publ.), Berlin, 722p.

66. Preko, K. (2007). Determination of Volumetric Soil Water Content Using Ground Penetrating Radar. PhD Dissertation.

67. Phillips, Steven P., Roger P. Denlinger, and Loren F. Metzger. Determination of specific yield and water-table changes using temporal microgravity surveys collected during the second injection, storage, and recovery test at Lancaster, Antelope Valley, California, November 1996 through April 1997. US Department of the Interior, US Geological Survey, 2003.

68. Reynolds, J.M. 2011. An Introduction to Applied and Environmental Geophysics. John Wiley & S o n s Ltd, Chichester, 2nd ed., 712.

69. Robinson, D.A., Jones, S.B., Wraith, J.M., Or, D. & Friedmann, S.P. (2003). A review of advances in dielectric and electrical conductivity measurement in soils using time domain reflectometry. Vadose Zone Journal, Vol. 2, pp. 444-475.

70. Scott,W. J., P.V. Sellmann & J.A. Hunter, 1978. Geophysics in the study of permafrost. Third International Conference on Permafrost: Edmonton, Alberta. National Research Council of Canada, Ottawa: 93–115.

71. Sellmann, P. V., A. J. Delaney & S. A. Arcone, 1992. Sub-bottom Surveying in Lakes with Groundpenetrating Radar. U.S. Army Cold Regions Research and Engineering Laboratories, Hanover, New Hampshire, 18 pp.

72. Sestini, G., 1973. Sedimentology of a paleoplacer: the gold bearing Tarkwaian of Ghana; in Amstutz, G. C. and A. J. Bernard (Eds): Ores in Sediments, pp. 275-305, Springer-Verlag, Heidelberg.

73. Sheriff, R. E. 2002. Encyclopedic Dictionary of Applied Geophysics, 4th Edition. Society of Exploration Geophysics. Tulsa, OK

74. Sheriff, R. E. & R. E. Geldart, 1982. Exploration Seismology, Volume 1: History, Theory, and Data Acquisition, Cambridge University Press, NewYork, 253 pp.

75. Sinai, G., D. Zaslavsky, and P. Golany. "The effect of soil surface curvature on moisture and yield-Beer Sheba observation." Soil Science 132, no. 5 (1981): 367-375.

76. Smith, M.C., Vellidis, G., Thomas, D.L., Breve, M.A., 1992. Measurement of water table fluctuations in a sandy soil using ground penetrating radar.

Transactions of the American Society of Agricultural Engineers 35, 1161–1166.

77. Sylvester, P. J., and K. Attoh, 1992. Lithostratigraphy and composition of 2.1 Ga greenstone belts of the West African Craton and their bearing on crustal evolution and the Archean-Proterozoic boundary. J. Geol., v. 100, pp. 337-393.

78. Takahashi, K; Igel, J; Preetz, H; and Kuroda, S. (2012). Basics and Application of Ground-Penetrating Radar as a Tool for Monitoring Irrigation Process, Problems, Perspectives and Challenges of Agricultural Water Management, Dr. Manish Kumar (Ed.), ISBN: 978-953-51-0117-8, InTech.

79. Taylor. P. N., Moorbath. S., Leube, A., and W. Hirdes, 1988. Geochronology and crustal evolution of early Proterozoic granite greenstone terrains in Ghana, West Africa. Abstracts, Intern. Conf. and Workshop on the Geology of Ghana with special emphasis on Gold: pp. 43 – 45, Accra.

80. Telford, W. M., L. P. Geldart, R. E. Sheriff & D.A. Keys, 1976. Applied Geophysics: Cambridge. Cambridge University Press, NewYork, 301 pp.

81. Thompson J.C. 1991. Behaviour and Prediction of Water Table Levels in Shallow Forest Soils, Southwestern British Columbia. Msc. Thesis, Simon Fraser University.

82. Topp, G.C., Davis, J.L. & Annan, A.P. (1980). Electromagnetic determination of soil water content: measurements in coaxial transmission lines. Water Resource Research, Vol. 16, pp.574-582.

83. Trashliev, S. S., 1972. The geology of 1/4° field sheets 82 (Wiawso SE) and 46 (Asankrangwa NE). Ghana Geol. Surv. Unpub. Rept., 88p (unpublished), Accra.

84. Ulaby, F.T., Moore, R.K. & Adrian, K.F. (1986). Microwave Remote Sensing: Active and Passive, volume 3: From Theory to Applications. Artech House, ISBN 0-89006-192-0, Norwood, MA

85. Ulriksen, C. P., 1982. Application of impulse radar to civil engineering. Published Ph.D. Thesis, Lund University of Technology, Lund, Geophysical Survey Systems, Inc. Hudson, New Hampshire, 179 pp.

86. Winter, Thomas C. Ground water and surface water: a single resource. Vol. 1139. DIANE Publishing, 1999.

87. Wright, J. B., Hastings, D. A., and W. B. Jones, 1985. Geology and Mineral Resources of West Africa. G. Allen and Unwin, 187p, London.

88. Ziaqiang, Z., Xianqi, H., Guangyin L., Qunyi L., and Jianhui L. (2009). Ground penetrating radar exploration for ground water and contamination. Geomatics and Info-physics School, Central South University, Changsha, China

APPENDICES

Appendix A:

Ground Penetrating Radar Profile Records Showing Water Table (WT) at Various Depths

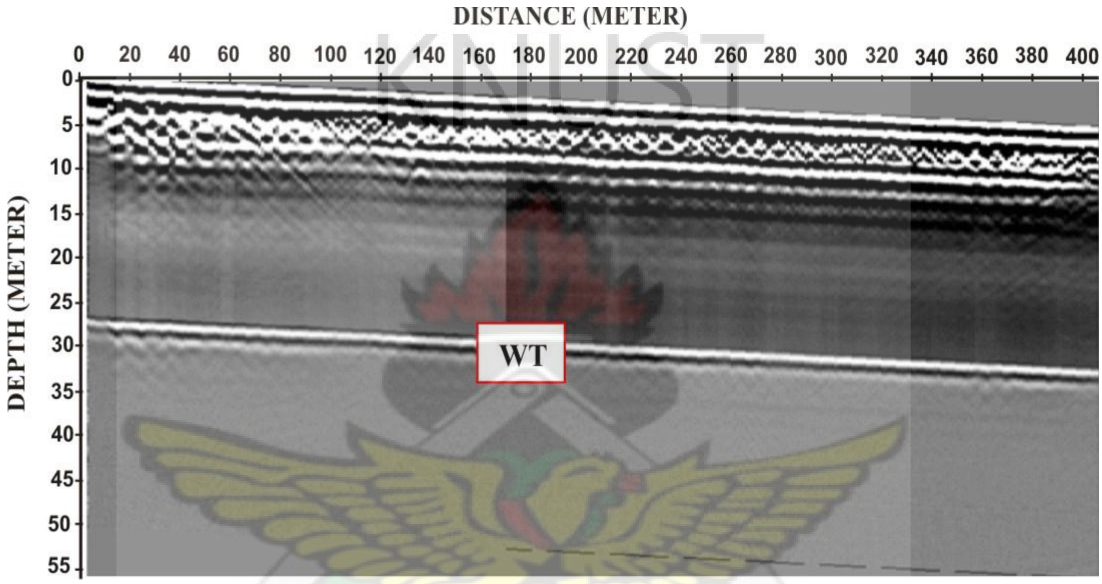

Figure A.1: Radar record for profile 4

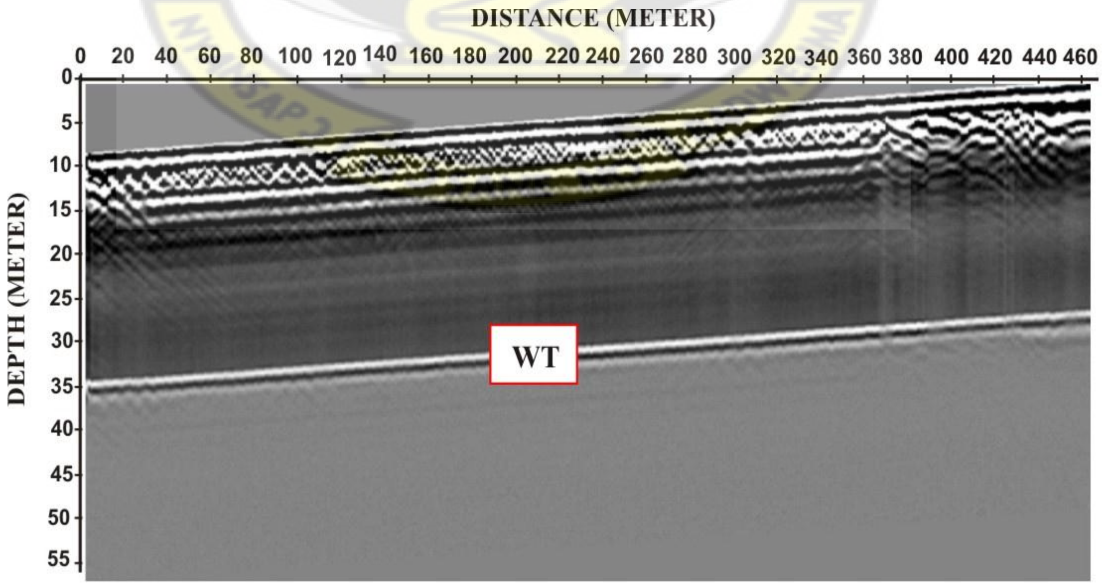

Figure A.2: Radar record for profile 5

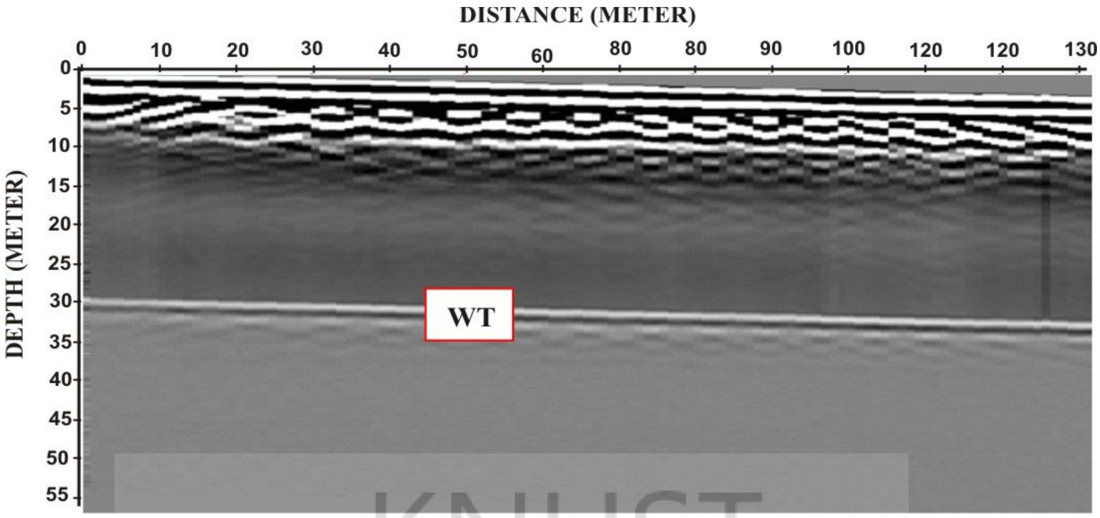

Figure A.3: Radar record for profile 6

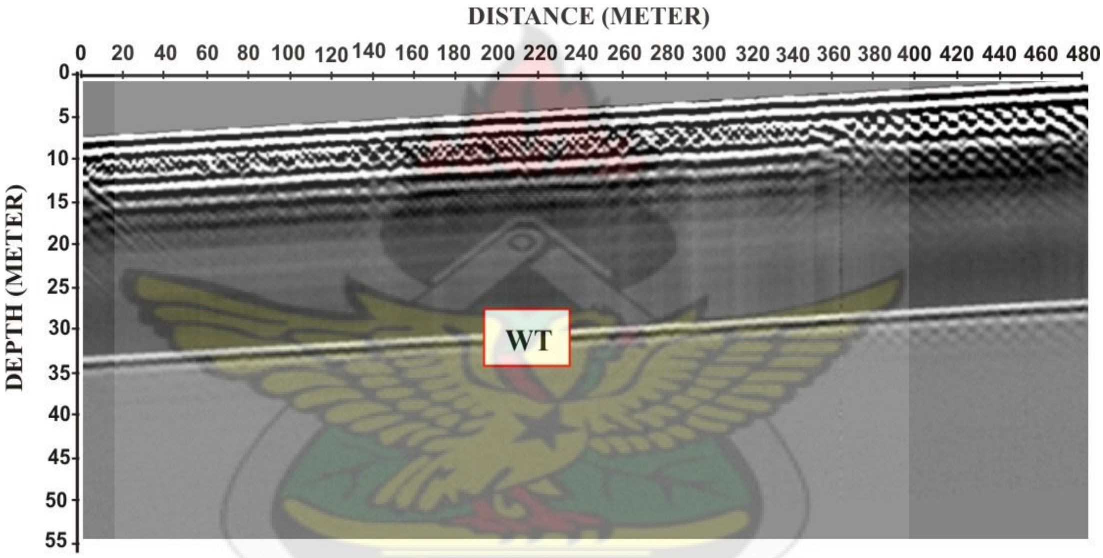

Figure A.4: Radar record for profile 8

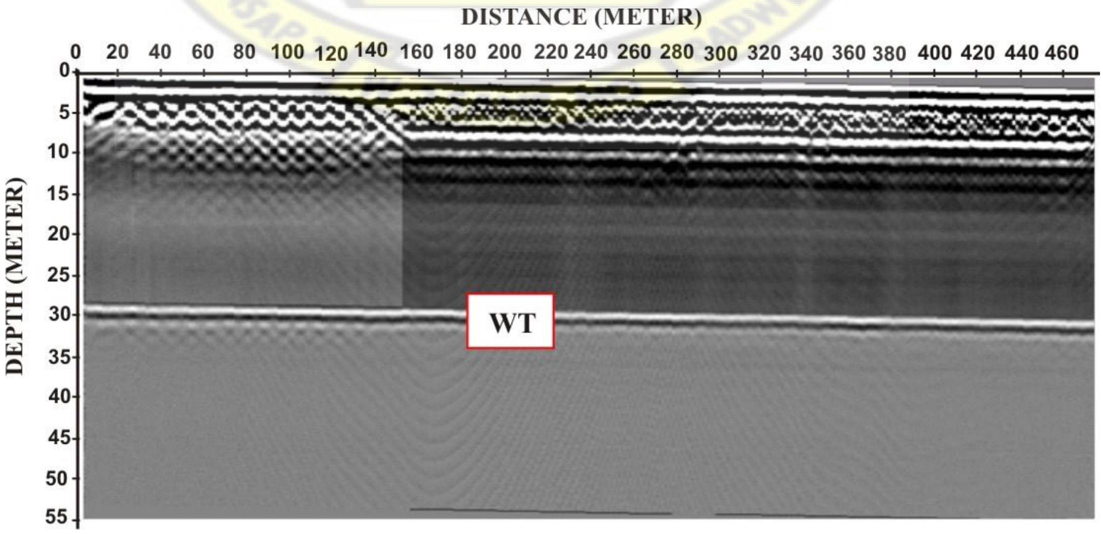

Figure A.5: Radar record for profile 9

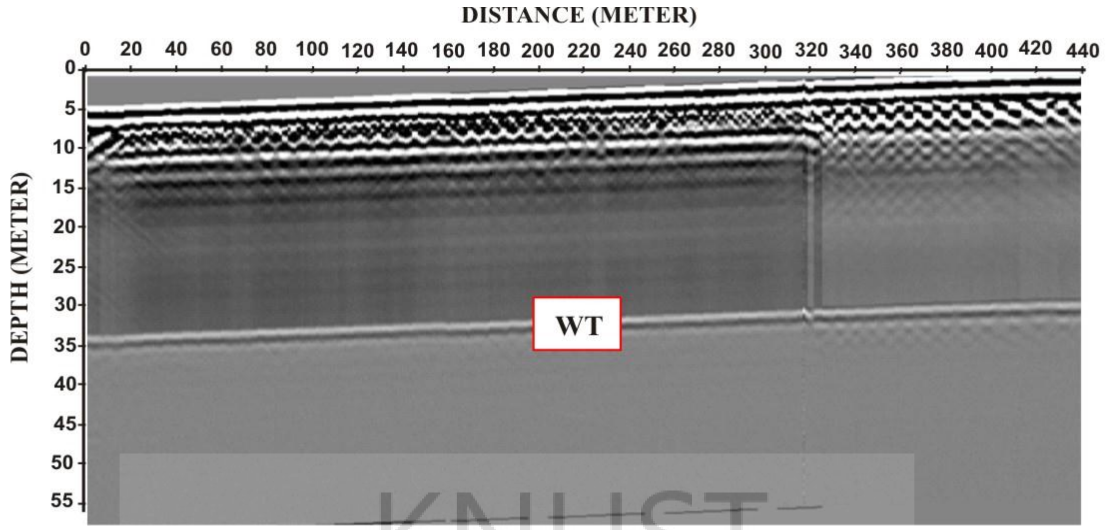

Figure A.6: Radar record for profile 10

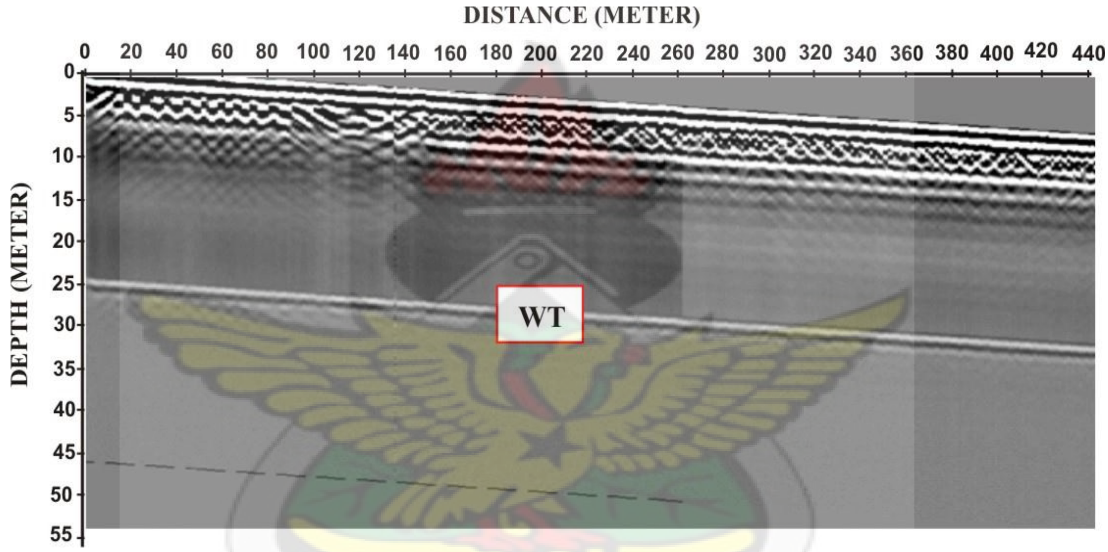

Figure A.7: Radar record for profile 11

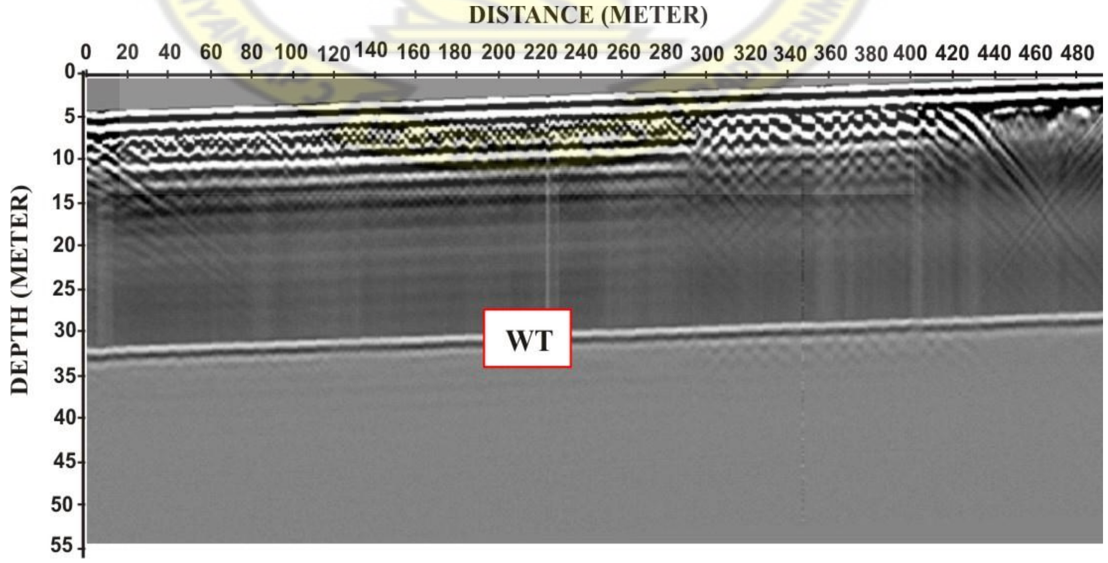

Figure A.8: Radar record for profile 12

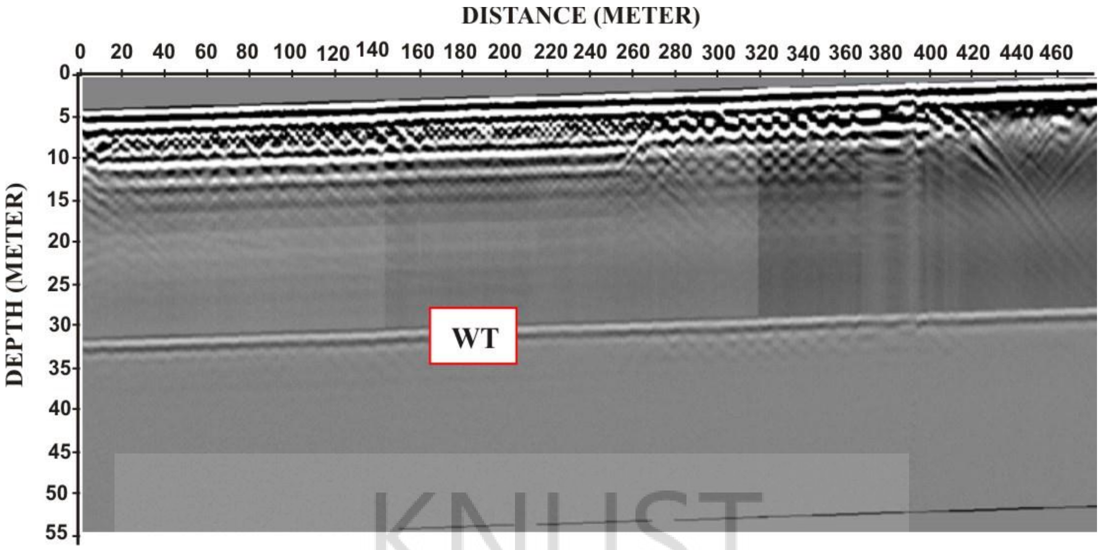

Figure A.9: Radar record for profile 14

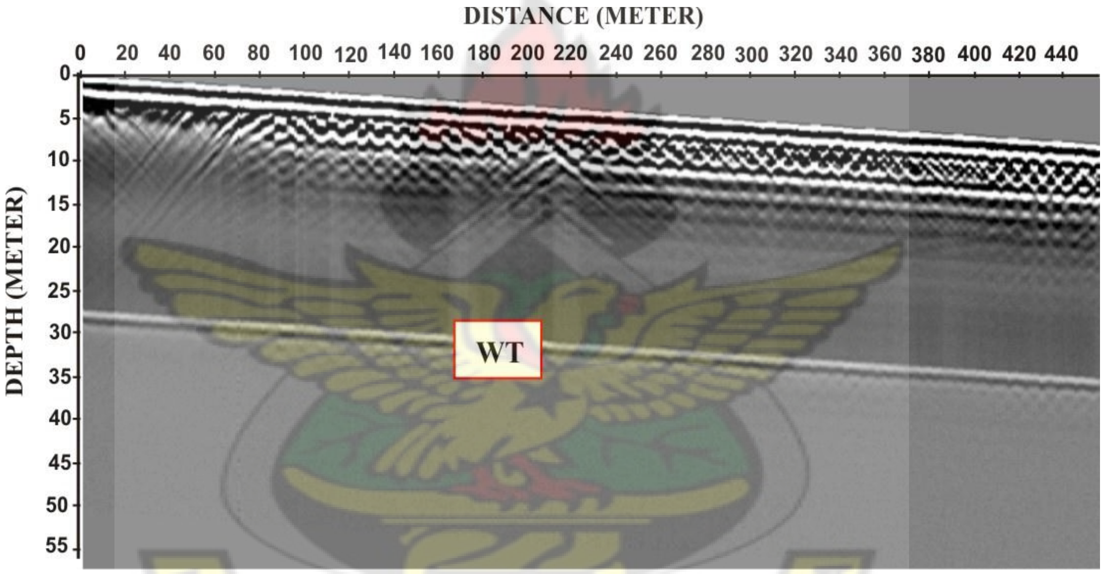

Figure A.10: Radar record for profile 15

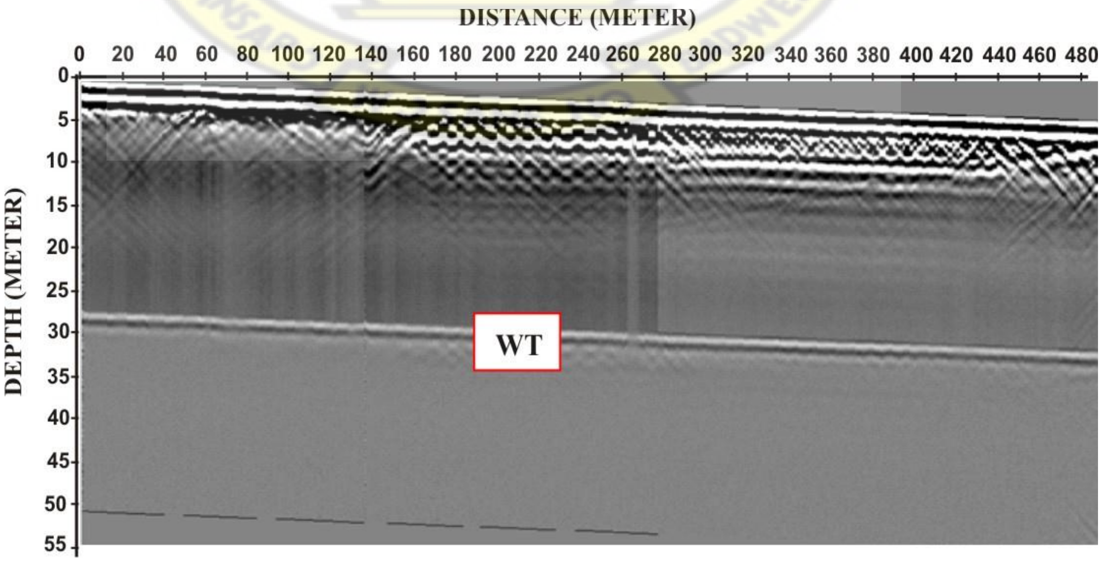

Figure A.11: Radar record for profile 17

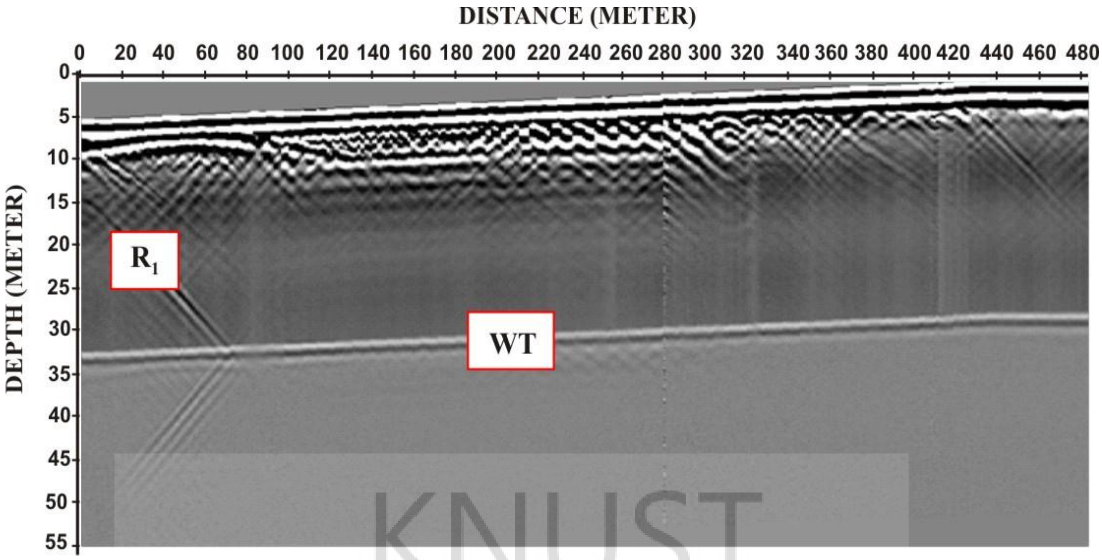

Figure A.12: Radar record for profile 18

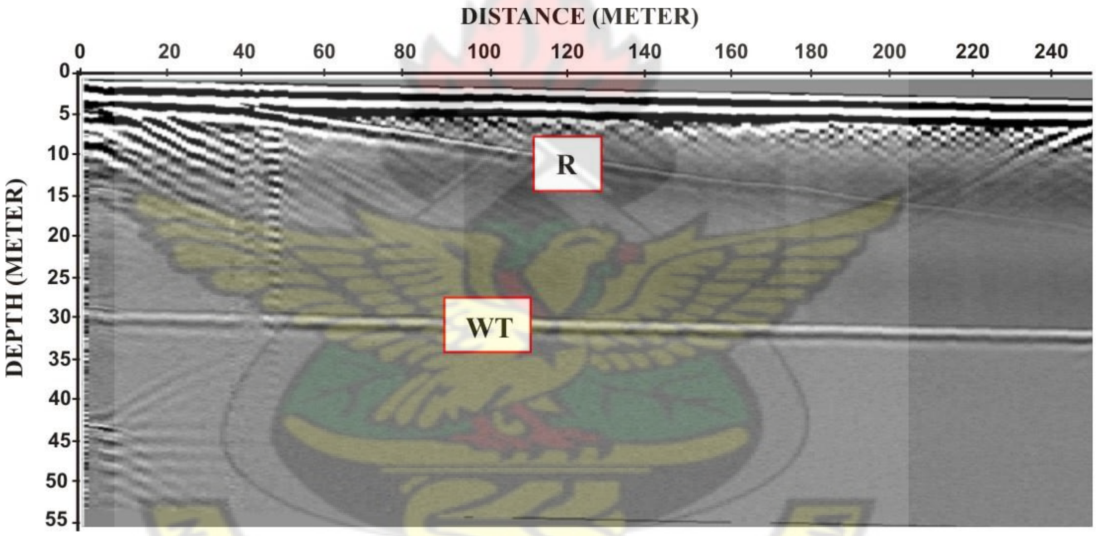

Figure A.13: Radar record for profile 20

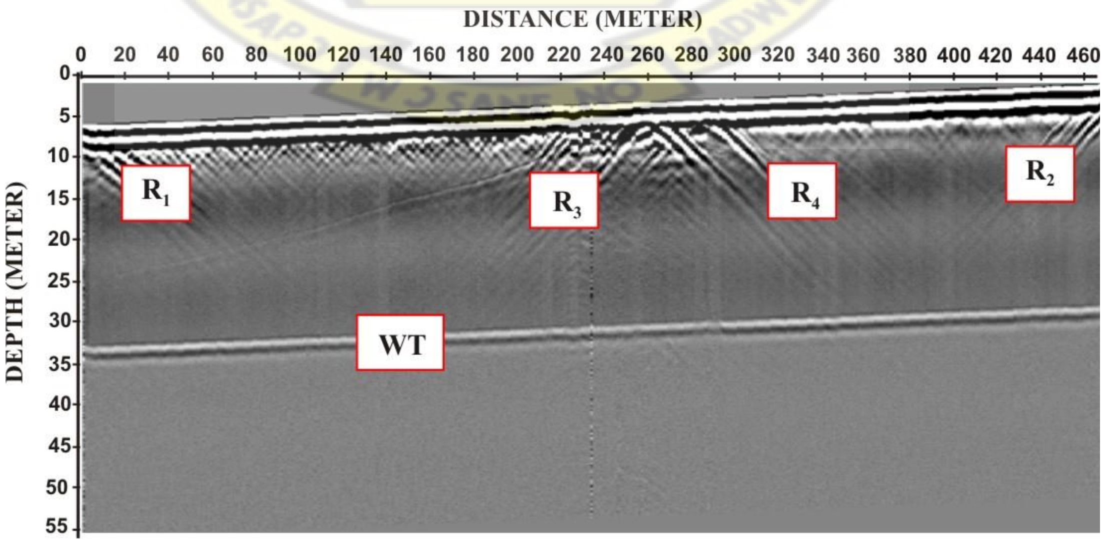

Figure A.14: Radar record for profile 21

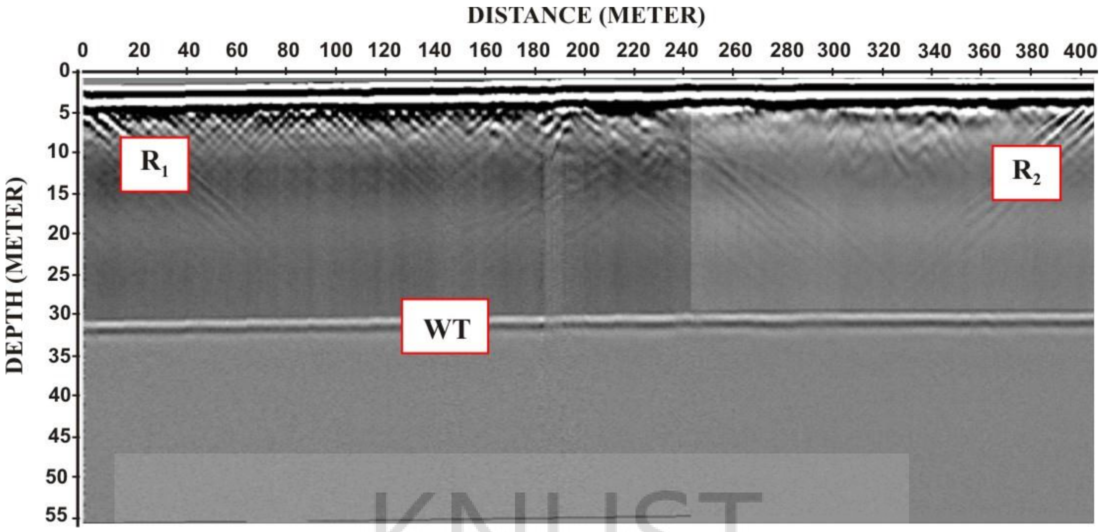

Figure A.15: Radar record for profile 23

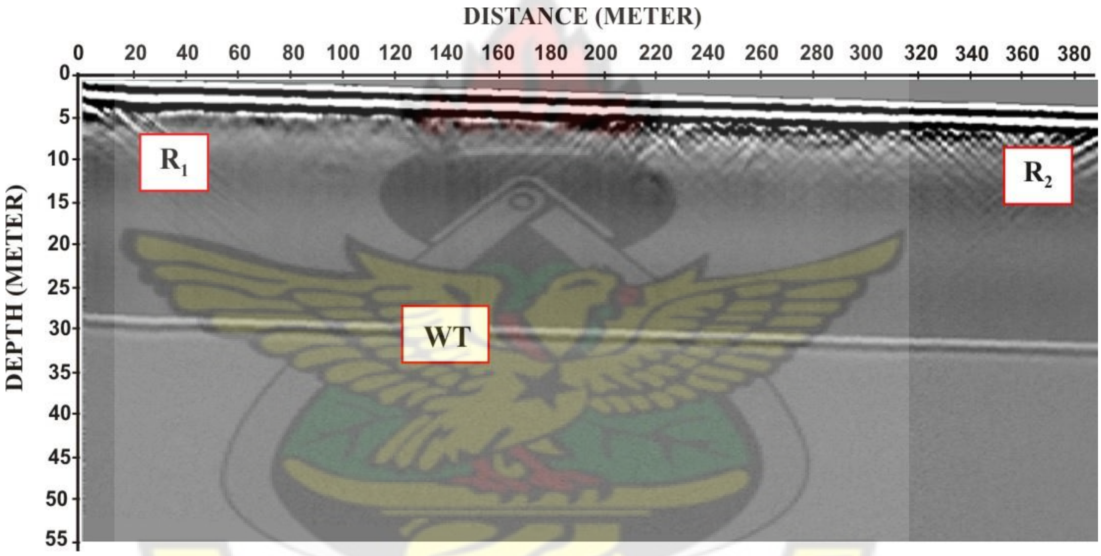

Figure A.16: Radar record for profile 24

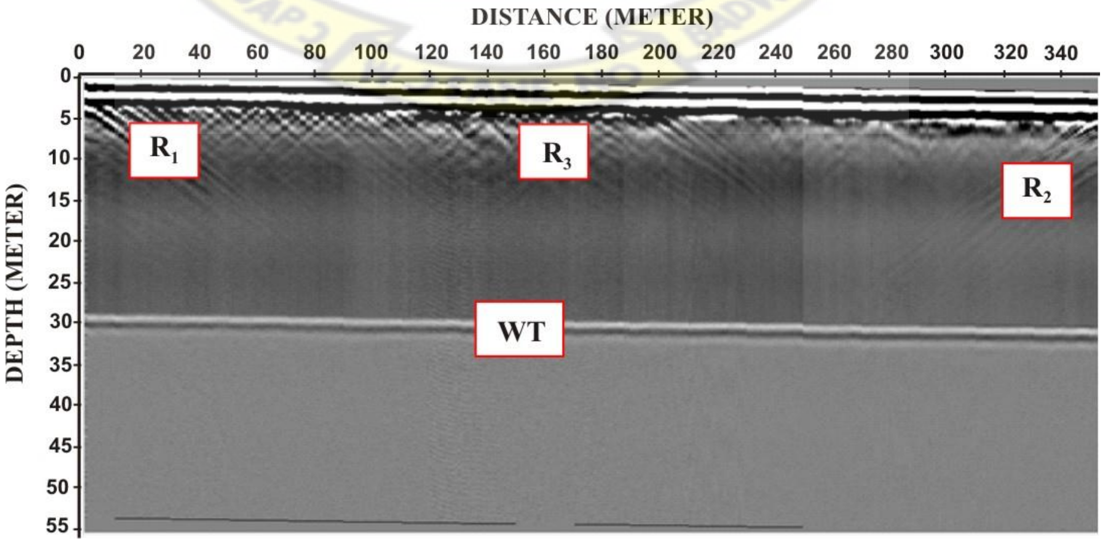

Figure A.17: Radar record for profile 25

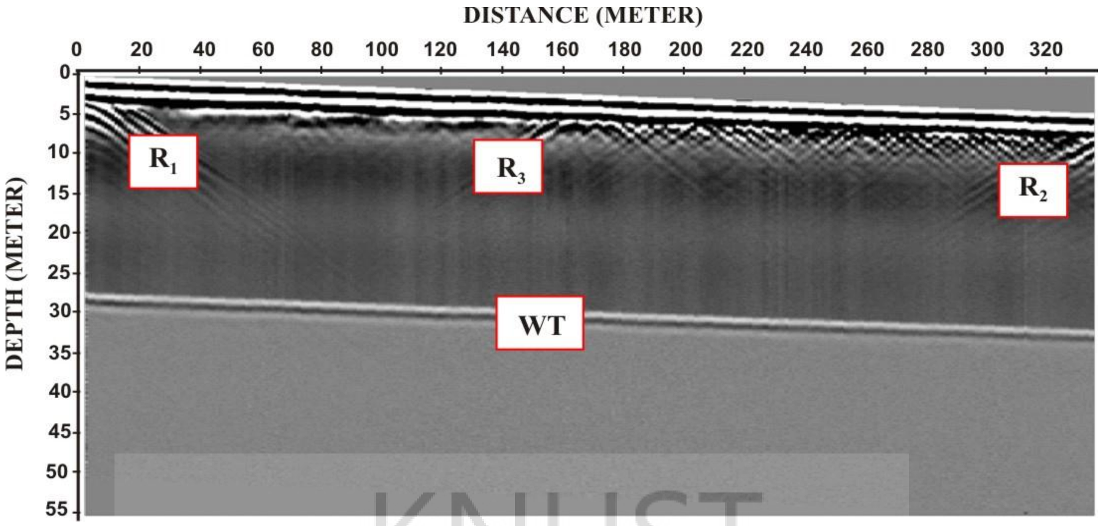

Figure A.18: Radar record for profile 26

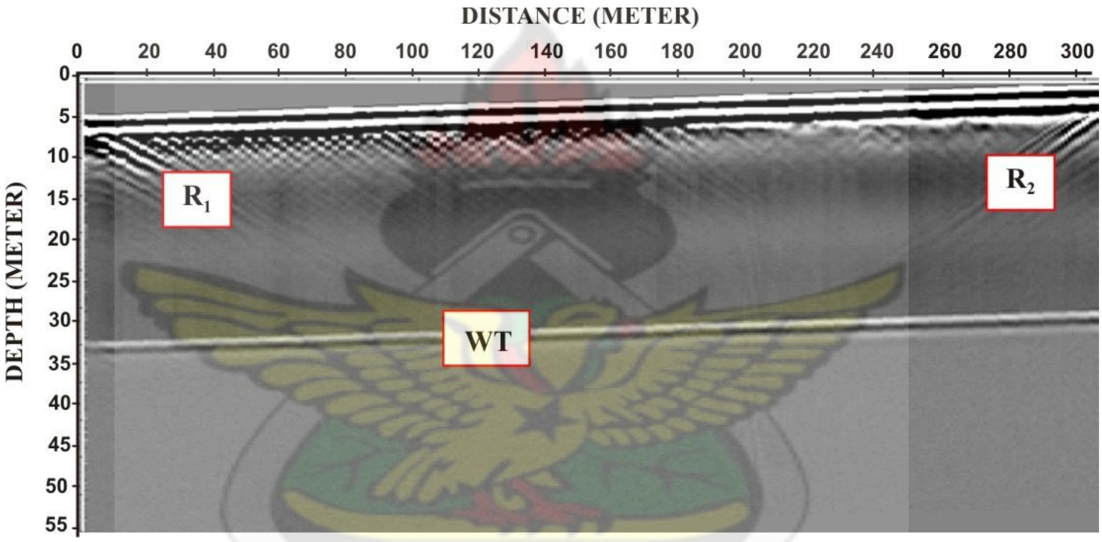

Figure A.19: Radar record for profile 27

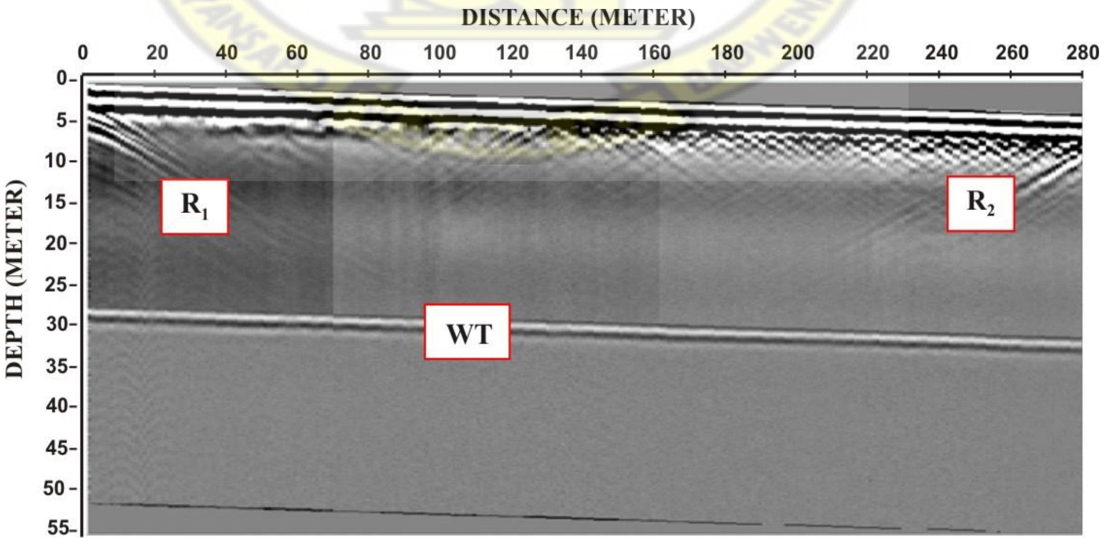

Figure A.20: Radar record for profile 28

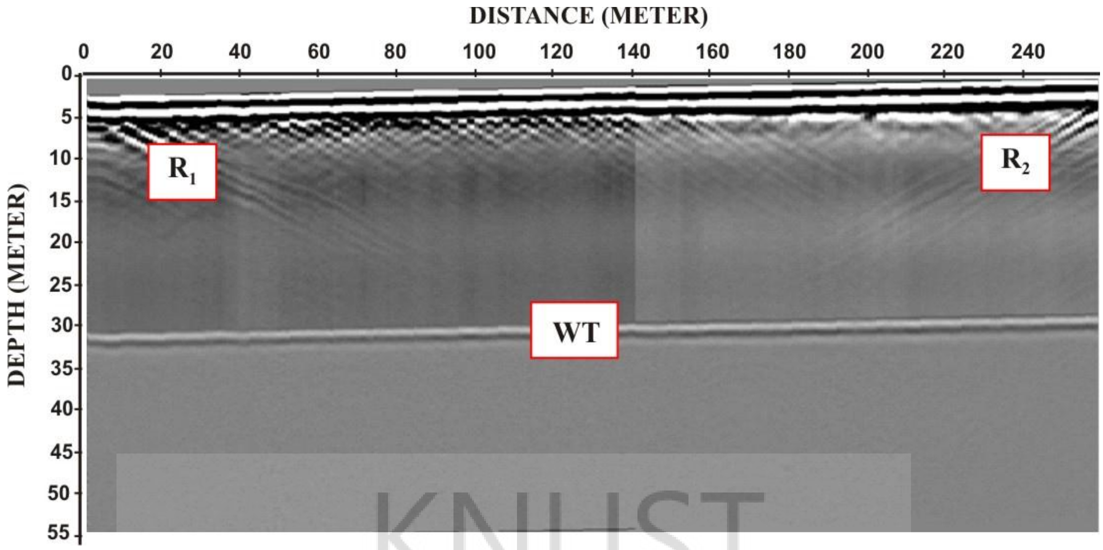

Figure A.21: Radar record for profile 29

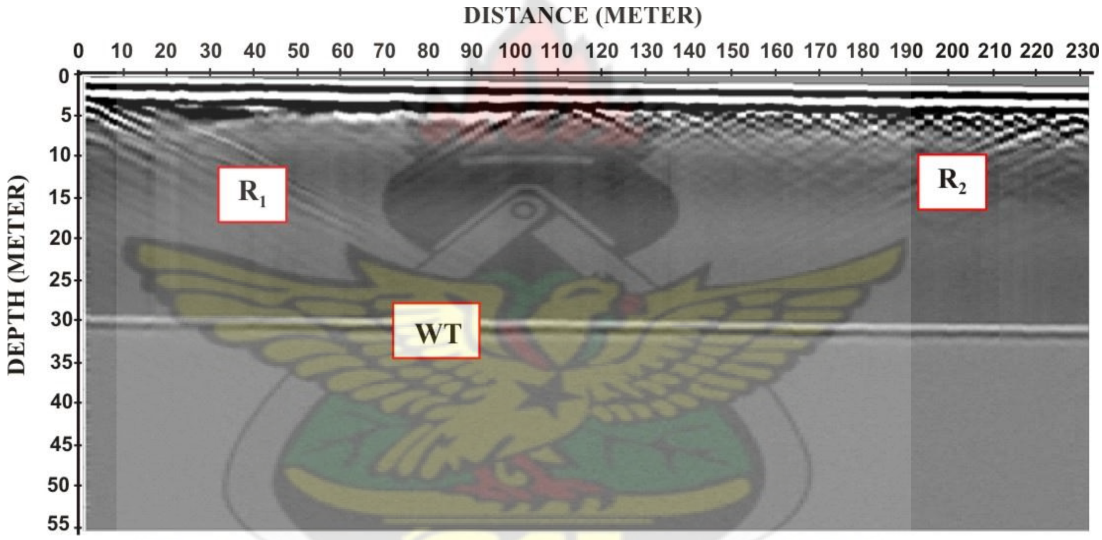

Figure A.22: Radar record for profile 30

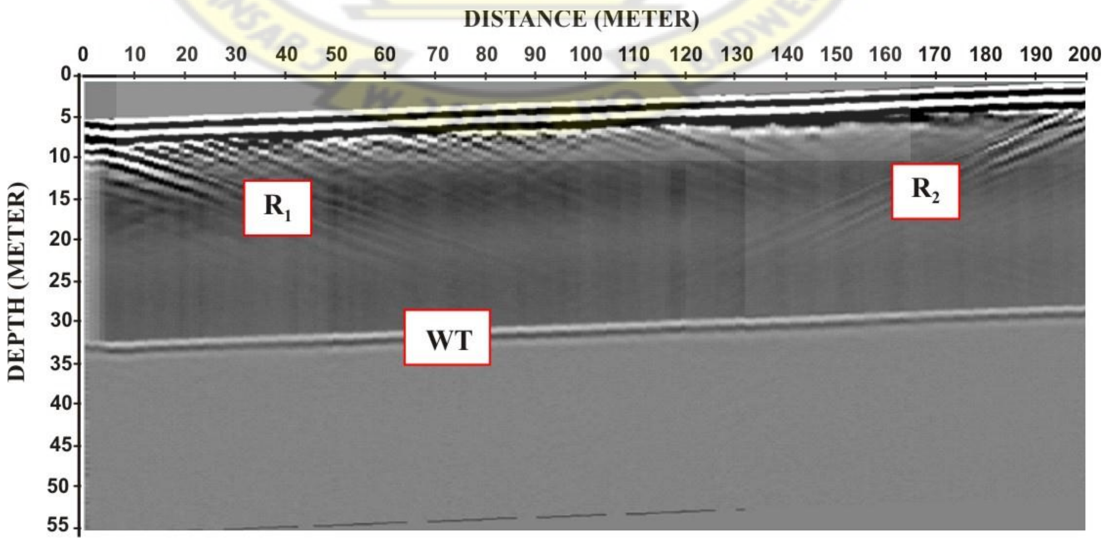

Figure A.23: Radar record for profile 31

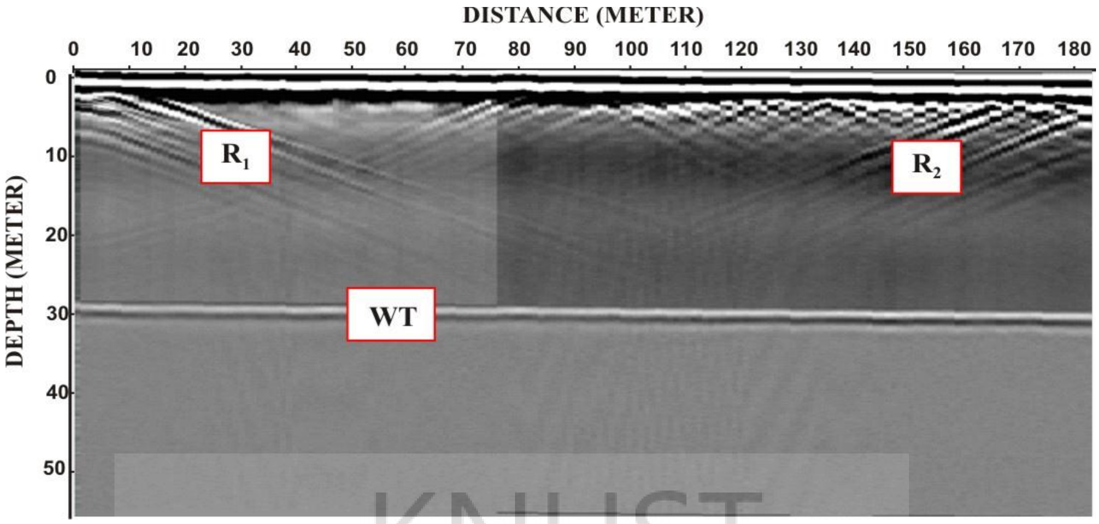

Figure A.24: Radar record for profile 32

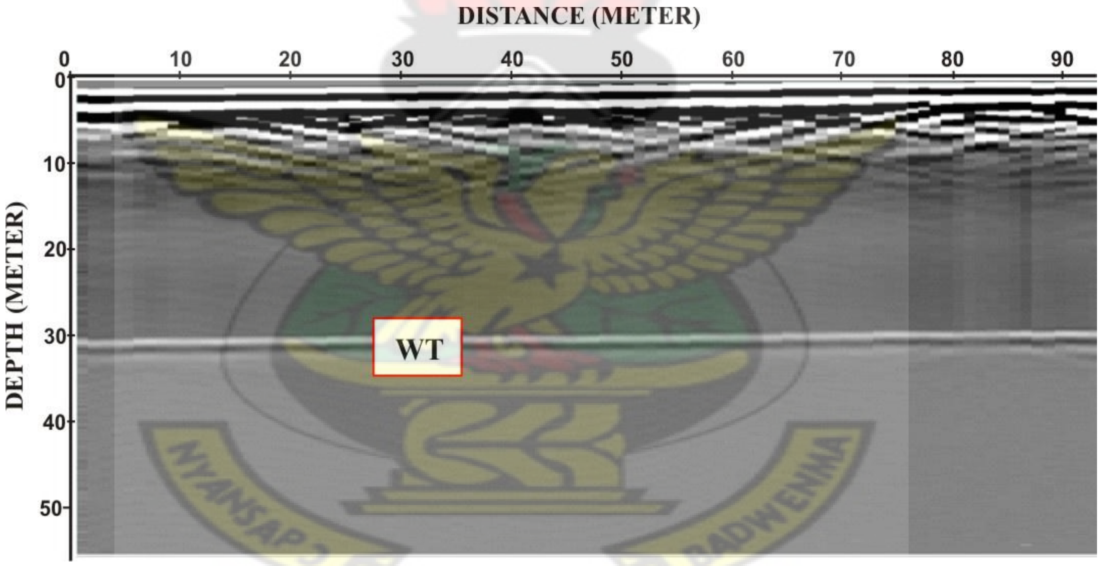

Figure A.25: Radar record for profile 35

APPENDIX B

ELEVATION MAP

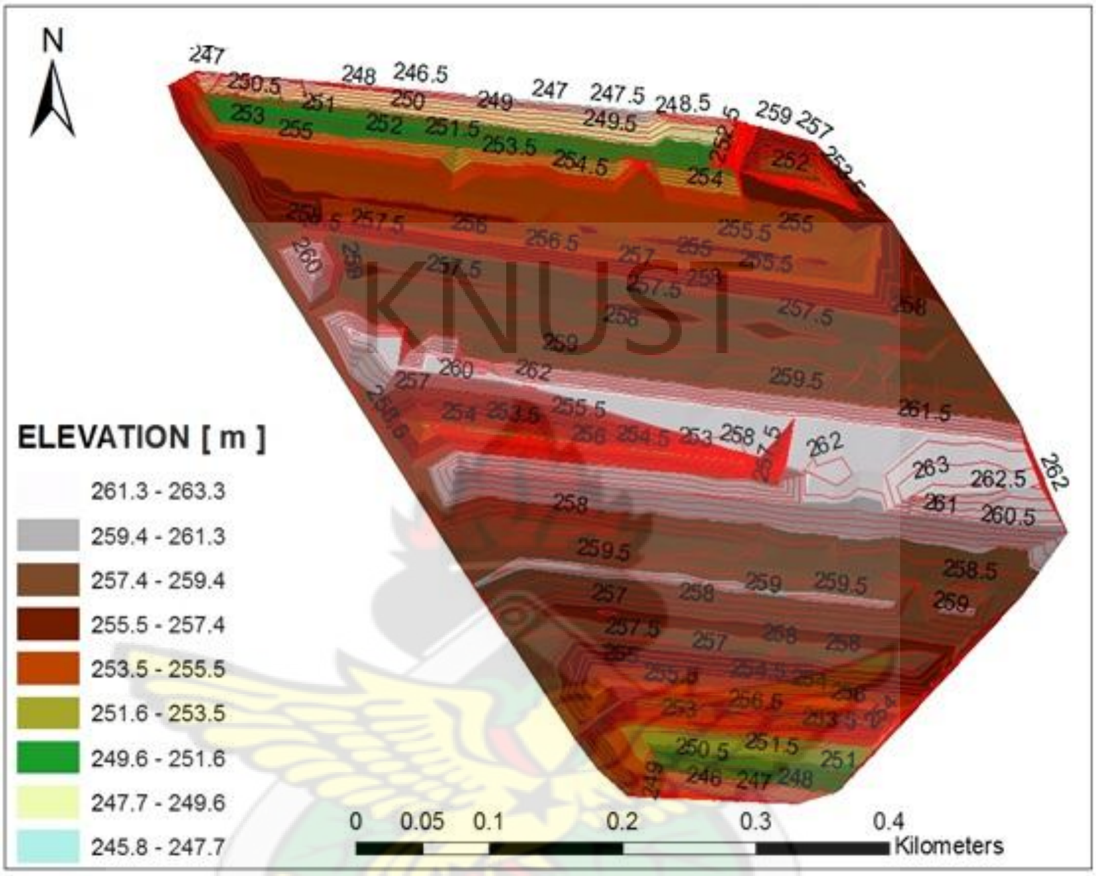

Figure B.1: Proposed Elevation Map of Project Site

APPENDIX C

Table C.1: GPS Data for Water Table and Elevation Maps

GPS Point	Latitude (˚)	Longitude (˚)	Y Projection (˚)	X Projection (˚)	Elevation (m)
363	6.693262	-1.525163	740084.8453	663018.9461	283.694
364	6.69433	-1.525459	740202.8476	662985.8667	286.3
365	6.697057	-1.526269	740504.1332	662895.4108	292.988
366	6.697044	-1.526238	740502.706	662898.8424	290.497
367	6.697978	-1.526163	740606.0135	662906.8242	293.653
368	6.692224	-1.523458	739970.6281	663207.7914	271.703
369	6.692218	-1.523451	739969.967	663208.5673	272.204
370	6.693648	-1.523589	740128.0521	663192.8353	274.721
371	6.695833	-1.523769	740369.6119	663172.2091	276.503
372	6.695875	-1.523869	740374.2231	663161.1394	279.887
373	6.695861	-1.523858	740372.6787	663162.3602	278.353
374	6.692197	-1.523491	739967.6315	663204.152	271.829
375	6.692274	-1.52366	739976.0901	663185.4421	271.265
376	6.696439	-1.524193	740436.4832	663125.1316	281.164
377	6.696921	-1.524448	740489.6986	663096.7795	286.431
378	6.695779	-1.524087	740363.5349	663137.0699	283.083
379	6.695791	-1.524111	740364.8539	663134.4126	282.099
380	6.692373	-1.523815	739986.9862	663168.2728	272.938
381	6.692526	-1.523941	740003.8632	663154.2917	279.079
382	6.695819	-1.524227	740367.9117	663121.5786	285.605
383	6.696824	-1.524504	740478.9537	663090.6206	287.509
384	6.696797	-1.524644	740475.9215	663075.1516	285.479
385	6.69263	-1.524093	740015.3132	663137.4524	283.34
386	6.692689	-1.524251	740021.785	663119.9647	281.299
387	6.695698	-1.524479	740354.4477	663093.7585	283.55
388	6.696741	-1.524761	740469.6901	663062.2351	286.012
389	6.69673	-1.524854	740468.4428	663051.957	285.384
390	6.692794	-1.524373	740033.3555	663106.4418	275.484
391	6.692918	-1.524516	740047.0201	663090.5909	283.547
392	6.69735	-1.525161	740536.9011	663017.8102	288.354
393	6.697343	-1.525335	740536.0693	662998.5757	287.81
394	6.692947	-1.524704	740050.1646	663069.7965	278.883
395	6.693063	-1.524814	740062.9555	663057.5967	284.445
396	6.693083	-1.524802	740065.1711	663058.9167	284.122
397	6.693085	-1.524797	740065.3939	663059.4688	284.07
398	6.697319	-1.525383	740533.3994	662993.277	288.713

399	6.697224	-1.525528	740522.8461	662977.2778	289.36
400	6.693156	-1.524949	740073.1947	663042.6405	280.37
401	6.693284	-1.525082	740087.305	663027.8939	283.105
402	6.697737	-1.525578	740579.5576	662971.5797	288.839
403	6.6978	-1.52574	740586.4704	662953.6486	289.494
404	6.693475	-1.525271	740108.3632	663006.9352	284.077
405	6.69379	-1.525276	740143.1946	663006.2779	283.825
406	6.693778	-1.525276	740141.8676	663006.2819	283.427
407	6.693803	-1.525284	740144.6295	663005.3891	283.356
408	6.693794	-1.525289	740143.6326	663004.8393	283.459
409	6.693581	-1.525411	740120.0384	662991.422	287.204
410	6.697832	-1.525898	740589.9566	662936.1701	292.213
411	6.697777	-1.526048	740583.8248	662919.6049	291.115
412	6.696366	-1.526198	740427.7453	662903.4896	288.133
413	6.69602	-1.525911	740389.5795	662935.3342	285.305
414	6.696027	-1.525925	740390.3489	662933.7841	285.004
415	6.696049	-1.525946	740392.7748	662931.4551	286.879
416	6.696079	-1.525954	740396.0895	662930.5607	287.754
417	6.696058	-1.525988	740393.7561	662926.8087	288.603
418	6.69605	-1.525986	740392.8721	662927.0325	288.898
419	6.696059	-1.525975	740393.8709	662928.2456	289.823
420	6.696058	-1.525968	740393.7627	662929.0198	290.443
421	6.696064	-1.525902	740394.4481	662936.3146	292.343
422	6.693776	-1.525771	740141.4822	662951.5566	283.319
423	6.696163	-1.526036	740405.3511	662921.4671	283.095
424	6.696152	-1.526144	740404.0989	662909.5307	290.057
425	6.693887	-1.525941	740153.7004	662932.7251	287.493
426	6.693987	-1.526065	740164.7173	662918.9828	285.766
427	6.698152	-1.526474	740625.1514	662872.3835	291.54
428	6.698	-1.526565	740608.3129	662862.3733	288.175
429	6.698037	-1.526597	740612.3938	662858.8232	289.382
430	6.694121	-1.52624	740179.4772	662899.5909	289.837
431	6.694166	-1.526265	740184.445	662896.812	289.636
432	6.694221	-1.526371	740190.4918	662885.0747	289.111
433	6.697874	-1.526745	740594.32	662842.5149	290.263
434	6.69783	-1.52686	740589.4163	662829.8155	288.973
435	6.694355	-1.526538	740205.2543	662866.5672	285.23
436	6.694411	-1.526667	740211.4041	662852.2868	289.972
437	6.697627	-1.527002	740566.9213	662814.1839	288.311
438	6.697535	-1.527084	740556.7207	662805.1487	289.041
439	6.694512	-1.526814	740222.524	662836.0014	283.679
440	6.69466	-1.52696	740238.8416	662819.811	283.245

441	6.697349	-1.527223	740536.1065	662789.8431	287.502
442	6.697262	-1.527367	740526.4382	662773.9518	288.386
443	6.694743	-1.527119	740247.9671	662802.2049	284.119
444	6.694855	-1.527281	740260.2985	662784.2576	283.459
445	6.697175	-1.527498	740516.7743	662759.4978	285.926
446	6.697178	-1.527502	740517.1047	662759.0545	286.556
447	6.697069	-1.527596	740505.0202	662748.6984	284.525
448	6.694978	-1.527417	740273.8549	662769.1811	283.015
449	6.69512	-1.527564	740289.5087	662752.8821	282.323
450	6.696897	-1.527725	740485.9576	662734.4936	287.578
451	6.696804	-1.527862	740475.6282	662719.3782	282.512
452	6.695176	-1.527722	740295.6489	662735.3956	281.83
453	6.6953	-1.527873	740309.3109	662718.6604	281.937
454	6.696677	-1.528031	740461.5284	662700.7362	280.317
455	6.695409	-1.528008	740321.3195	662703.6991	277.049
456	6.6955	-1.528154	740331.334	662687.5277	278.251
457	6.696316	-1.528231	740421.5424	662678.7445	284.287

Appendix D:

D.1 Regional Geology

Regionally Ghana falls mostly within the West African Craton which features a wide variety of geological terrains with a complicated geological history. Although a broad geological framework was established by pioneer workers much earlier, it has only been in the last few decades that more detailed regional studies have emerged. Petters (1991) and Dallimore and Davis (1987) have summarised much of the regional information in several texts.

The West African Craton is made up of an Archean core which is also referred to as the Man Shield and Paleoproterozoic domain with relics of Archean basement (Wright et al., 1985)

D.1.1 Archean

The Archean features old Precambrian rocks surrounded by younger Precambrian units. The southern part of this craton is now generally referred to as the Man Shield (Milesi et al., 1991).The oldest Precambrian rocks are the Archean in age (> 2500 Ma)and appear to be limited to a core zone along the coastal region extending from western Cote d'Ivoire through Liberia, Sierra Leone and into southern Guinea (Wright et al., 1985)

The geology of the Archean core is believed to be similar to major Archean shield areas in many parts of the world. Most of the region appears to consist of highly metamorphosed mafic to felsic gneisses and migmatites representing old basements. (Wright et al., 1985)

Wedged into the basement rocks are narrow greenstone belts of less metamorphosed suprecrustal rocks with extensive tholeiitic basalts and sequences of metasediments that include turbidities, conglomerates and extensive banded iron formation. The banded iron formations have been developed on a substantial scale in Liberia and both Sierra Leone and Guinea have large resources with excellent potential for future development. These belts contain numerous gold occurrences and some indications of base metals. Also within the greenstone belts are some intermediate to felsic volcanic units; late-stage intrusive complex are also quite widespread (Brabham, 1998).

The Prominent Sassandra fault bounds the Archean Units on the east in Cote d'Ivoire. The Sassandra fault is a large N-S regional feature, which generally separates the Archean unit from younger Paleoproterozoic metasedimensta and metavolcanic units still further to the east (Milesi et al., 1991)

Radiometric age-dating has established two widespread thermo-tectonic events; the most widespread one is dated at about 2750-2900 Ma and is called Liberia event. This event metamorphosed all of the supracrustal rocks and surrounding basement. Limited data suggest an even earlier Archean event (greater than 3000 Ma), referred to as Leonian but its extent is not well established as yet (Griffis et al., 2002)

D.1.2 Paleoproterozoic

The most extensive units of the Man shield are the Paleoproterozoic metasediments, metavolcanics and associated intrusive complexes that are exposed and covers Ghana, Cote d'Ivore, Burkina Faso and into southern Mali, northern Guinea and SW corner of Niger (Wright et al., 1985). Virtually all of the Volta Basin in northern and eastern

Ghana is underlain by Paleoproterozoic units and there are also equivalent rocks in NW Africa, which suggests that much of the Western Sahara has the same but buried Paleproterozoiccratonic units. The Paleoproterozoic metasediments, volcanic and related intrusive are economically important as they host majority of the substantial old resources of the region and in addition they also host important manganese deposits (Brabham, 1998)

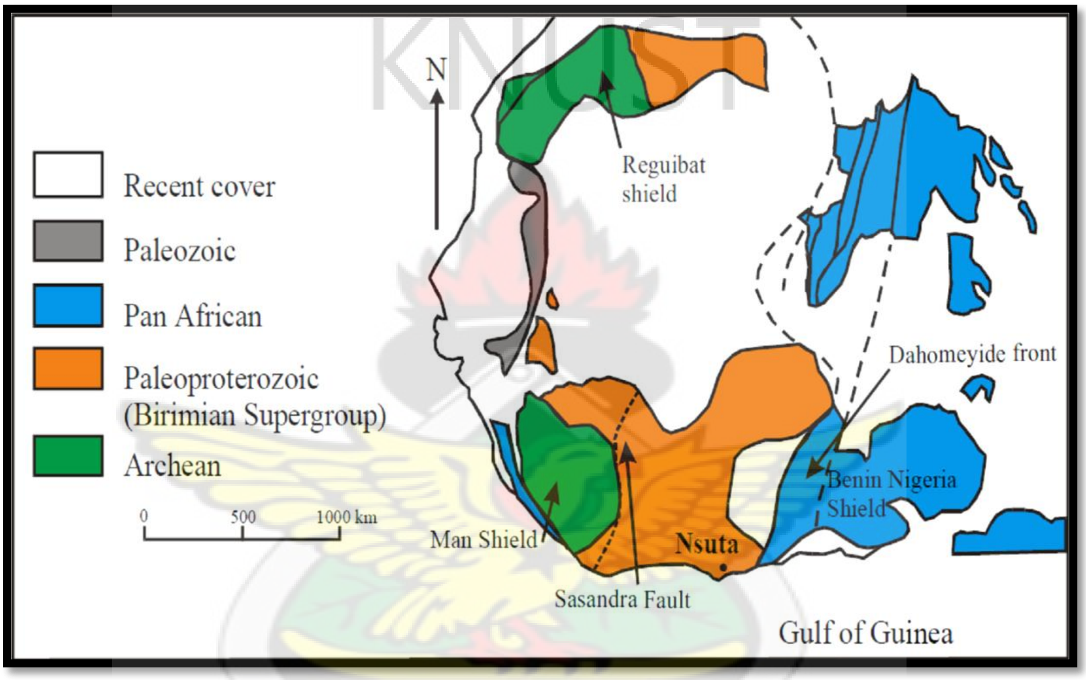

Figure D.1: Precambrian geology of West Africa with the Archean Man Shield boarded on the west by the Birimian Supergroup (Milesi et al., 1991)

D.2. Geology of Ghana

Ghana is mostly underlain by metamorphosed rocks of the Paleoproterozoic age that fall mainly within the age range of 2300-1900 Ma. It is mostly believed that some the granitic complexes in some parts of both southern and northern Ghana represented the Archean basement units. However subsequent age-dating has confirmed that most of these are actually Paleoproterozoic in age and related to the Eburnean Orogenic cycle (Griffis et al., 2002)

Kesse (1985) has done extensive and detailed description of the historical nature on the geology of Ghana and have also worked on the various aspects of the geology of southern and northern Ghana.

D.2.1 The Birimian Supergroup

The Birimian rocks derived their name from the Birim River valley in Ghana (Kesse, 1985). The Birimian system in Ghana is grouped under the dominant sedimentary units called the 'Lower Birimian' series and the dominantly metavolcanic units called the 'Upper Birimian' System. (Griffis et al., 2002)

According to Junner (1940), the Lower Birimian sedimentary packages represent classical 'miogeosynclinal' basin sediments whereas the volcanic-rich units were believed to represent 'eugeosynclinal units. Griffis et al., (2002) believe the extensive folding and faulting and limited exposure have made it difficult to estimates the total thickness of the Upper and Lower series. However, Junner (1940) made a general estimate of 10,000-15,000m for the Upper Series (volcanic units) and it could be assumed that at least a comparable thickness would apply to the Lower Series of Predominantly sedimentary units. This should be considered as a very minimum estimated thickness (Griffis et al., 2002). The thickness of the Tarkwaian metasediments in the Bui syncline indicate a thickness of about 9000 m (Kiessling, 1997) and this represents the most recent measurements.

These are thinner than the volcanic-sedimentary units, which they overlie and also much thinner than the mainly sedimentary units in adjacent basins.

According to Griffis et al., (2002), later works by different groups retained the basic Upper and Lower series but with additional details on each series. Particularly, Soviet geologists in the early 1960's gave a more detailed analysis of the Lower Birimian sedimentary series. Trashliev (1972) and Dabowski (1972) worked extensively in the Kumasi basin and established several flysch, argillaceous, and arenaceous formations within the Lower Birimian Series. Although similar lithologic units were observed in most of the sedimentary basin areas, it is reasonable to say that considerable difficulty was encountered in establishing consistent stratigraphic correlations from area to area.

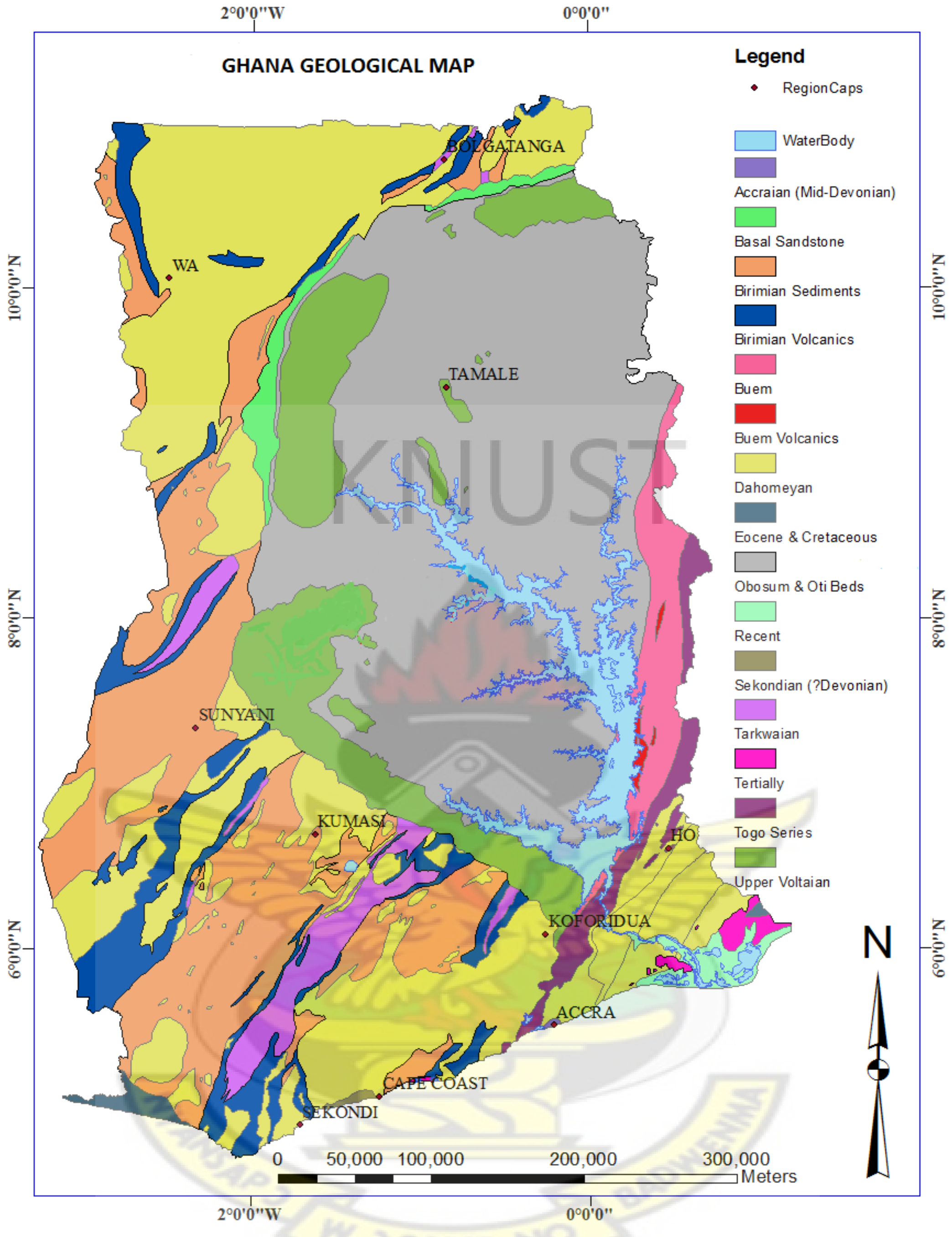

Figure D.2: Geology of Ghana (modified after Ghana Geological Survey Department, 2009)

The Upper Suite according to works done by the Soviet group was made up of diabase, quartz porphyries, tuffs and interbedded phyllites along with a Middle suite of mainly phyllites, quartz porphyries and tuff. These are underlain by a Lower suite of felsites, felsite porphyries with interbedded tuffaceous greenstone and agglomerate (Kesse, 1985).The Soviet classification scheme applied mainly to the northern Bui and Bole areas. Dabowski (1972) proposed a similar general breakdown with an Upper basic volcanic complex (metabasalt and andesite), a Middle acid metavolcanic complex (quartzite, quartz schist and metarhyolite) and a Lower volcanic arenaceous complex (greywackes, conglomerate and grit).

As a lithostratigraphic unit, Birimian rocks occupy the southern part of the West African Craton. Birimian strata were deformed and metamorphosed during the ~2.2 Ga Uburnean Orogeny. This orogeny is characterised by isoclinals folding as well as intrusion of pretectonic and post-tectonic granites (Eisenlohr and Hirdes, 1992)

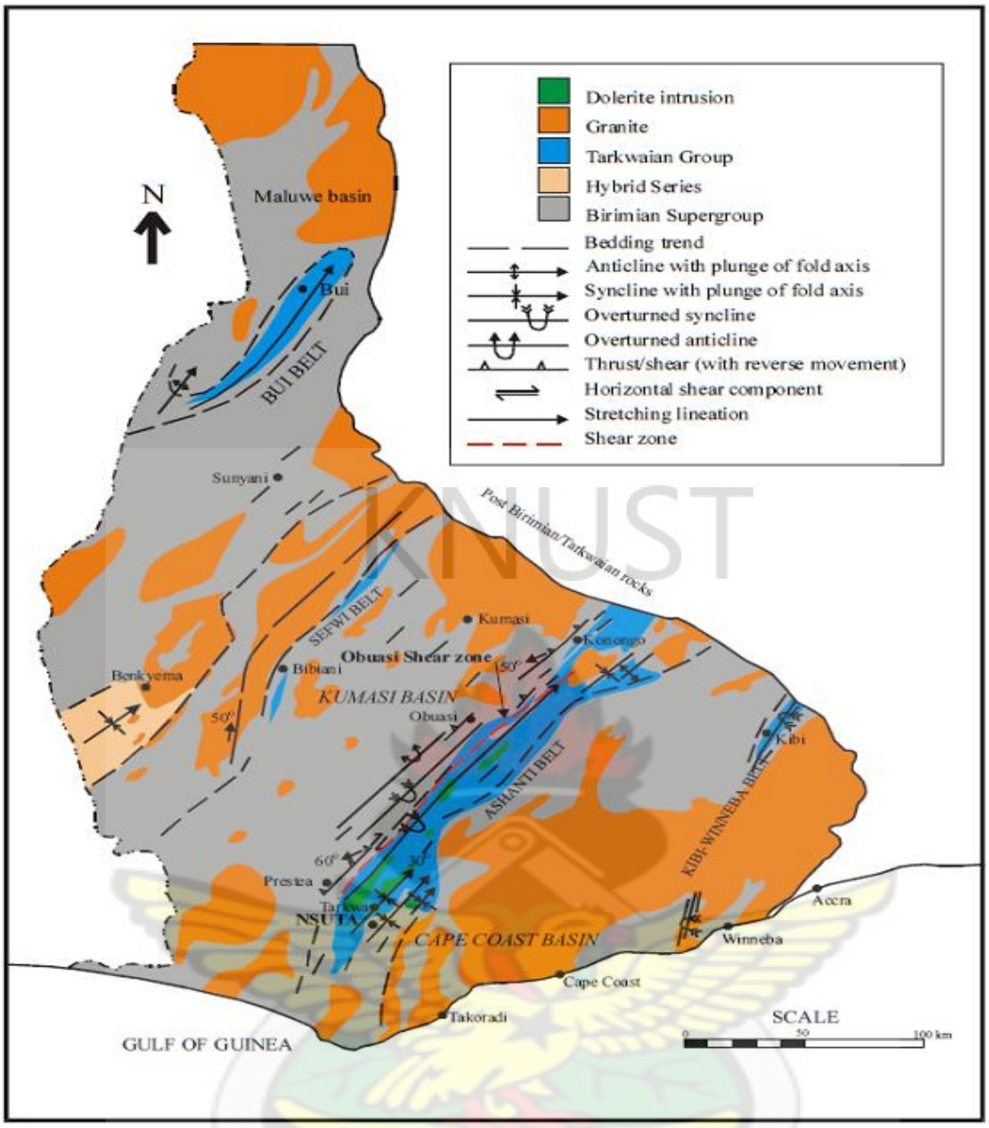

Figure D.3: General geology and structure of the southern Ashanti Belt and Western Ghana (modified after Eisenlohr and Hirdes, 1992)

Recent geochronological and geochemical data suggests contemporaneous volcanism and sedimentation. ''Although the geochemistry of the volcanic units in Ghana are dominantly of tholeitic character, there are some indications of units with calc-alkaline characteristics; for example, Sylvester and Attoh (1992) have noted the bi-modal occurrence of tholeitic basalts and calc-alkaline felsic volcanic in several of the volcanic belts of Ghana.

Similar affinities have been recognised in various other volcanic belts in West Africa (Liegeois et al., 1991; Ledru et al., 1991). In many of the belts, volcani clastic units (both pyroclastic and epiclastic) form a very important component and, in places, argillites and chemical sediments are widespread (Griffis et al., 2002).''

Sm-Nd isotopic dating of samples from the Birimian volcanic and sedimentary rocks by Taylor et al., (1988) for example confirmed the suspected contemporaneity of Birimian sedimentary rocks and volcanic. Model ages for eight samples of Birimian sedimentary rocks range from 2.01 Ga to 2.31 Ga (Eisenlohr and Hirdes, 1992; Davis and Annan 1989). They differ very little from the analysed Birimian volcanic rocks dated at 2189 $\pm$ 1Ma (Hirdes and Davis, 2002). Detrital input into the Birimian sedimentary basins from ancient crustal sources has thus been insignificant; instead a derivation of clastic sediments from contemporaneous igneous activity in the volcanic belts is confirmed by isotopic data (Leube et al; 1990).

The Birimian Supergroup is unconformably overlain by coarse fluvial sedimentary rocks also referred to as the Tarkwain Group (fig 2.5) which contains auriferous conglomerates. Authors like Junner (1940) and Kesse (1985) regard the Birimian and Tarkwaian as two separate entities.

D.2.2 The Tarkwaian Formation System

The Tarkwaian Group has been well studied in the region of the Tarkwa goldfield. The Group consists of a thick series (1800-3000m) of argillaceous and arenaceous sedimentary rockswith two well-defined zones of auriferous conglomerates in the lower formations of the succession and a variety of sandstones (quartzites), conglomerates and argillites (phyllites) (Junner, 1940)

The Tarkwa district has seen most of the extensive sedimentological study by Sestini (1973) research work who concluded that the Tarkwaian units were largely deposited in shallow, non-marine, basins along the flanks of a volcanic chain. Fast flowing streams transported much of the sediments. The coarse loads were discharged into alluvial fans and in deltas along the margins of the basin and the fan deposite were progressively re-worked by braided river channels. This general pattern also fits the model established more recently in the Bui syncline by Keissling (1997) who recognised several major cycles of sedimentation in two separate basins, which eventually became linked.

Various stratigraphic subdivisions have been proposed for the Tarkwaian Group (Junner, 1940; Kesse, 1985; Hirdes & Nunoo, 1994). The latest subdivision that was officially accepted by the Geological Survey Department of Ghana is that of Hirdes and Nunoo (1994) (Table 2.1)

Table D.1. Stratigraphic subdivisions in the Tarkwaian Group in the Tarkwa mine area(modified by Hirdes and Nunoo, 1994, after Junner, 1940)

Series	**Thickness (m)**	**Composite Lithology**
Huni Series	1370	Sandstone, grits and quartzites with phyllites
TarkwaPhyllite Series	120 – 400	Huni sandstone transitional beds and green and greenish grey chloritic and sericiticphyllites and schists.
Banket Series	120 – 160	Tarkwaphyllitetransisional beds and sandstones, quartzites, grits, breccias and aufiferous conglomerates
Kawere Series	250 – 700	Quartzites, grits, phyllites and conglomerates.

Based on the study of detrital zircon populations, Hirdes and Davis (2002) suggest that the formation of Tarkwaian depositories and their sedimentary infill took place between 2132 $\pm$ 3 Ma and 2097 $\pm$ 2 Ma. Seventeen of twenty investigated detrital zircon grains from the Tarkwaian depository investigated by Hirdes and Davis (2002) fall within the age range of 2194 Ma to 2155 Ma. This confirms that the principal provenance of the Tarkwaian zircons in the Ashanti Belt was the Birimian Supergroup (Leube et al., 1990; Taylor et al., 1992).

D.3 Intrusives

There are a variety of intrusions throughout the Birimian sedimentary basins and volcanic belts. However two major types of occurrences have been recognised in many parts of the region which are the 'Cape Coast' and 'Dixcove' types (Griffis et al., 2002)

D.3.1 Cape Coast Type

The 'cape coast' type batholiths are more massive, foliated, syntectonic and dominantly intermediate intrusive which are generally rich in calcium with biotite being the most common mafic minerals. Typical lithologies include diorite, tonalities, granodiorites, adamellites and granites. They have extensive contact metamorphic aureoles with mineral assemblages that indicate pressures of at least 4 kb and temperature 500°C

D.3.2 Dixcove Type

The 'Dixcove' type occurs mainly within the confines of the volcanic belts and are generally of an intermediate composition although more mafic and felsic phases are not common. Hornblende is usually the dominant mafic mineral and in some instances the intrusive lack strong foliation. They occur in small plutons to very large batholiths, although not as extensive as the major 'Cape Coast' complexes. They are frequently described as discordant intrusive (Griffis et al., 2002). The 'Dixcove' units were considered to be late-tectonic to post-tectonic

There is also the Bongo-Type granitoid bodies which intrude the Tarkwaian sediments in the Bole-Navrongo belt, and show unusually high K-concentrations. These granitoids lack foliation i.e they are post tectonic in origin and are petrographically characterised by pink phenocrysts of alkali feldspar.

Appendix E:

E.1 Softwares Used:

- ReflexW
- MapInfo 10.5-Discover
- ArcGIS
- Coral Draw X5: Radar records